Self-sensing magnetic levitation : a feasibility study

van Acht, V.M.G.

Award date:
1997

University of Technology Eindhoven
Department of Electrical Engineering
Measurement and Control Section

Self-Sensing Magnetic Levitation A Feasibility Study

by V.M.G. van Acht

09-06-97 22:08:00, 25, UK
Master of Science Thesis
Carried out from October 1996 to June 1997
Commissioned by prof.dr.ir. P.P.J. van den Bosch
Under supervision of dr.ir. A. Damen

ABSTRACT

At the Eindhoven University of Technology research is carried out at a three dimensional laser interferometer, which can be used to measure the position of an object. (For example the tool centre point of a robot.) In the laser-interferometer a mirror is used to direct the laser-beam onto a retro-reflector on the object to be measured. The position and orientation of this mirror must be controlled extremely accurate and fast.
One way to realise the laser deflection system is to use magnetic bearings. Magnetic bearings have the advantage that friction is extremely low, tracking can be extremely accurate (in principle) and hardware is cheap. Magnetic bearings use several electromagnetic coils to exert positioning forces onto the freely levitated ferromagnetic mirror. One way to obtain the position and orientation of the mirror (necessary for the position control system of the mirror) is to measure the inductances of the same coils which are used to levitate the mirror. This is called *self sensing* magnetic levitation. Self sensing magnetic levitation has the advantage that no additional position sensors are necessary. Therefore it can be cheaper and smaller.

In this master of science thesis a pilot project for the magnetic levitated mirror is discussed. A steel ball is to be levitated and controlled in the two directions of the vertical plane by four coils. Position of the ball must be obtained by measuring the inductances of the coils.
First the magnetic, electrical and mechanical parameters of the levitation system are measured. After that, the equations of a one-dimensional magnetic levitation system are derived for current controlled coils and voltage controlled coils. Then the two different actuators (current source and voltage source) are examined in detail. It will be shown that, in contrary to a voltage source, a current source is very likely to oscillate and suffers from a lot of output voltage noise when loaded with a coil. Next, five different ways to measure the inductances of the coils are discussed and examined in detail, and the best actuator/sensor combination is chosen. It will appear that this is a voltage controlled current source with an additional HF-component to measure the inductance of the coil.
After that, a controller is designed for the magnetic levitated ball, using the previously chosen actuator/sensor combination, and simulations with the proposed controller are done.
Finally the designed actuator and sensor are tested in practice, and recommendations are given regarding the magnetic levitated mirror system.

CONTENTS

LIST OF FIGURES

LIST OF TABLES

LIST OF USED SYMBOLS

In this list only global symbols are given. They can be overrid by local definitions.

A	= coil model parameter	[H]	[kg m^2 s^{-2} A^{-2}]
A_0	= open loop amplification opamp	[]	
B	= coil model parameter	[m^{-1}]	
C_f	= filter capacitance	[F]	[A^2 s^4 kg m^{-2}]
f	= frequency of additional high freq.	[s^{-1}]	
f_0	= resonance frequency	[s^{-1}]	
f_g	= gravitational force	[N]	[kg m s-2]
f_m	= magnetic reluctance force	[N]	[kg m s^{-2}]
f_{osc}	= oscillation frequency oscillator	[s^{-1}]	
g	= gravitational acceleration	[m s^{-2}]	
i_L	= current through coil	[A]	
L	= inductance of the coil	[H]	[kg m^2 s^{-2} A^{-2}]
L_f	= filter inductance	[H]	[kg m^2 s^{-2} A^{-2}]
L_s	= leak inductance	[H]	[kg m^2 s^{-2} A^{-2}]
m	= mass of the levitated ball	[kg]	
N	= number of winding	[1]	
R_f	= filter resistance	[Ω]	[kg m^2 s^{-3} A^{-2}]
R_L	= resistance of the coil	[Ω]	[kg m^2 s^{-3} A^{-2}]
$(SNR)_{in}$	= signal to noise ratio, input signal	[]	
$(SNR)_{out}$	= signal to noise ratio, output signal	[]	
T	= period of switched power supply	[s]	
U_L	= coil voltage	[V]	[kg m^2 s^{-3} A^{-1}]
V_{dd}	= supply voltage	[V]	[kg m^2 s^{-3} A^{-1}]
V_L	= coil voltage	[V]	[kg m^2 s^{-3} A^{-1}]
V_n	= noise voltage	[V]	[kg m^2 s^{-3} A^{-1}]
V_s	= signal voltage	[V]	[kg m^2 s^{-3} A^{-1}]
V_{ss}	= ground voltage or negative supply	[V]	[kg m^2 s^{-3} A^{-1}]
x	= gap length	[m]	
δ	= duty cycle of switched power supply	[]	
Φ	= flux	[Wb]	[kg m^2 s^{-2} A]
μ_0	= permeability of vacuum	[H/m]	[kg m s^{-2} A^{-2}]
μ_r	= relative permeability	[]	
τ	= time constant opamp	[s]	

1. INTRODUCTION

At the Eindhoven University of Technology, Measurement and Control Section, research is done at a three dimensional laser interferometer, which can be used to measure to position of an object (for example the tool centre point of a robot) very accurately in all three degrees of freedom. In figure 1 the 3D interferometer system is depicted.

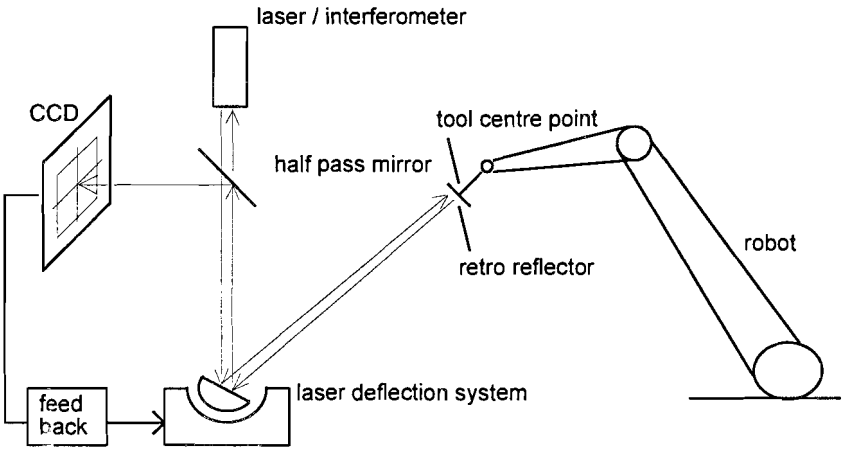

figure 1: 3D laser interferometer

In figure 1 a laser beam goes through a half pass mirror and is directed by the laser deflection system onto the retro reflector on the tool centre point (TCP) of the robot. The retro reflector reflects the laser beam back via the laser deflection system on the half pass mirror. Half of the laser-beam is then reflected onto the CCD (charge coupled device), and the other half is reflected back into the laser interferometer. The interferometer is now able to measure the distance the laser light has travelled.
A control system controls the direction of the deflection mirror in such way that the laser beam hits the CCD in the middle. The orientation of the mirror determines (in combination with the distance) the position of the tool centre point.

Biggest problem of the 3D laser interferometer as described above, is that the position and the orientation of the deflection mirror must be controlled extremely accurate and fast. (Goals are an accuracy of 1μrad with a bandwidth of 300 Hz) Therefore special bearings are necessary. At the Measurement and Control Section, an air bearing is used to control the position and angles of the mirror to deflect the laser beam. As this bearing has its limitations, the idea of developing a magnetic bearing was suggested. A magnetic bearing could be realised as shown in figure 2. Here the mirror is levitated and rotated by the same magnets. Probably this will lead to various problems, but figure 2 is only intended as an illustration of the magnetic bearing for the laser deflection mirror.

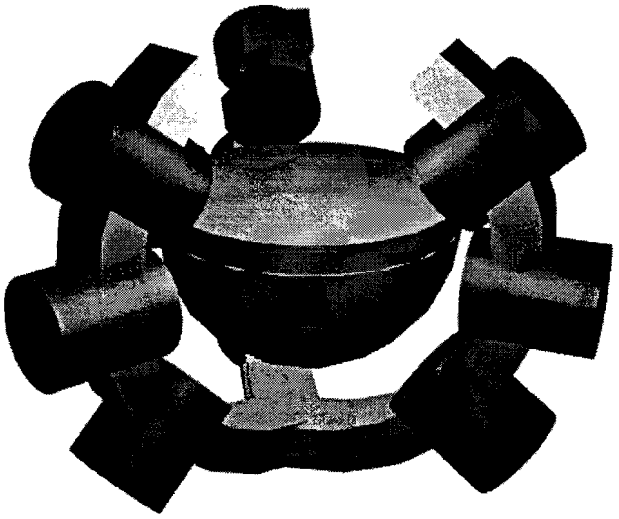

figure 2: Magnetic levitated mirror

As a pilot project for the magnetic levitated mirror, to learn about magnetic bearings, a magnetic levitation system as in figure 3 has been developed.

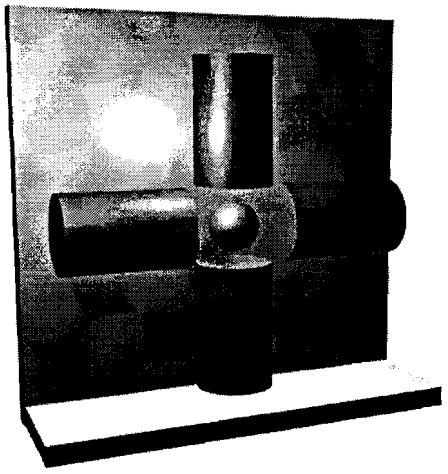

figure 3: Magnetic bearing, pilot project

The system as depicted in figure 3 consists of four electromagnets to position a steel ball in two directions. The currents through the magnets are supplied by four power amplifiers, which are controlled by a controller.
Special about this system is that it is *self sensing*. This means that no explicit position sensor is used in the levitation system but that the position of the ball is obtained by measuring the inductances of the coils. Self sensing magnetic bearing are described in [1], [2], [3] and [5]. The advantage of self sensing magnetic levitation is that it can be cheaper and smaller, evidently because of the absence of position sensors.

The pilot project, as described above, was already realised. However, there were a few major problems. First of all, the current through the coil was supplied by a **current** source. This has some disadvantages, as will be made clear in chapter 4. The next problem was that the position of the ball was not measured with the upper coil as it was levitated with, but with the bottom coil. Further on, the ball was not positioned in two dimensions but in the vertical direction only. And last but not least, the controller was not able to stabilise the ball very accurately.
Goal of this Master Science Thesis was to solve (some) of the problems of the self sensing magnetic levitated ball.
To write this Thesis the author has intensively used three other theses of the Eindhoven University of Technology, [10], [11] and [12]. Citations from these reports will be made without further notice.

2. MODEL PARAMETERS

Before any hardware or a controller can be designed the model parameters for the two dimensional magnetic levitation system must be obtained. This will be described in this chapter.
The dimensions and some of the magnetic properties of the physical process are depicted in figure 4 and table 1.

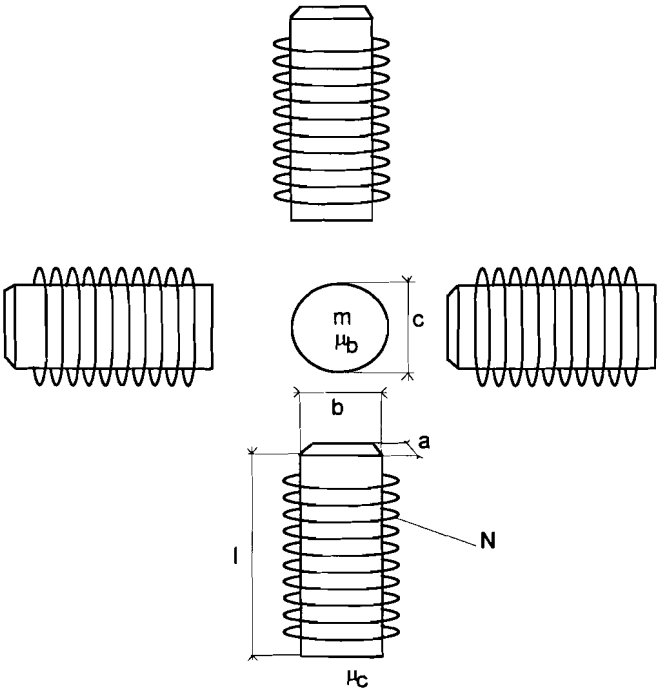

figure 4: Physical dimensions of the process

variable	description	value	unit
a	depth of coil	0.025	[m]
b	width of coil	0.025	[m]
l	length of coil	0.010	[m]
$A\ (=a \cdot b)$	area of coil	0.0625	[m^2]
N	number of turns	1000	
μ_c	rel. permeability coil (ferrox cube)	≈1000	
c	diameter ball	0.020	[m]
m	mass of ball	0.080	[kg]
μ_b	rel. permeability ball (steel)	≈1000	

table 1: Physical dimensions of the process

Note that the upper coil has two separate windings, so there is a total of five coils. (not four)

2.1. MEASURING COIL SATURATION

The magnetic flux through the core of a coil does not only depend on the current through the windings, but also on the magnetic properties of the coil material. The material used suffers from saturation (as every weak magnetic material). This leads to a reduction of the inductance of the coil, because the magnetic permeability decreases with increasing current.
This can be understood by the fact that there are only a finite number of elementary magnets in the material. With increasing current, more and more elementary magnets are aimed in the direction of the magnetic field, and thus the magnetic field is amplified by those elementary magnets. But at a certain point, all elementary magnets point in the direction of the magnetic field already, so no further amplification due to the aiming of the elementary magnets can be expected. The B-field then only increases because of increasing μ_0H. (See figure 5.)
For small variations in the current through the coil i_L, the inductance of the coil is given by:

$$L = \frac{N^2 \mu_0 \mu_r A}{l} \qquad (1)$$

In (1) μ_r depends on the current through the coil, as described above. Normally μ_r is defined as the relative permeability of the magnetic material for small magnetic field strengths, that is for small currents i_L. In that case the magnetic field strength B is proportional with the current through the coil.

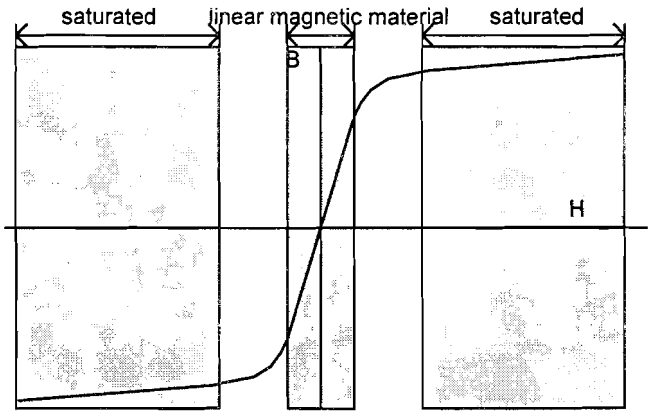

figure 5: Plot of saturation of coil material

Although it was impossible to change the material of the core of the coils due to lack of time, the magnetic properties of two materials other than the currently used ferrox cube were measured. In figure 6 (see also Appendix A.) the magnetic field strength B is plotted against the current I_L through the coil for different materials.
It is obvious that the material currently in use (ferrox cube) suffers from saturation at relatively low currents.
The cheapest form of steel (steel-37 (also: Fe 37, Fe 360), which has the lowest amount of carbon) saturates at much higher currents, but suffers from excessive hysterese. This can be

seen best in the right part of figure 6. The curve of steel-37 does not start and end in the origin of the co-ordinate system.
Weak iron is the best material for the coil, because it suffers the least from saturation and hysterese. However, because weak iron (and also steel-37) is a conductor it suffers from a effect which is not discussed here, viz Eddy-currents. Eddy currents can be largely avoided by laminating or sintering the core of the coil.

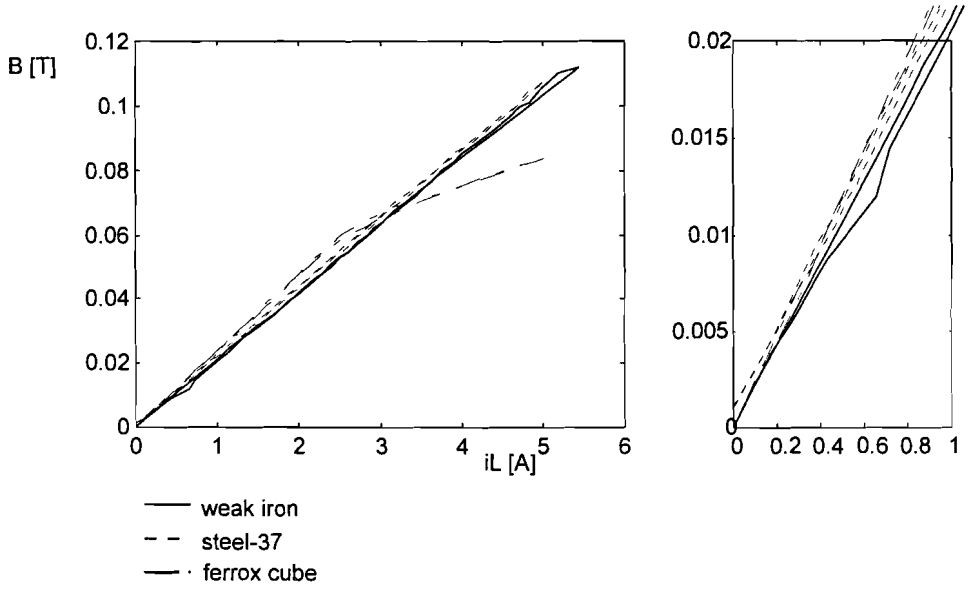

figure 6: Magnetic properties of materials

The magnetic field strength was measured using a Gauss-meter (10000 Gauss = 1 Tesla) for different DC-currents through the coil. The current through the coil was monotonously increased in discrete steps until the maximum current through the coil was reached. After that the current was monotonously decreased again in discrete steps to measure the hysterese of the material.
Note that the measurements used for the plots in figure 6 were taken after the coil material was pre-magnetised by a current through the coil of approximately 5A to emphasise hysterese effects of the material.

As already indicated in chapter 1, the position of the ball is obtained by measuring the inductance of the coil. Because it is unknown (at this point) whether saturation and hysterese are frequency, temperature, or time dependent it is not possible to compensate the position measurement for the effects of saturation and hysterese. It is therefore **very** important that the current through the coil does not exceed 2A (when using ferrox cube), to minimise the effects of saturation. Probably even a smaller maximum current is necessary to measure the position of the ball accurately.

2.2 MEASURING SMALL-SIGNAL COIL PARAMETERS

Because saturation (see previous section) must be avoided, the currents applied to the coil are relatively small. The small signal coil parameters can be measured very accurately using a simple ohm-meter and an inductance-meter. The inductance is measured when the distance between the ball and the coil is infinitely large. The results can be found in table 2.

	Resistance [Ω]	Inductance [mH]
Upper coil	3.570	108.70
Bottom coil	3.409	111.10
Left coil	3.406	107.12
Right coil	3.465	106.80
Gravity coil	4.720	109.18

table 2: Small signal coil parameters

The values in table 2 show the great similarity between the five coils. The inductances and DC-resistances are about all the same, except for the gravity coil. Its DC-resistance is much higher than that of the other four coils. This can be explained by the fact that the gravity coil is winded around the upper coil, so that the radius of the windings is larger and the total length of the wire is longer.
Although the position of the ball is obtained by measuring the inductance of the coil, the exact value of the inductances in table 2 is not interesting. The position of the ball is calculated by measuring the deviation of the inductance from the value in table 2.

2.3 MEASURING POSITION / INDUCTANCE RELATION

The relation between the position of the ball and the inductance of the coil is depicted in figure 7. See also appendix B. Measurements were made by measuring the inductance of the coil with an inductance-meter for different distances between the ball and the coil.

When an inverse proportional model is fitted on the measurement data, using a vertical least means square method, the result is a model that does not describe the behaviour of the process very well. (This will be discussed in detail in chapter 3.) So an exponential model is used for the process. (2)
Because the vertical least mean square method was used to fit the model on the measurement data, most data points were chosen around the steady state operating point of the system (x=0.005 [m]) , and only a few with larger distance between the coil and the ball. Therefore the model is not fitted very well on the data for larger distances between coil and ball.

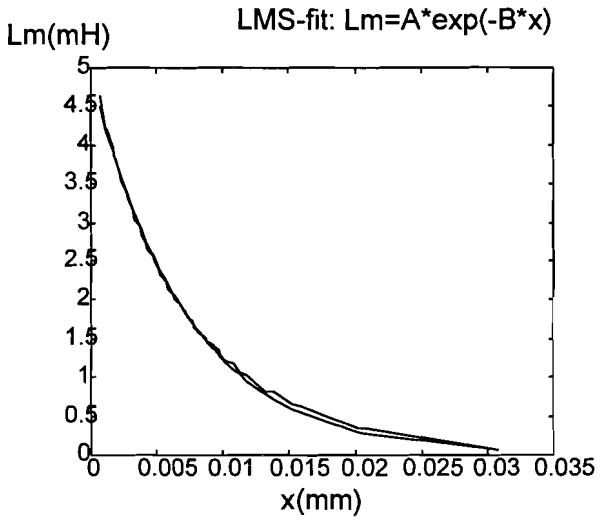

figure 7: Position / inductance relation

The values L_S, A and B found for the for the process are:

$$L = L_s + A \cdot e^{-B \cdot x}$$

$$L_s = 102.89[mH]$$
$$A = 4.941[mH]$$
$$B = 138[m^{-1}]$$

(2)

Note that L_S in (2) does not comply with L_S in table 2. This is because L_S can change significantly when the amount of magnetic material in the direct environment of the coil is changed. However, because exact value of L_S is unimportant, L_S will be approximated by the value 0.11H.

Note that the relation between the induction of the coil and the distance between the ball and the coil is measured when the ball moves in the vertical direction only. Variation in induction by horizontal displacement is not measured. This means that the levitation system will be one dimensional.

3. THEORY OF MAGNETIC LEVITATION

In this chapter the equations of a magnetic levitation system are derived. For simplicity, the ball is assumed to move in the vertical direction only. This means that the coils for horizontal movements are assumed to be absent, and thus have no influence on the ball.
When the position of the ball must be controlled in two directions, the relation between the position of the ball and the inductance of the coil (figure 7), must be measured in two dimension. Furthermore, the magnetic reluctance force (as will be derived in the chapter) would be a function of the vertical as well as the horizontal position of the ball. Also, the **(varying!)** mutual coupling between the coils influences the magnetic reluctance force and the relation between the position of the ball and the inductance of the coil. This would complicate the system very much. Therefore only the one dimensional levitation system is examined in this thesis.

The coils can be operated in two different ways. The first is to apply a certain voltage over the coil (voltage control) by a voltage source, the current through the coil is then given by the impedance of the coil, according to:

$$i_L = \frac{1}{|j\omega L + R_L|} \cdot U_L \qquad (3)$$

In formula (3) i_L is the current through the coil, U_L is the voltage over the coil, L is the induction of the coil and R_L is the serie resistance.

The other way to control the coil is to force a certain current through the coil (current control) by a current source. The voltage over the coil is then given by:

$$U_L = |j\omega L + R_L| \cdot i_L \qquad (4)$$

In this chapter the relation between the current through the coil and the position of the ball as well as the relation between the voltage over the coil and the position of the ball are derived. After that, those relations are linearised in an operating point of the process to calculate the linearised transfer function of the one dimensional levitation system.

3.1 DERIVATION OF THE COIL EQUATIONS

In this section the equations of the one dimensional magnetic levitation system are derived. The symbols as in figure 8 will be used.

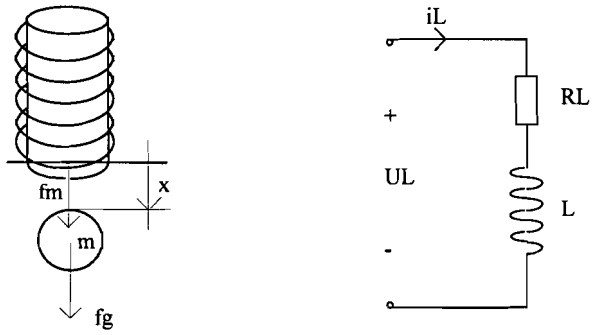

figure 8: One dimensional levitation system

In figure 8 f_m is the magnetic reluctance force exerted by the coil on the ball, f_g is the gravitational force, m is the mass of the ball, x is the distance between the coil and the ball, R_L is the DC-resistance of the coil and L is the inductance of the coil, i_L is the current through the coil and U_L is the voltage over the coil (serial connection of the inductance L and its resistance R_L).

In most literature about magnetic levitation (e.g. [1], [5], [8], [10], [11] and [12]) it is assumed that the number of magnetic flux lines running through the ball does not depend on the distance between the ball and the coil. However, this is **not** true for the physical process used for this report. (See also section 2.3.)
Nevertheless we can easily set up a derivation based on the assumption that the number of flux lines through the ball is independent of the position of the ball. When further assumed that:

- The flux lines through the coil have only two paths: One path from one end of the coil directly to the other. The other path is from one side of the coil, through the ball, to the other side of the coil.
- The permeability of the material of the coil and ball is infinite large, and does not depend on the amount of flux lines through it. (No saturation)
- The material of the coil has no memory effect. (No hysterese)
- The permeability of air is one.

the relation between the coil inductance and the position of the ball can be derived using Hopkins' law. [13] This leads to [10], [11], [12]:

$$L = \frac{\Phi}{i_L} = L_m + L_s = \frac{\mu_0 A N^2}{(X + 2x)} + L_s \qquad (5)$$

In (5) Φ is the magnetic flux, i_L is the current through the coil, L_s is the inductance of the coil which does not depend on the position of the ball ('parasitic inductance'), L_m is the position depended part of the inductance of the coil, X is a constant depending on the geometry, A is a constant depending on the geometry, N is the number of windings on the coil and x is the distance between the ball and the coil.
Formula (5) shows that the inductance should be inversely proportional to the position of the ball. However, when the constants X and A were fitted on measurements of the real process as obtained in chapter 2 with a vertical least mean square fit, it was clear that the model described in (5) was not a good description of the process. (See figure 9.)

Experiments with different models have shown that the relation between the inductance of the coil and the position of the ball is best described by:

$$L = L_s + A \cdot e^{-B \cdot x} \qquad (6)$$

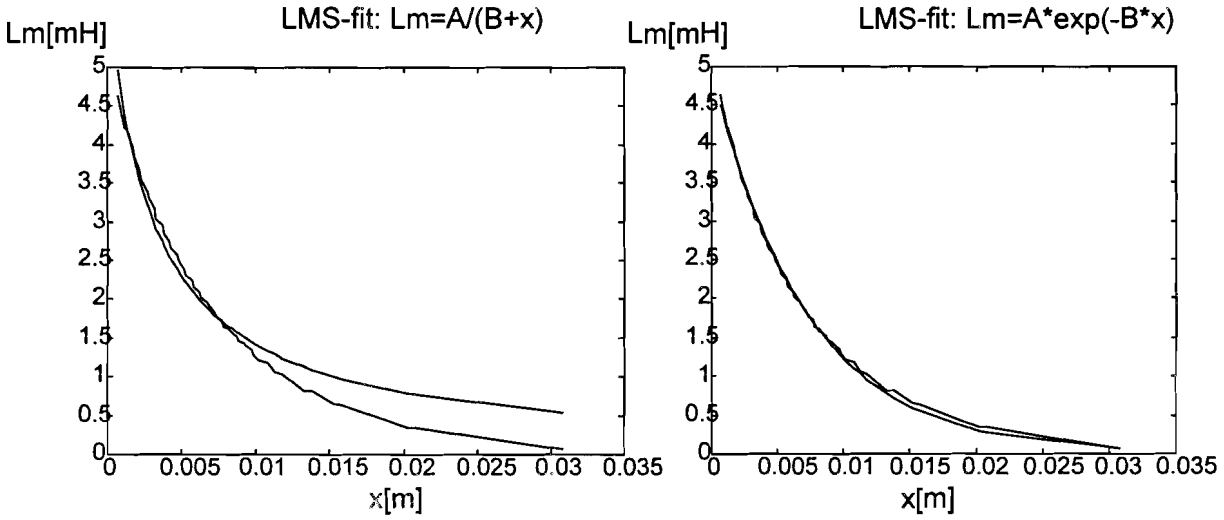

figure 9: Vertical least mean square fits on coil measurements

A physical explanation of the exponential model (6) is that the pattern of the magnetic flux lines of the coil is best depicted in figure 10b rather than in figure 10a. The closer the ball is to the coil, the more flux lines run through the ball. Above experiments show that this relation is approximately exponential for the process under study.

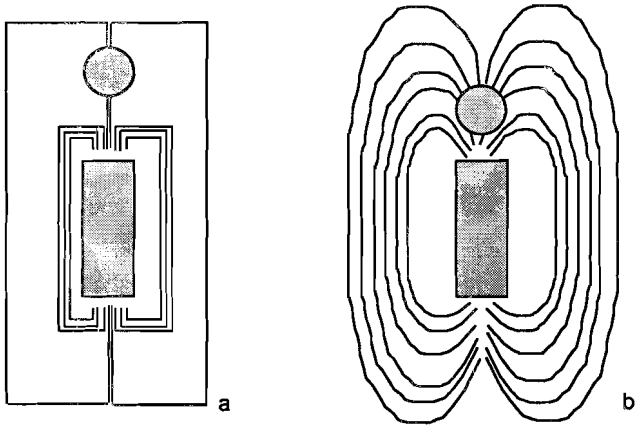

figure 10: Flux lines through coil and ball

The magnetic reluctance force f_m by the coil in the quasi-static situation (that is, when the kinetic energy of the ball is small) can be calculated using the law of energy conservation: When the current through the coil is held constant, any variation in the energy of the magnetic field is due to movement of the ball. This leads to: [13]

$$\left.\begin{aligned} dW_m(\Phi,x) &= i_L \cdot d\Phi \\ dW_m(\Phi,x) &= f_m \cdot dx \end{aligned}\right\} \Rightarrow i_L \cdot d\Phi - f_m \cdot dx = dW_m(\Phi,x) = \frac{\partial W_m}{\partial \Phi} d\Phi + \frac{\partial W_m}{\partial x} dx$$

$$f_m = \frac{-\partial W_m(\Phi,x)}{\partial x} \overset{lin.magn.material}{=} \frac{1}{2} i_L^2 \frac{dL}{dx} = \frac{1}{2} i_L^2 \frac{d}{dx}\left(L_s + A \cdot e^{-B \cdot x}\right) = -\frac{1}{2} AB \cdot e^{-B \cdot x} \cdot i_L^2$$

(7)

where Φ is the magnetic flux W_m is the magnetic field energy and f_m is the magnetic reluctance force.

Remark that the partial derivation $\frac{-\partial W_m(\Phi,x)}{\partial x}$ in (7) means that the magnetic field energy must be differentiated with respect to x when Φ (and so i_L) is held constant. So the magnetic reluctance force is given by $f_m = \frac{1}{2} i_L^2 \frac{dL}{dx}$ and **not** by $f_m \neq \frac{1}{2} \frac{d\left(i_L^2 \cdot L\right)}{dx}$. [13]

The voltage over the coil, given a certain current i_L through the coil is given by:

$$U_L = R_L \cdot i_L + \frac{d\Phi}{dt} = R_L \cdot i_L + \frac{\partial \Phi}{\partial i_L} \cdot \frac{di_L}{dt} + \frac{\partial \Phi}{\partial x} \cdot \frac{dx}{dt} \overset{lin.magn.material}{=}$$

$$U_L = R_L \cdot i_L + L \frac{di_L}{dt} + i_L \frac{dL}{dx} \cdot \frac{dx}{dt}$$

(8)

It is assumed that the ball moves in the vertical direction only, so the dynamic equations of the ball can easily be derived using Newton's second law.

$$m \cdot \frac{d^2x}{dt^2} = f_g + f_m$$

(9)

Combining (7) and (9) gives a relation between the current through the coil i_L and the position of the ball x:

$$\begin{cases} f_m = m\frac{d^2x}{dt^2} - f_g \\ f_m = -\frac{1}{2} i_L^2 ABe^{-Bx} \end{cases} \Rightarrow m\ddot{x} - f_g = -\frac{1}{2} i_L^2 ABe^{-Bx}$$

(10)

When formula (10) is combined with (8), it gives a relation between the voltage over the coil U_L and the position of the ball x.
Obvious, the relations between current and position or voltage and position are not linear. However they can be linearised in an operating point (x_0, $i_{L,0}$) respectively (x_0, $U_{L,0}$) using the Taylor approximation. In this manner the linearised transfer function of the system can be derived. First this is done for current control, after that the transfer function of the voltage controlled system is derived.

3.1.1 CURRENT CONTROL

Formula (10) gives the non linear relation between the current through the coil i_L and the position of the ball x. It is repeated below:

$$m\ddot{x} = f_g - \frac{1}{2} i_L^2 ABe^{-Bx} \tag{11}$$

Formula (11) linearised in an operating point ($i_{L,0}$, x_0) gives:

$$m\Delta\ddot{x} = f_g - \frac{1}{2} i_{L,0}^2 ABe^{-Bx_0} - ABe^{-Bx_0} i_{L,0} \cdot \Delta i_L + \frac{1}{2} i_{L,0}^2 AB^2 e^{-Bx_0} \cdot \Delta x \tag{12}$$

In the equilibrium point holds:

$$f_g - \frac{1}{2} i_{L,0}^2 ABe^{-Bx_0} = 0 \tag{13}$$

This means that the DC current to hold the process in the equilibrium point is:

$$i_{L,0} = \sqrt{\frac{2mg}{ABe^{-Bx_0}}} \tag{14}$$

Substituting (14) in (12) gives:

$$m \cdot \Delta\ddot{x} = -ABe^{-Bx_0} \sqrt{\frac{2mg}{ABe^{-Bx_0}}} \cdot \Delta i_L + \frac{1}{2} \frac{2mg}{ABe^{-Bx_0}} AB^2 e^{-Bx_0} \cdot \Delta x$$

$$m \cdot \Delta\ddot{x} = -\sqrt{2ABmge^{-Bx_0}} \cdot \Delta i_L + mgB \cdot \Delta x \tag{15}$$

So the linearised transfer function in the operating point ($i_{L,0}$, x_0) is:

$$H(s) = \frac{\Delta x}{\Delta i_L} = \frac{-\sqrt{2mgABe^{-Bx_0}}}{ms^2 - mgB} \tag{16}$$

A DC-current $i_{L,0}$ must be added to the output current of the controller to set the system in the equilibrium point (x_0, $i_{L,0}$). This extra DC-current is given in (14).

When (16) is factorised the following relation is obtained:

$$H(s) = \frac{x(s)}{i(s)} = -\sqrt{\frac{2ABge^{-Bx_0}}{m}} \frac{1}{\left(s+\sqrt{gB}\right)\left(s-\sqrt{gB}\right)} \tag{17}$$

One can see that poles of the linearised transfer function are independent of the linearisation point x_0. Only the gain of the linearised transfer function depends on the linearisation point. This is only true when for the relation between the position of the ball and the inductance of the coil an exponential model is used.

One other point of attention is that the gain of the linearised system is **negative.** When designing a controller for the system, one has to be careful to not to generate a positive feedback, instead of a negative.

A pole zero map of the current controlled system will be displayed in chapter 7, when a controller is designed for the system.

3.1.2 VOLTAGE CONTROL

Formula (10) gives the non linear relation between the current through the coil i_L and the position of the ball x; formula (8) between the voltage over the coil U_L, the current through the coil i_L, and the position of the ball x. They are repeated below:

$$\begin{cases} m\ddot{x} = f_g - \frac{1}{2} i_L^2 ABe^{-Bx} \\ U_L = R_L \cdot i_L + L\frac{di_L}{dt} + i_L \frac{dL}{dx} \cdot \frac{dx}{dt} \end{cases} \tag{18}$$

The bottom relation of formula (18) linearised in an operating point ($U_{L,0}$, x_0) gives:

$$U_{L,0} + \Delta U_L = R_L \cdot i_{L,0} + R_L \cdot \Delta i_L + \left(L_s + Ae^{-Bx_0}\right) \cdot \Delta \dot{i}_L - i_{L,0} ABe^{-Bx_0} \cdot \Delta \dot{x} \tag{19}$$

In the equilibrium point holds:

$$U_{L,0} = R_L \cdot i_{L,0} \tag{20}$$

Substituting (14) in (20) gives the DC-voltage over the coil necessary to hold the process in the equilibrium point. The DC-voltage is:

$$U_{L,0} = R_L \cdot i_{L,0}$$
$$U_{L,0} = R_L \cdot \sqrt{\frac{2mg}{ABe^{-Bx_0}}}$$

(21)

Substituting (14) in (19) and using (15) gives:

$$\Delta U_L = R_L \cdot \Delta i_L + \left(L_s + Ae^{-Bx_0}\right) \cdot \Delta \dot{i}_L - i_{L,0} ABe^{-Bx_0} \cdot \Delta \dot{x}$$
$$\Delta U_L = R_L \cdot \frac{mgB \cdot \Delta x - m \cdot \Delta \dot{x}}{\sqrt{2ABmge^{-Bx_0}}} + \left(L_s + Ae^{-Bx_0}\right) \cdot \frac{mgB \cdot \Delta \dot{x} - m \cdot \Delta \ddot{x}}{\sqrt{2ABmge^{-Bx_0}}} - \sqrt{\frac{2mg}{ABe^{-Bx_0}}} ABe^{-Bx_0} \cdot \Delta \dot{x}$$

(22)

So the linearised transfer function in the operating point ($U_{L,0}$, x_0) is:

$$H(s) = \frac{\Delta x}{\Delta U_L} = \frac{\sqrt{2mgABe^{-Bx_0}}}{-\left(L_s + Ae^{-Bx_0}\right)m \cdot s^3 - Rm \cdot s^2 + \left(\left(L_s + Ae^{-Bx_0}\right)mgB - 2mgABe^{-Bx_0}\right) \cdot s + R_L mgB}$$

(23)

A DC-voltage $U_{L,0}$ must be added to the output current of the controller to set the system in the equilibrium point ($U_{L,0}$, x_0). This extra DC-voltage is given in (21).

When (23) is factorised the following relation is obtained:

$$H(s) = \frac{x(s)}{U_L(s)} = \frac{\sqrt{\frac{2ABge^{-Bx_0}}{m}}}{\left(L_s + Ae^{-Bx_0}\right)} \cdot \frac{1}{\left(s + \frac{R}{L_s + Ae^{-Bx_0}}\right)\left(s + \sqrt{gB}\right)\left(s - \sqrt{gB}\right)}$$

(24)

When looking at the linearised transfer function of the voltage controlled system, one observes that the poles of this system are simply those of the current controlled system, with one additional pole of the resistance / inductance serial connection. $\left(s + R/\left(L_s + Ae^{-Bx_0}\right)\right)$
Only the position of this additional pole depends on the linearisation point x_0. The gain of the linearised transfer function also depends on the linearisation point.
One other point of attention is that the gain of the linearised system is **negative.** When designing a controller for the system, one has to be careful to not to generate a positive feedback, instead of a negative.

3.2 CONCLUSIONS

In the previous section the linearised transfer functions of the one dimensional magnetic levitation system were derived for both current controlled coils and voltage controlled coils.

When examining the differences in the two linearised transfer functions, one can see that from the point of view of the controlling of the levitated ball, the current controlled coil is the most attractive, because its transfer function is only of the second order. Further on, the poles of the linearised transfer function of the current controlled system do not depend on the linearisation point. Only the gain of the transfer function depends on the linearisation point.
In the next chapter will become clear that from the point of view of the actuator current control has some disadvantages. (See chapter 4.)

4. ACTUATORS

The magnetic reluctance force f_m exerted on the ball by the coil depends on the current through the coil i_L. So the current through the coil must be supplied by a **controlled** power supply to control the exerted force on the ball.
Because the target of this thesis is self sensing magnetic levitation, the power supply has to meet one other restriction, namely that the inductance of the coil can be measured at the same time. (See next chapter.) In all proposed power supplies this is done by measuring a high frequency component in the current through the coil, or the voltage over the coil. Because actuator and sensor depend on each other, this chapter must be read in combination with the next chapter, which will handle about various ways to measure the inductance of the coil.

As already indicated in the previous chapter, there are two ways the coil can be controlled, viz. current control and voltage control. In the first case a current source forces a current through the coil, in the latter a voltage source applies a voltage over the coil. Both actuators will be examined throughout this chapter.
Also the possibilities of using a switched voltage source are examined. The advantage of a switched power supply is that there is virtually no power dissipation in the power supply. A switched current supply is not examined, but it is in principle the dual case of the switched voltage source.

4.1 LINEAR CURRENT SOURCE

As formula (7) shows, the magnetic reluctance force exerted on the ball by the coil depends directly on the current through the coil. Consequently it is straightforward to use a voltage controlled current source as the power supply for the coil.

4.1.1 PROBLEMS WITH THE CURRENT SOURCE

As already indicated above, the inductance of the coil must be measured to obtain a measurement for the position of the ball. This can be done by adding an extra high frequency current on top of the actuating current through the coil. The voltage over the coil, at that high frequency is a measurement for the inductance of the coil. The frequency of this extra component must be much higher than the highest frequency of the mechanical system. To add an additional 1 kHz component would be a good choice.
Note that this additional high frequency current has not necessarily to be supplied by the same current source which supplies the low frequency actuating current. However, when the high frequency current is supplied by an extra (low power) current source, the actuating current source must have a high output impedance at that high frequency. So the bandwidth of the actuating current source must be high, which leads to the same design criteria as when the current source must supply the high frequent current itself.

A voltage controlled current source can be realised as in figure 11. The resistor R is for sensing the current through the coil. The power MOSFET is controlled by the controller. In

most cases the controller is nothing more than a proportional controller with a very large gain (e.g. an opamp). But in this application, the controller must be designed, using sophisticated design tools, to avoid oscillation and excessive noise.

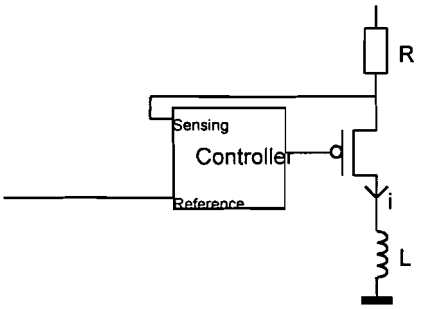

figure 11: Voltage Controlled Current Source

Oscillation of the current source loaded with a coil comes from the fact that a coil opposes against variations in the current i_L through it. For this reason the coil can be interpreted as a current source (for small signals, for a short period of time). This gives the equivalent circuit as in figure 12.

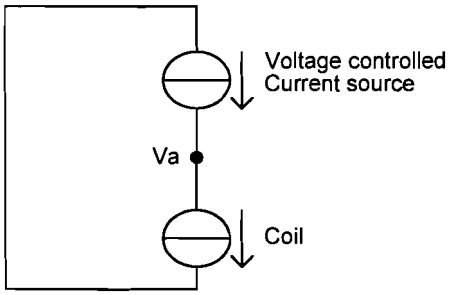

figure 12: Equivalent circuit of a current source loaded with a coil

The voltage at node V_a in figure 12 is not defined because of the serial connection of the two current sources. (In practice the coil is not an ideal current source, so the voltage over the coil is defined, of course.) However, an additional high frequent (noise) voltage at node V_a, does not lead to a high frequent current through the coil, because of the high impedance of the inductance at that frequency. The voltage controlled current source senses only the current through the coil, so a high frequent voltage at node V_a is not observed. Because of this, a high frequency voltage oscillation over the coil is poorly damped. This will lead to noise problems when a high frequent voltage over the coil is measured for sensing the inductance of the coil.

4.1.2 H∞ CONTROLLER DESIGN, CURRENT SENSING

The controller of figure 11 is designed using the H_∞ toolbox MHC in Matlab [15]. The augmented plant is depicted in figure 13 and the generalised plant in figure 14.

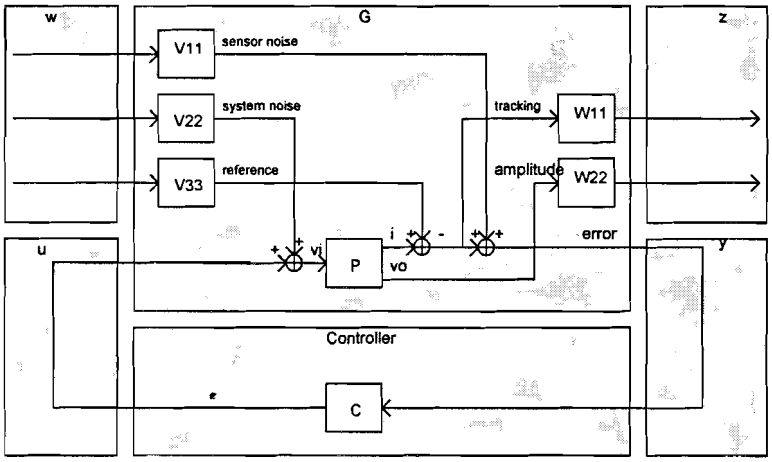

figure 13: Augmented plant

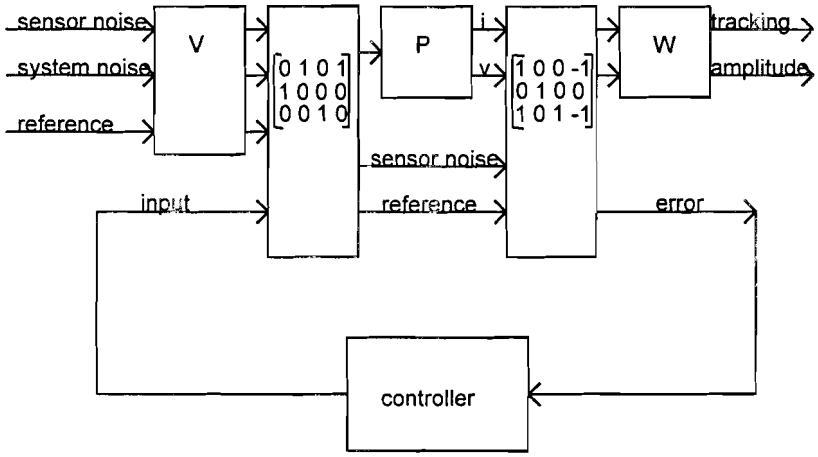

figure 14: Generalised plant for MHC-Toolbox

In figure 13 the plant P is the MOSFET, the coil L and the resistor R of figure 11. The input of the plant is the voltage at the gate of the MOSFET v_i, the two outputs of the plant are the output current i_L and output voltage of the current source v_o (when loaded with the coil). Although the current through the MOSFET is given by a non linear relation with the gate-source voltage, the plant is assumed to have a linear transfer function. (Any non linearity of the process is eliminated by the enormous gain of the controller. See further on)
As resistor R is assumed to be 1Ω, the transfer function P_{11} is 1 [A/V], which means that 1V at the gate of the MOSFET gives 1A through the coil. Transfer function P_{12} is given by the inductance of the coil and its serie resistance. (4) An extra pole at an unimportant high frequency is added to the zero, to make transfer function P_{12} bi-proper. This gives:

$$P_{12} = \frac{110s + 3.5}{0.0159s + 1}$$

The plant has three exogenous inputs. The first is the sensor noise, with its shaping filter V_{11}. It is assumed that the signal to noise ratio of the current sensor (and its additional electronics) is 40dB at all frequencies. This means that $V_{11} = -40dB = 0.01$
The second exogenous input of the plant is system noise, with its shaping filter V_{22}. System noise is for modelling the noise of the electronics of the controller. The signal to noise ratio of

the electronics of the controller is assumed to be 40dB at all frequencies. This means that $V_{22} = -40dB = 0.01$

The third exogenous input of the plant is the reference signal, with its shaping filter V_{33}. The reference signal is shaped by V_{33} in such way, that the current source is able to supply the demanded current, at all frequencies. (This means that the output voltage of the current source does not exceed the supply voltage of the current source V_{dd}, which is 30V). An additional zero is added to make V_{33} bi-proper. This gives for V_{33}: $V_{33} = \frac{0.055s + 3.5}{110s + 3.5}$

Note that weighting filter V_{33} as state above does **not** guarantee that the input signal of the current source is small enough to avoid saturation of the current source. It only gives an rough estimation of the input signals of the current source for designing the H_∞ controller for the current source.

Further on it is assumed that: $\|w_1\|_2, \|w_2\|_2, \|w_3\|_2 < 1$

The generalised plant has two exogenous outputs. First of all the tracking error, with its shaping filter W_{11}. This filter is designed in such way that tracking errors for small frequencies and tracking errors at the position measurement frequency are weighted heavily. This gives for W_{11}: $W_{11} = \frac{18.7s^3 + 1229s^2 + 3445s + 2469}{s^3 + 13.88s^2 + 47.32s + 24.76}$. In this way the weighting upon tracking errors in the interesting frequency bands is 40dB (This gives a tracking error of 10..30mA) It is not possible to increase weighting on tracking errors, because the sensor noise is only -40dB. Again the weighting filter is made bi-proper by adding an additional zero at an unimportant (high) frequency.

The other exogenous output is the output voltage of the current source with its shaping filter W_{22}. The maximum output voltage of the current source is bounded by its supply voltage V_{dd}, which is 30V. This means that $W_{22} = 0.0333$

Note that (as with all other signals which are bounded to certain value in the time domain) weighting filter W_{22} gives **no** guarantee that the output voltage of the current source never exceeds 30V.

Finally it is assumed that: $\|z_1\|_2, \|z_2\|_2 < 1$

Note that all transfer functions are bi-proper, which means that the order of the numerator polynomial is equal to the order of the denumerator polynomial. This is necessary when calculating an H_∞ controller because else the weighting on very high frequencies would be zero or infinite (depending on the transfer function). This would give incorrect answers. For this reason extra poles or zeros are added (at very high, unimportant frequencies) to each transfer function to make them proper. The transfer function of the process P_{12} is proper too, which means that an additional high pass filter must be added parallel to the coil so that the simulations agree with practice. (See section 4.1.4.)

Note that all frequencies are expressed in krad rather then in rad, to avoid numerical problems when calculating the H_∞ controller

The transfer functions of the plant and the weighting filters are repeated below:

$$P_{11} = 1$$
$$P_{12} = \frac{110s + 3.5}{0.0159s + 1}$$

$$V_{11} = 0.01$$
$$V_{22} = 0.01$$
$$V_{33} = \frac{0.055s + 3.5}{110s + 3.5}$$
$$W_{11} = \frac{18.7s^3 + 1229s^2 + 3445s + 2469}{s^3 + 13.88s^2 + 47.32s + 24.76}$$
$$W_{22} = 0.0333$$

(25)

The transfer functions of the plant and the weighting filters are plotted in figure 15.

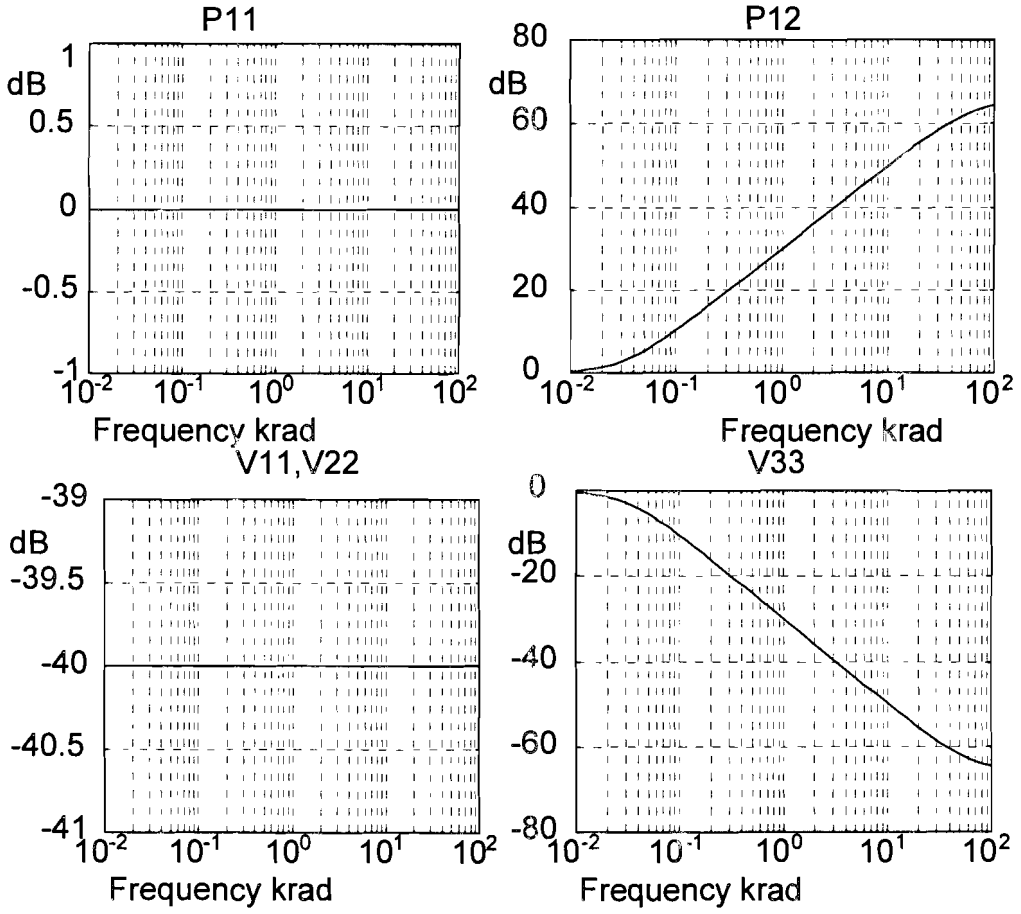

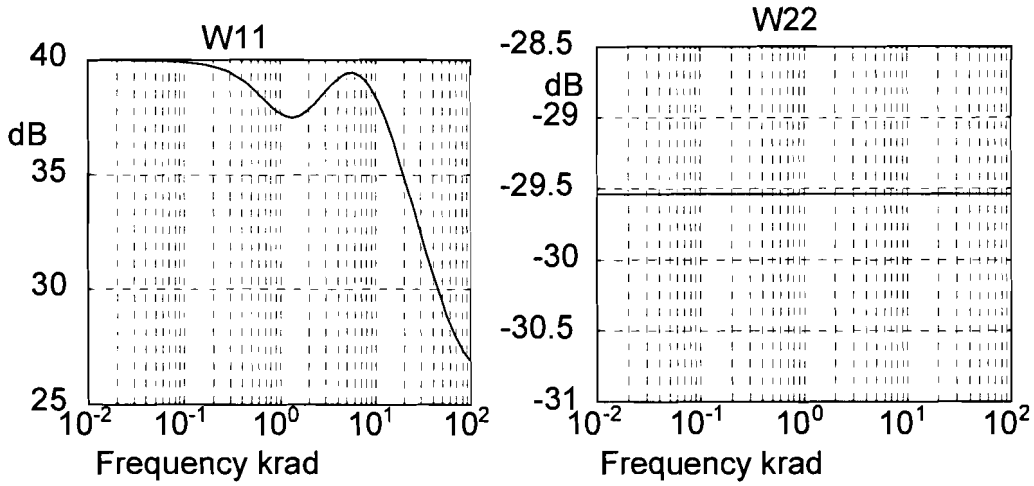

figure 15: Weighting filters for MHC-Toolbox

When a controller is designed using the weighting filters as in (25) the H_∞ toolbox for Matlab MHC gives the results as in figure 16. The solid line is the transfer function from a certain input of the augmented plant to a certain output. The dashed line is the boundary of guaranteed stability (when γ is equal to 1). The optimum γ was found to be 0.998, which is close to 1, as it should be.

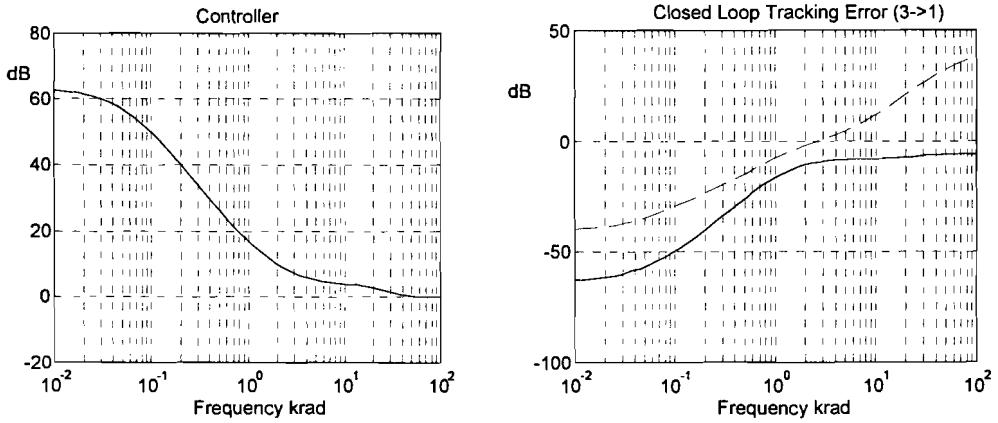

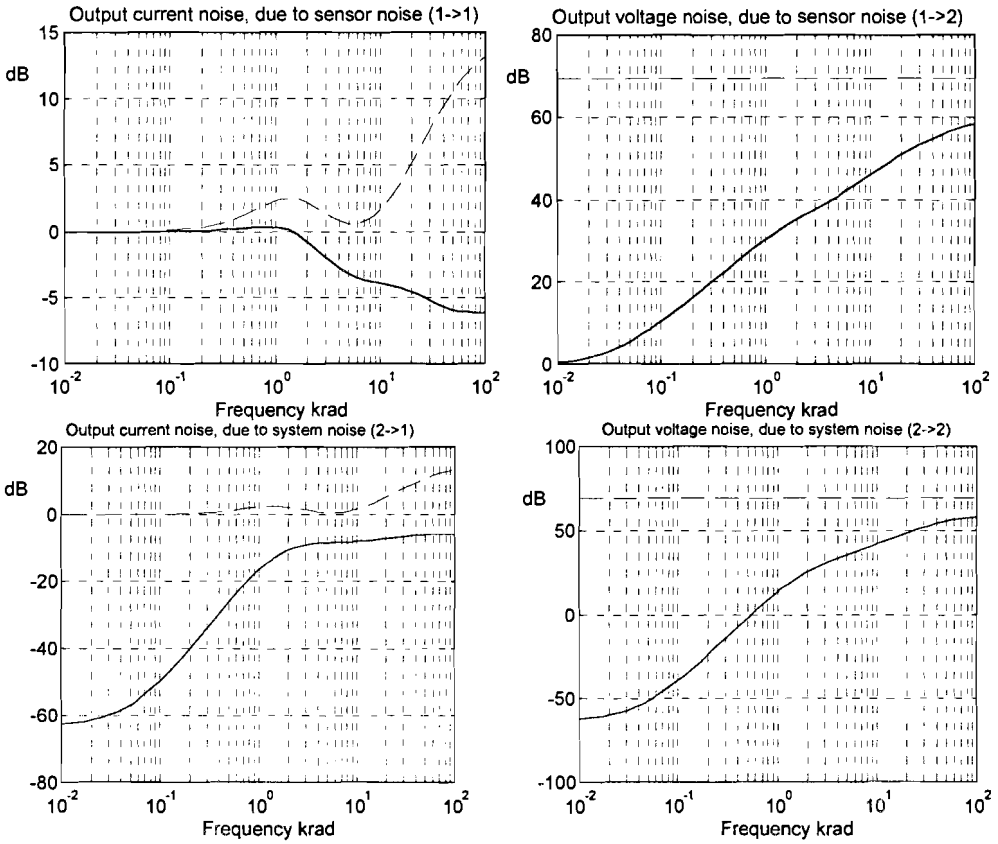

figure 16: Controller designed by MHC-Toolbox

The upper left plot in figure 16 shows that the designed controller has a second order low pass characteristic in the concerned frequency band. The -6dB point is 80 at rad/sec. The controller has a second break point around 3 krad/sec, so frequencies higher than 500Hz have a gain of approximately one.
The upper right part of figure 16 shows the tracking error of the output current with an applied input voltage. The tracking error for low frequencies is smaller than -50 dB (<0.3%) However, around the inductance measurement frequency of 6 krad/sec the tracking error is as much as -10dB, which means that the output impedance of the current source is not very high at that frequency. This has its consequences for the sensor as will be made clear in the next chapter.
The plot on the bottom left part of figure 16 shows that the output **current** noise damping for system noise is for low frequencies higher than 60 dB (>1000x)
The plot on the bottom right part shows that the output **voltage** noise amplification (!) for system noise at the inductance measurement frequency of 1 KHz is about 40 dB (≈100x) This means that when the system noise amplitude is assumed to be 1 [mV], the noise in the coil voltage at 1 kHz is 0.1 [V] (!)

The controller design by MHC is of fifth order, but can be approximated by a second order transfer function. (26)

$$C(s) = \frac{(s+3000)(s+3000)}{(s+80)(s+80)}$$

(26)

Although the controller designed in this section is able to stabilise the current source when it is loaded with a coil (in contrary to a simple proportional controller), it will inevitably cause noise problems with position sensor. As already indicated, the output voltage noise amplification is approximately 40dB. So another H_∞ controller is designed in the next section, which suffers less from output voltage noise.

4.1.3 H∞ CONTROLLER DESIGN, CURRENT AND VOLTAGE SENSING

As already indicated in the section 4.1.2, the output voltage of the current source is not observed. Because of this, an H_∞ controller must be designed to avoid oscillation and excessive noise. However, the controller as designed in the previous section still suffers from a system noise **amplification** of 40dB at the inductance measuring frequency, which is not tolerable.
Therefore in this section a current source is designed, which senses not only the current through the coil, but also the voltage over the coil. Minor drawback is that this leads to some additional electronics. The controller for the current source, as depicted in figure 17, is designed using the H_∞ toolbox MHC in Matlab [15].

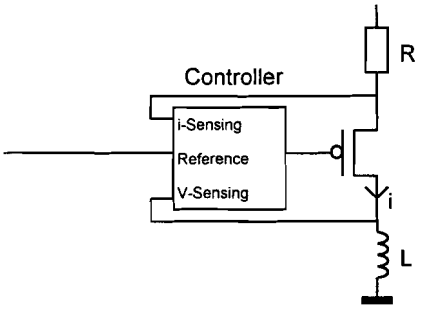

figure 17: Voltage Controlled Current Source with voltage sensing

The augmented plant is depicted in figure 18 and the generalised plant in figure 19.

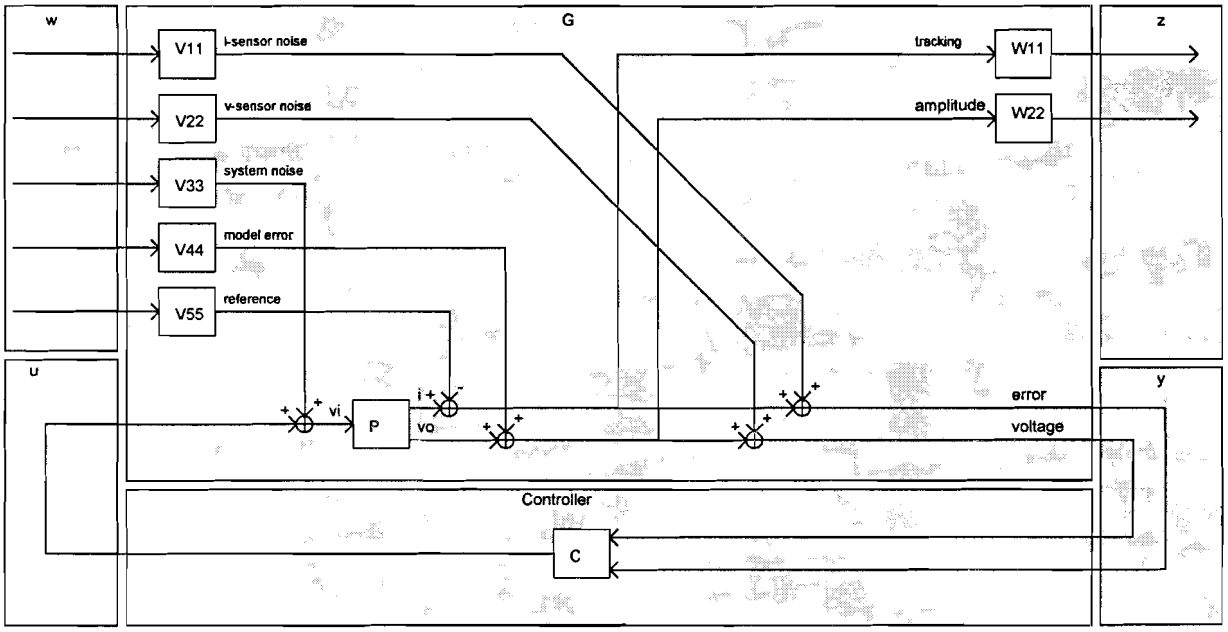

figure 18: Augmented plant VCCS with voltage sensing

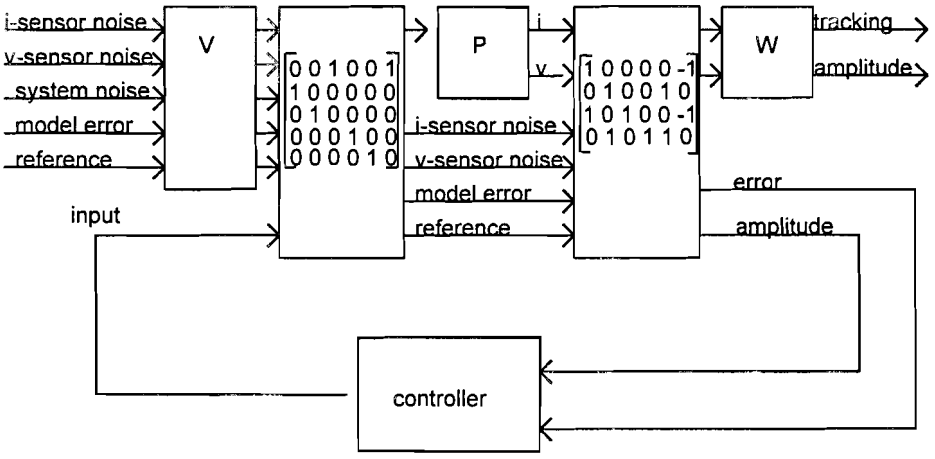

figure 19: Generalised plant for MHC-Toolbox VCCS with voltage sensing

In figure 18 the plant P is the MOSFET, the coil L and the resistor R of figure 17. The input of the plant is the voltage at the gate of the MOSFET v_i, the two outputs of the plant are the output current and output voltage of the current source v_o (when loaded with the coil). As in the previous section, the plant is assumed to have a linear transfer function. The resistor is again assumed to be 1Ω. The transfer function P_{11} is then given by: P_{11}=1 [A/V]
Transfer function P12 is given by the inductance of the coil and its serial resistance. An extra pole is added to the zero to make P12 bi-proper. This gives: $P_{12} = \dfrac{110s + 3.5}{0.0159s + 1}$

The plant has five exogenous inputs. The first two are the current sensor noise and the voltage sensor noise, with their shaping filter V_{11} and V_{22} respectively. The signal to noise ratio of the sensors (with their additional electronics) is assumed to be at least 40 dB for all frequencies. This means that $V_{11} = -40dB = 0.01, V_{22} = -40dB = 0.01$

The third exogenous input of the plant is system noise, with its shaping filter V_{33}. System noise is for modelling the noise of the electronics of the controller. This signal to noise ratio is assumed to be al least 40dB at all frequencies. This means that $V_{33} = -40dB = 0.01$
The fourth exogenous input of the plant is the coil-model error, with its shaping filter V_{44}. The variation of the inductance of the coil because of the movement of the ball is modelled by V_{44}. Its value will be calculated below:
Formula (2) shows that the minimum, maximum and nominal coil inductances are:

$$\begin{aligned} L_{\min} &= 102.89[mH] \\ L_{nom} &= 105.11[mH] \\ L_{\max} &= 107.83[mH] \end{aligned}$$

(27)

This gives a maximum coil voltage variation due to the inductance variation of the coil of:

$$\left.\begin{aligned} \frac{L_{nom}}{L_{\min}} &= 1.0216 \\ \frac{L_{\max}}{L_{nom}} &= 1.0259 \end{aligned}\right\} \Delta L_{\max} = 2.59\%$$

(28)

When assumed that the high frequent inductance measurement signal has an (voltage) amplitude of 10% of the maximum output voltage of the current source V_{dd} (which is assumed to be 30V), the maximum variation of the coil voltage due to variation in the inductance of the coil is:

$$0.0259 \cdot 0.10 \cdot V_{dd} = 0.077[V]$$

(29)

Thus V_{44} is 0.077

The last exogenous input of the plant P is the reference signal, with its shaping filter V_{55}. The reference signal is shaped by V_{55} in such way, that the current source is able to supply the demanded current, at all frequencies. An additional zero is added to make V_{55} bi-proper, This gives $V_{55} = \dfrac{0.055s + 3.5s}{110s + 3.5}$
Note that weighting filter V_{55} as stated above does not guarantee that the input signal of the current source is small enough to avoid saturation of the current source. It only gives a rough estimation of the input signals of the current source for designing the H_∞ controller for the current source.
Further on it is assumed that: $\|w_1\|_2, \|w_2\|_2, \|w_3\|_2, \|w_4\|_2, \|w_5\|_2 < 1$

The generalised plant has two exogenous outputs. The first is the tracking error, with its shaping filter W_{11}. Filter W_{11} is chosen in such a way that tracking errors for low frequencies and tracking errors at the induction measurement frequency are weighted heavily. This gives: $W_{11} = \dfrac{18.7s^3 + 1229s^2 + 3445s + 2469}{s^3 + 13.88s^2 + 47.32s + 24.76}$. In this way the weighting upon tracking errors in the

interesting frequency bands is 40dB (this gives a tracking error of 10..30mA) Again W_{11} is made bi-proper by adding an additional zero at an unimportant high frequency.
The other exogenous output of the plant P is the output voltage of the current source with its shaping filter W_{22}. As the maximum output voltage of the current source is bounded by its supply voltage, which is assumed to be 30V, this gives: W_{22}=0.0333
Note that (as with all other signals which are bounded to certain value in the time domain) weighting filter W_{22} gives **no** guarantee that the output voltage of the current source never exceeds 30V.
Finally it is assumed that: $\|z_1\|_2, \|z_2\|_2 < 1$

Note that all frequencies are expressed in krad rather then in rad to avoid numerical problems when calculating the H_∞ controller

The transfer functions of the plant and the weighting filters are repeated below:

$$P_{11} = 1$$
$$P_{12} = \frac{110s + 3.5}{0.0159s + 1}$$

$$V_{11} = 0.01$$
$$V_{22} = 0.01$$
$$V_{33} = 0.01$$
$$V_{44} = 0.077$$
$$V_{55} = \frac{0.055s + 3.5}{110s + 3.5}$$
$$W_{11} = \frac{18.7s^3 + 1229s^2 + 3445s + 2469}{s^3 + 13.88s^2 + 47.32s + 24.76}$$
$$W_{22} = 0.0333$$

(30)

The transfer functions of the plant and the weighting filters are plotted in figure 20.

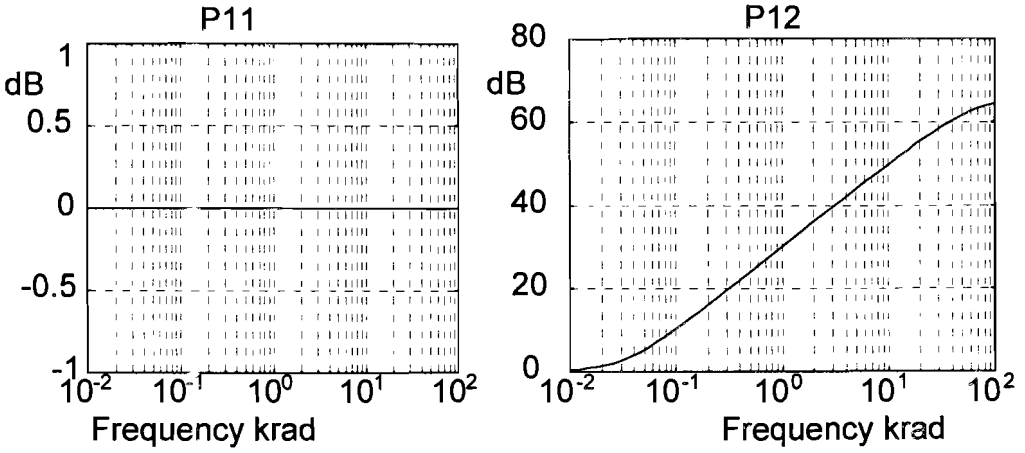

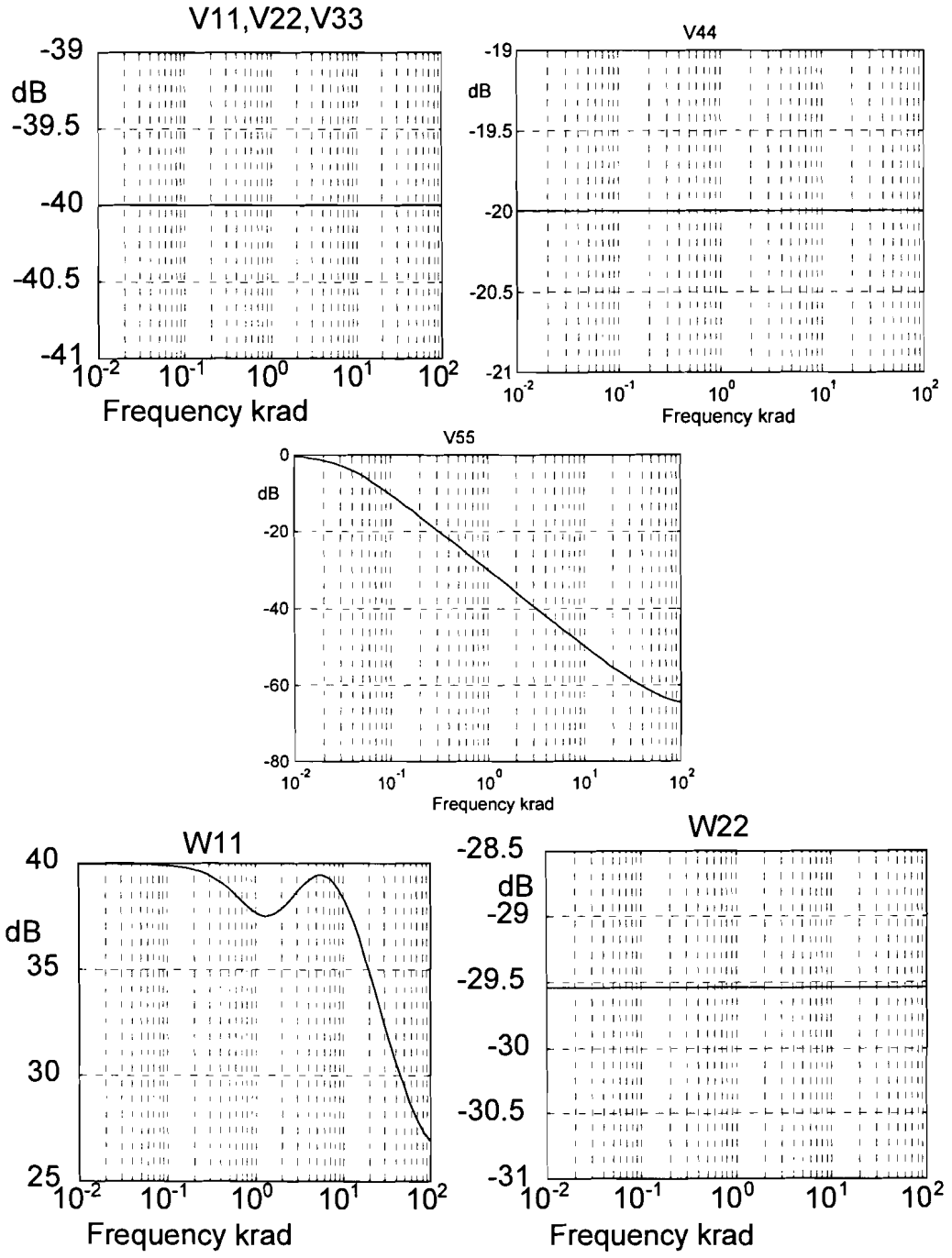

figure 20: Weighting filters for MHC-Toolbox, VCCS with voltage sensing

When a controller is designed using the weighting filters as in (30) MHC gives the results as in figure 21. The solid line is the transfer function from a certain input of the augmented plant to a certain output. When γ is equal to one, the dashed line is the boundary of guaranteed stability. The optimum γ was found to be 1.008, which is close to 1, as it should be.

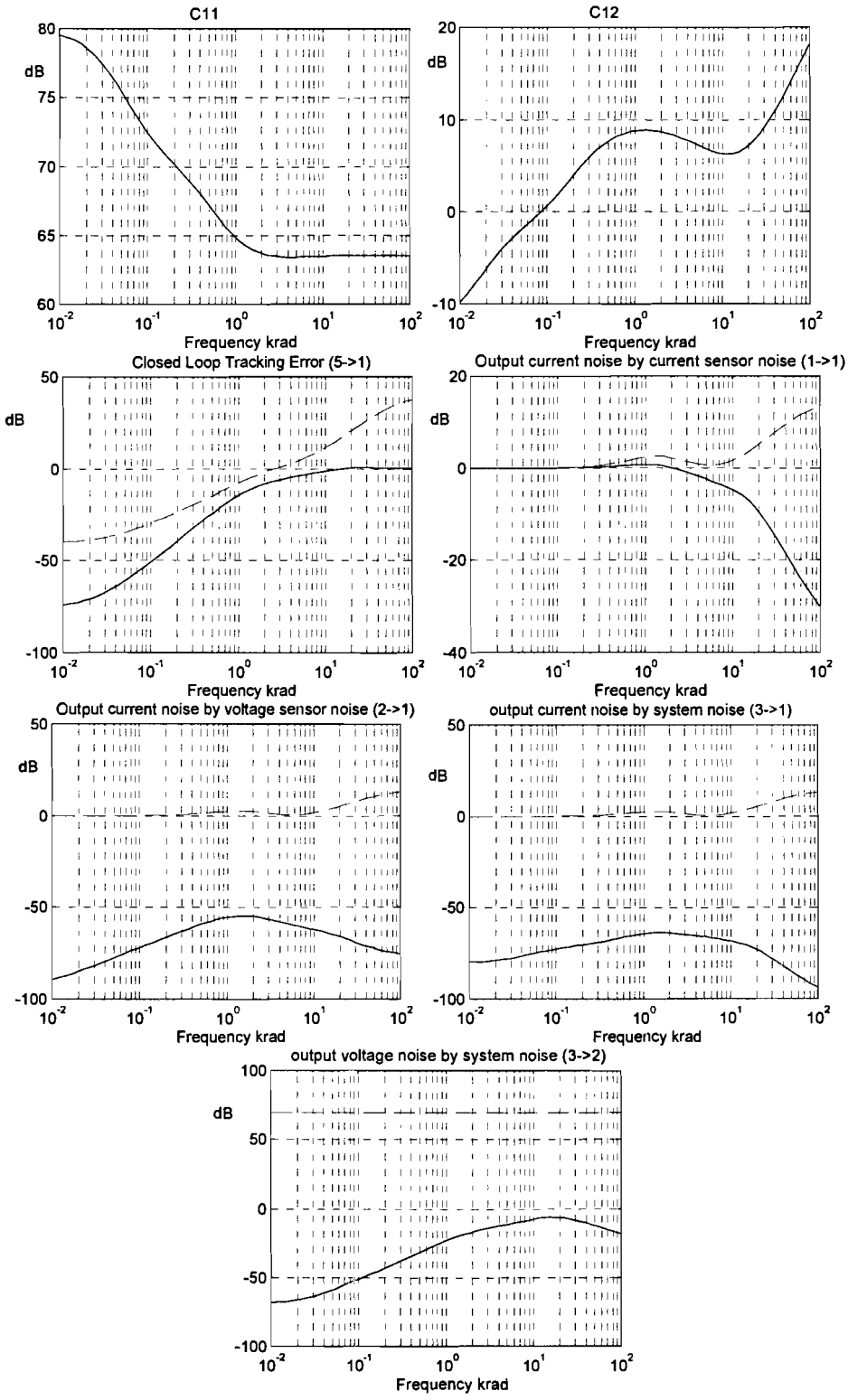

figure 21: Controller designed by MHC-Toolbox, VCCS with voltage sensing

The upper two plots in figure 21 show the transfer functions of the designed controller. One can see that the voltage sensing plays an important role for high frequencies only, and that for low frequencies current sensing is important.
Most important plot is in the bottom of figure 21. In contrary to the current source described in the previous section, the current source in this section **damps** voltage noise at its output by system noise for **all** frequencies (!!!)

The plots of the transfer functions of the sensor noises to the tracking error show that voltage sensor noise as well as current sensor noise is damped for all frequencies.
The closed loop tracking error is also plotted in figure 21. One can see that the tracking error for low frequencies is -70dB.($3e^{-4}$) However, the tracking error around the measuring frequency of 6 Krad/sec is around 0 dB, which means that MHC gives **no** guarantee that the inductance measurement signal can be provided by this current source. However, in the plots of figure 21 both magnitude and phase are negotiated. The phase of the high frequent inductance measurement signal is not important (Although it should be constant, see chapter 5.) So it is possible that the H_∞ controller designed in this section can provide the inductance measurement signal. This will be examined in the next section.

The controller design by MHC is of fifth order, but can be approximated by one first and one third order controller. (31)

$$C_{11}(s) = \frac{500 \cdot (s+200)}{(s+35)}$$

$$C_{12}(s) = \frac{(s+1)(s+10000)(s+10000)}{1000000 \cdot (s+1000)(s+1000)} \qquad (31)$$

Note that the voltage sensing current source as described in this section can only be used when no additional sources are connected to the coil. In other words the voltage sensing current source must be the one and only current source connected to the coil. This means that, in contrary to what is described in section 4.1.1, a high frequent current for inductance measurement must be supplied by this voltage sensing current source, and that the inductance measurement schemes involving an oscillator cannot be used in combination with this current source. (See next chapter)

4.1.4 Simulations of the Designed Current Sources

The reduced controllers as designed in the previous sections (26) and (31) are simulated using PSpice 5.1 for Windows. For comparison, a voltage controlled current source with a simple P-controller is simulated too. In the simulations the current sources are loaded with a coil.
For the simulations the circuits as in figure 22, figure 23 and figure 24 are used. The input signal for the current source used in the simulations is a sine wave. The frequency, phase, amplitude and offset voltage of the input signal are unimportant, only the tracking error of the output current on the input voltage is examined.

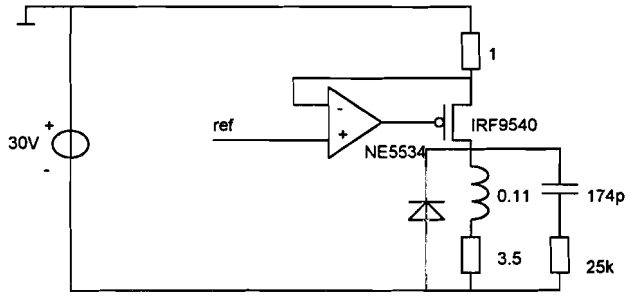

figure 22: Circuit of VCCS with P-controller

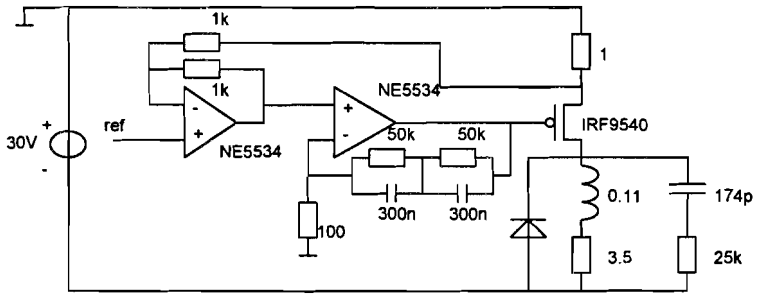

figure 23: Circuit of VCCS with H_∞ controller, current sensing only

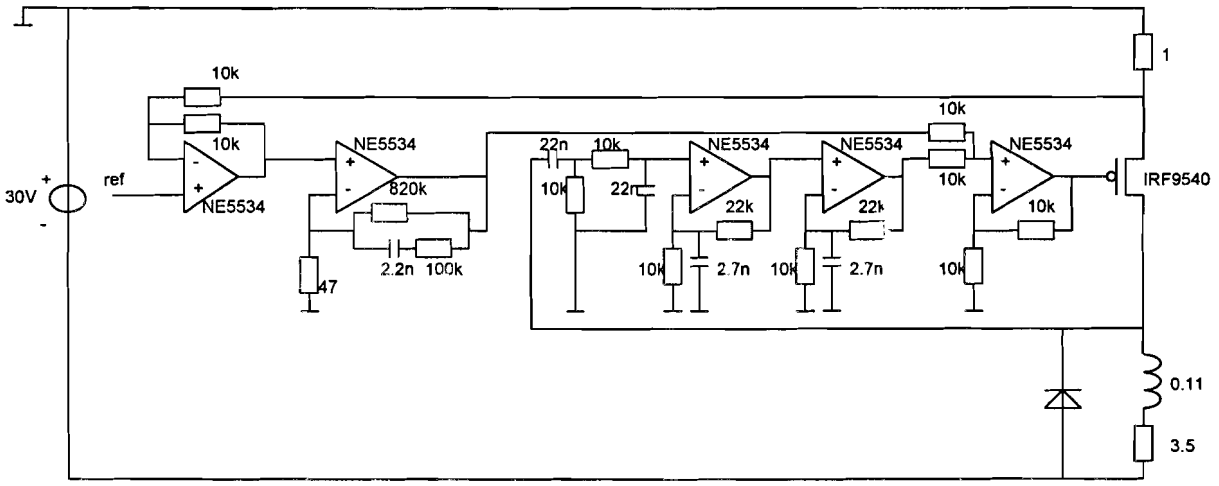

figure 24: Circuit of VCCS with H_∞ controller, current and voltage sensing

In figure 22, figure 23 and figure 24 a diode is connected anti parallel to the coil. This diode serves two goals. The first is that when a diode is connected the voltage at the drain of the MOSFET can never exceed the negative supply voltage. When this would possible, the MOSFET could be damaged.
The second reason for the extra diode, is to avoid limit cycles. At power-on, fast non linear transients flow trough the coil, because the controller is not yet operating. When the diode is connected to the coil, limit cycles by these transients are avoided.

P-controller

In figure 25 the output voltage of a VCCS with a P-controller is plotted. Obviously a P-controller is not able to stabilise a current source loaded with a coil. A high pass filter (as in figure 22) is connected parallelly to the coil. Even with this additional filtering the P-controller is unable to stabilise the process.

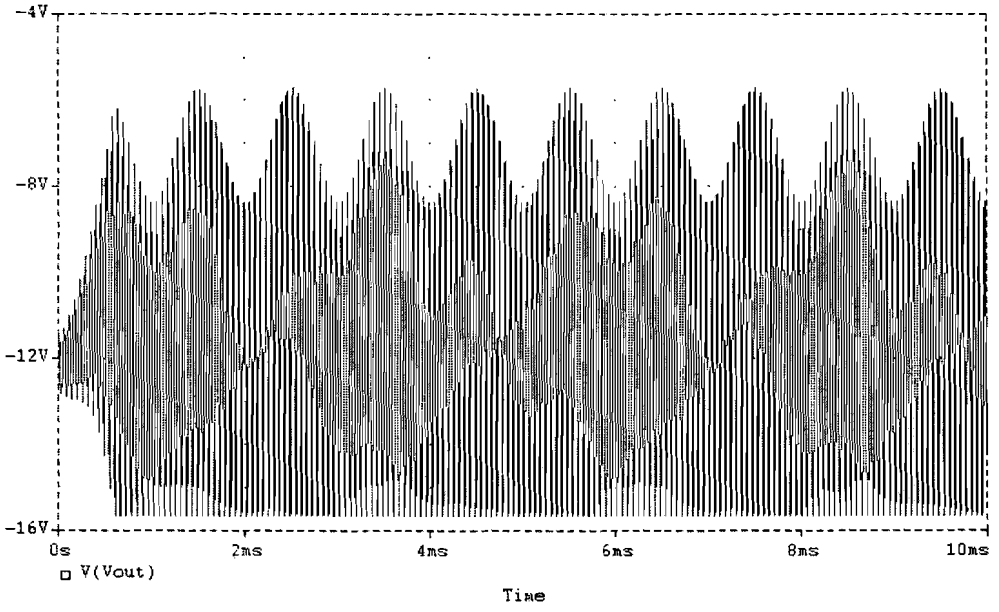

figure 25: Output voltage VCCS with P-controller

H_∞ controller, current sensing only

In figure 26 the output voltage of a voltage controlled current source with the H_∞-controller of section 4.1.2. is plotted. An additional high pass filter (as in figure 23) is connected parallelly to the coil. The controller is not able to stabilise the process without this filter. The oscillation at the beginning of the simulation is cause by power-on transients and are damped by the high pass filter.
The influence of this high pass filter on the inductance measurement will be examined in the next chapter.

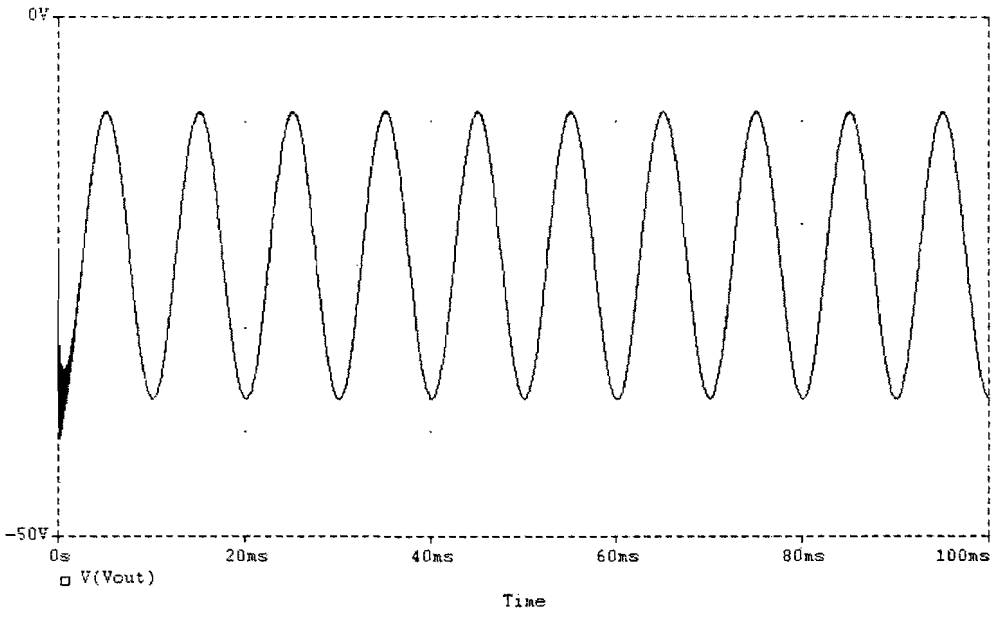

figure 26: Output voltage VCCS with H_∞ controller, current sensing only

In figure 27 the tracking of the VCCS with the H_∞ controller is plotted. One can see that the tracking (amplitude) is very good for frequencies up to 1KHz (the measuring frequency)
In figure 28 the phase of the output current is plotted. For frequencies up to 100 Hz the phase shift is very small. This means that no delay is introduced in the levitation system by the actuator. At the high frequent inductance measurement frequency, the phase error is approximately 10 degrees. Depending on what inductance sensor is used, this can have two effects. First of all, the output impedance of the current source is not very high, so the oscillation of an LC-oscillator (see section 5.1, section 5.2, section 5.3) is damped, and its frequency is influenced. When using an additional high frequency component and an AM-demodulator (see section 5.4) the phase of the synchronous carrier must be phase shifted too, to ensure 90° phase shift between carrier and detection signal.

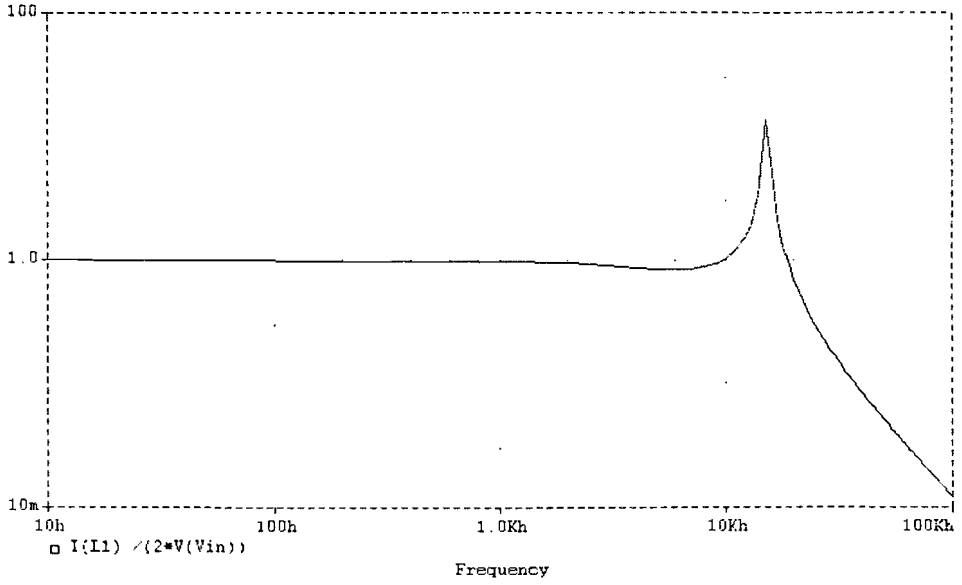

figure 27: Tracking VCCS with H_∞ controller, current sensing only

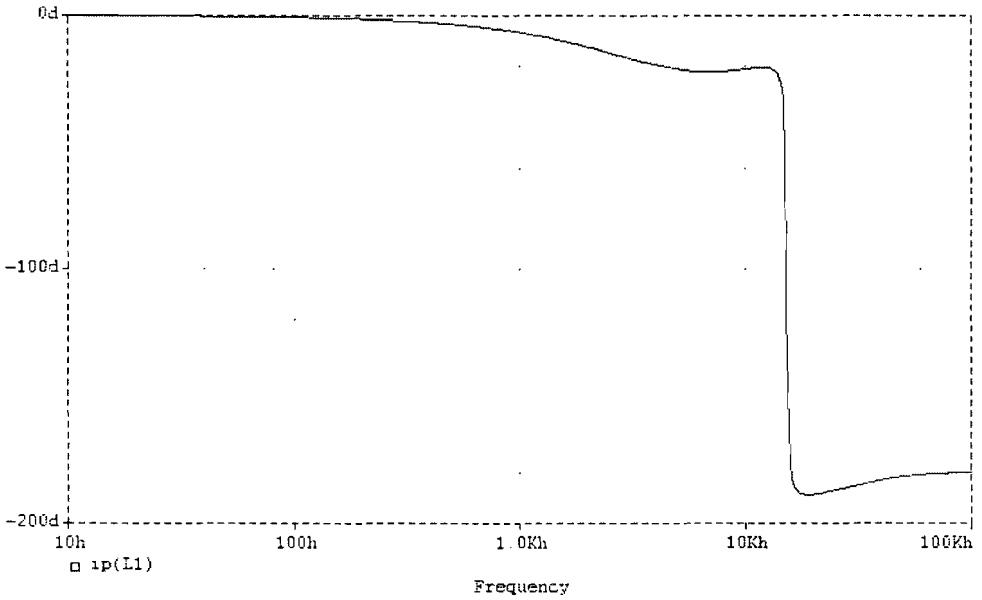

figure 28: Phase shift of output current H_∞ controller, current sensing only

In figure 29 the sensor noise attenuation to the output current is plotted. For frequencies up to the inductance measurement frequency (the frequency band of interest) the transfer function from sensor noise to output current is a unity gain function. At the resonance frequency of the high pass filter with the coil, sensor noise is amplified by 20dB. (But this noise can easily be filtered at the input of inductance sensor)
In figure 30 the system-noise amplification of the H_∞ controlled current source is plotted. As already described in section 4.1.2, the system noise amplification at the measuring frequency of 1kHz is 100x (!!!) This is too much.

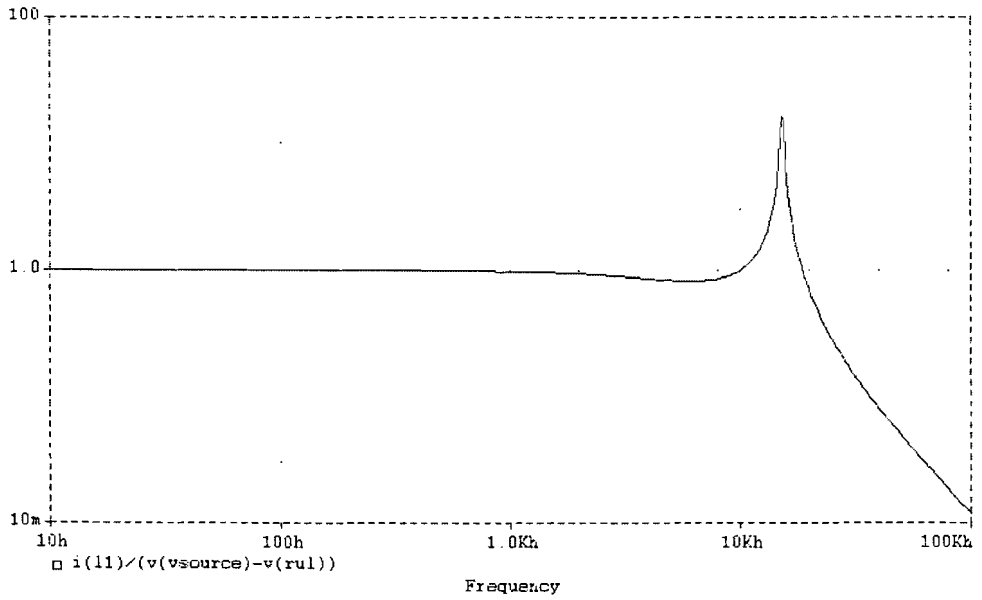

figure 29: Sensor noise to output current of H_∞ controller, current sensing only

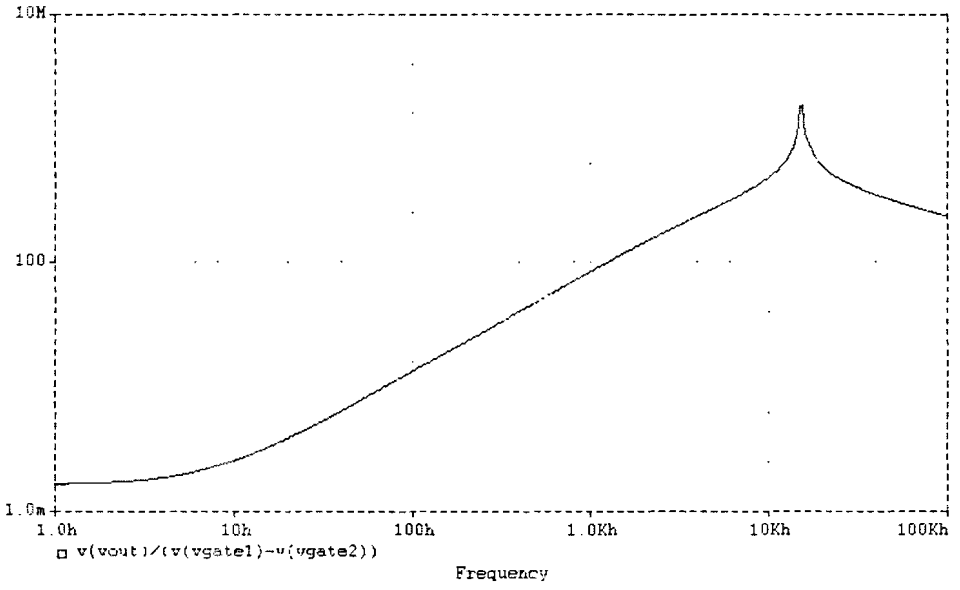

figure 30: System noise to output voltage of H_∞ controller, current sensing only

H_∞ controller, current and voltage sensing

In figure 31 the output voltage of a voltage controlled current source with the H_∞-controller of section 4.1.3. is plotted. No additional high pass filter is connected parallelly to the coil. The controller is able to stabilise the process without this filter.(!!!)

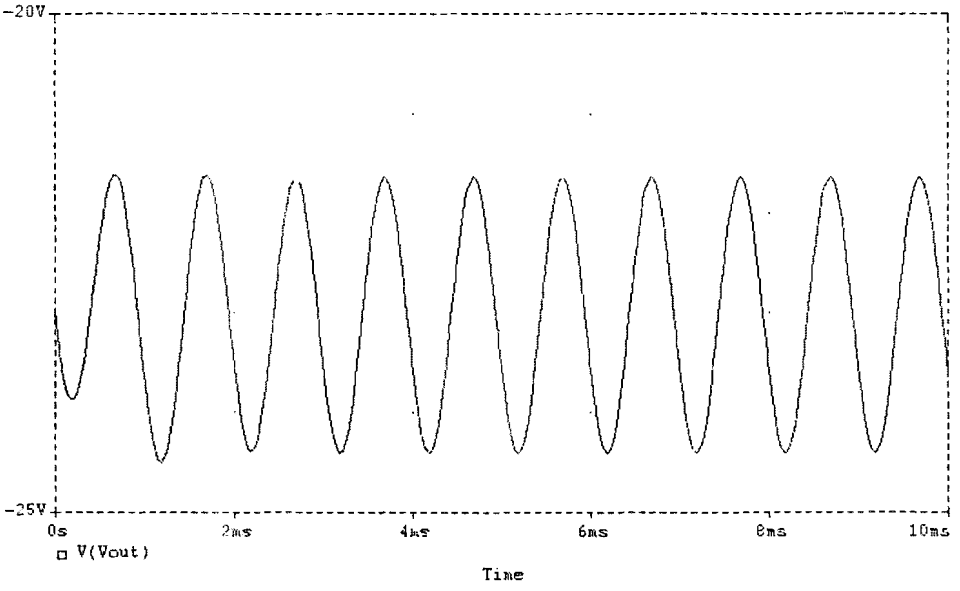

figure 31: Output voltage of VCCS with H_∞ controller, current and voltage sensing

In figure 32 the tracking of the VCCS with the H_∞ is plotted. One can see that the tracking is very good for frequencies up to 100Hz and at the measuring frequency of 1kHz
In figure 33 the phase of the output current is plotted. For frequencies up to 300 Hz the phase shift is very small. This means that no delay is introduced in the levitation system by the

actuator. At the high frequent inductance measurement frequency, the phase error is approximately 65° degrees. In combination with this current source only the additional high frequency component sensor can be used to measure the inductance of the coil (see section 5.4). The phase of the synchronous carrier must not need to be shifted 90°, but only 25° to ensure 90° phase shift between carrier and detection signal.

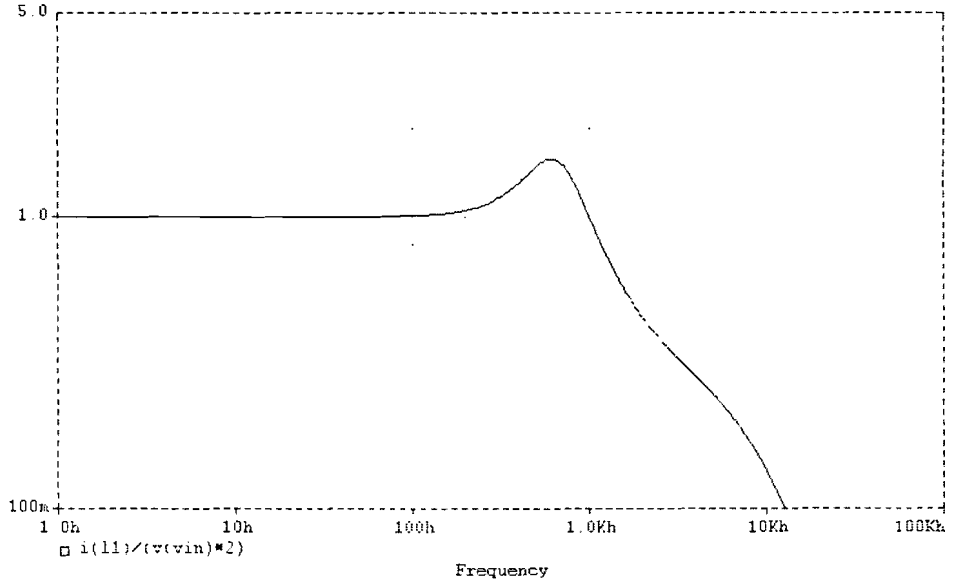

figure 32: Tracking VCCS with H_∞ controller, current and voltage sensing

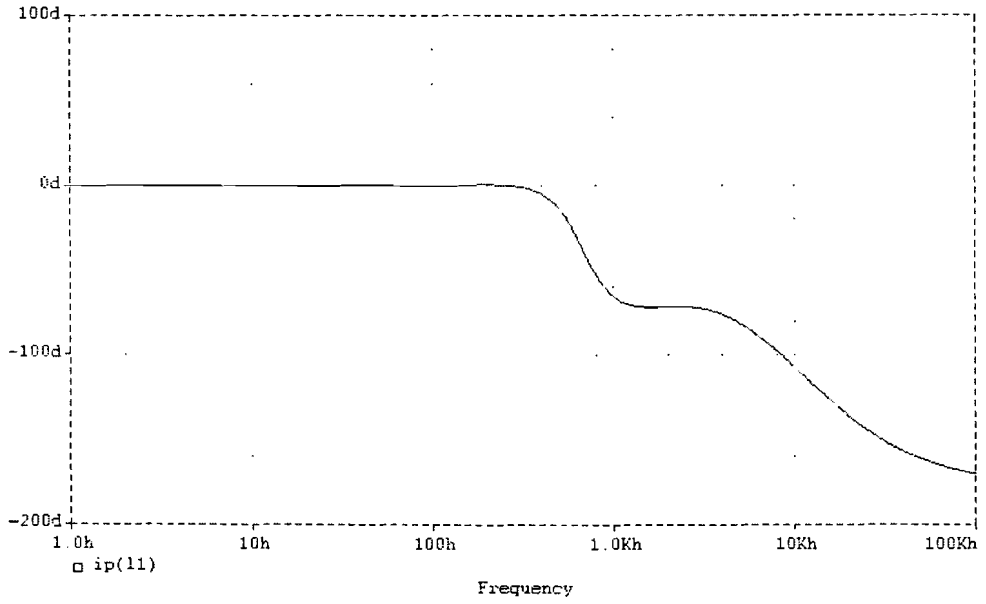

figure 33: Phase output current H_∞ controller, current and voltage sensing

In figure 34 the noise in the output current due to the current sensor noise is plotted. The current sensor noise has a unity gain at the interesting frequencies.
In figure 35 the noise in the output current due to voltage sensor noise is plotted. The voltage sensor noise is attenuated least at the inductance measurement frequency of 1 kHz, but attenuation is still 30dB.

In figure 36 the system-noise amplification of the H_∞ controlled current source is plotted. As already described in section 4.1.3, the system noise is damped at all frequencies. This is even true when no additional high pass filter is connected parallelly to the coil.

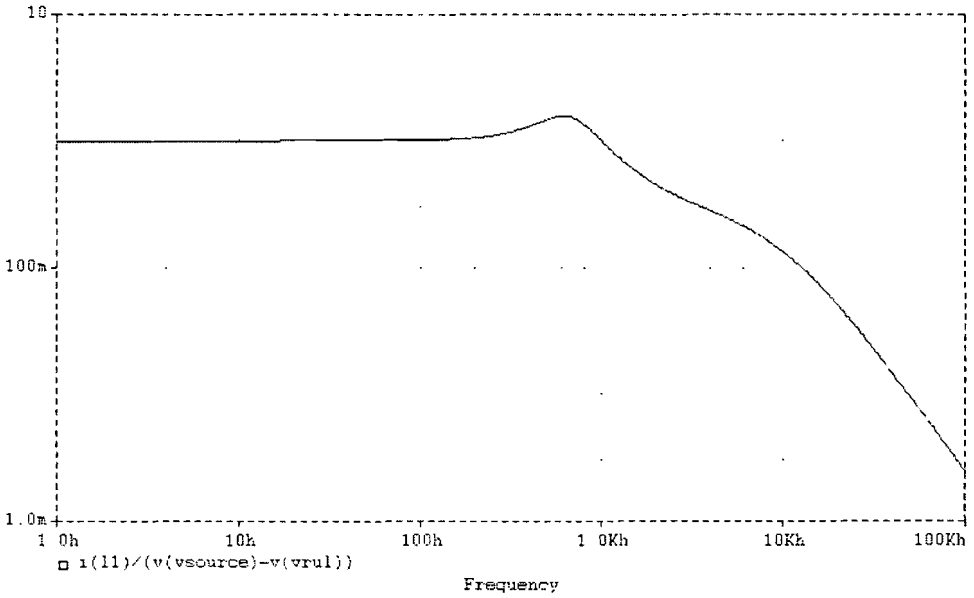

figure 34: Current sensor noise to output current H_∞ controller, current and voltage sensing

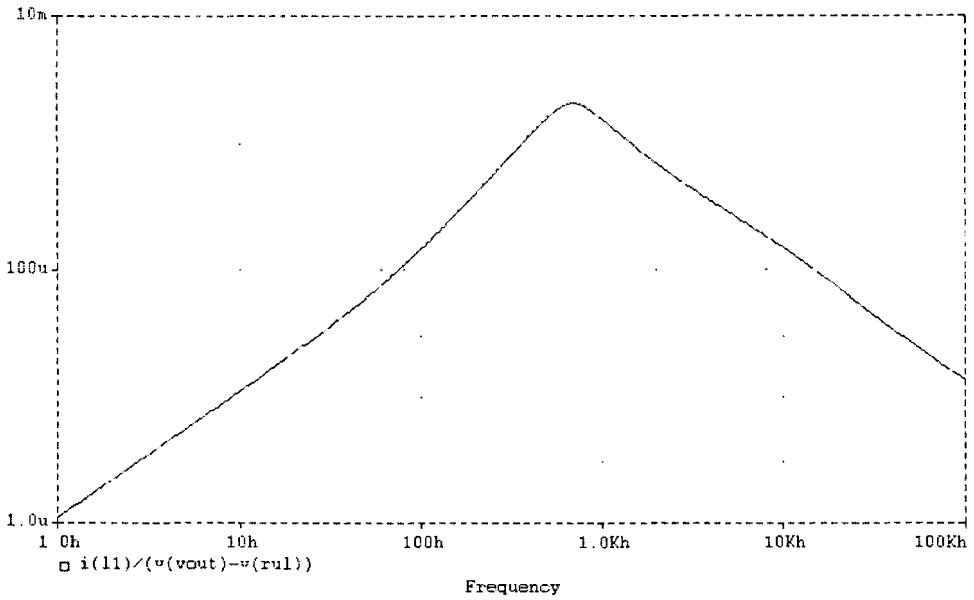

figure 35: Voltage sensor noise output current H_∞ controller, current and voltage sensing

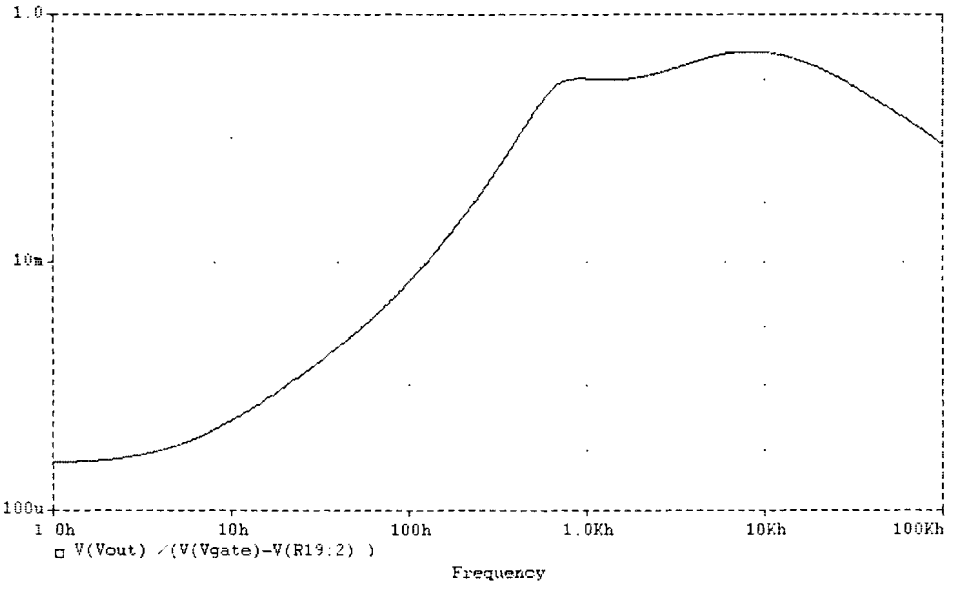

figure 36: System noise amplification output voltage H_∞ controller, current and voltage sensing

4.1.5 Conclusions Regarding Current Sources

In the previous sections the voltage controlled current source was examined as the actuator in the magnetic levitation system. It appeared that it is very difficult to stabilise a current source loaded with coil, and that the output voltage of the current sources suffers from a lot of noise. This will lead to problems with the inductance measurement.

For these reasons the voltage controlled voltage source is examined as the actuator for the magnetic levitation system in the next section.

4.2 Linear Voltage Source

The power supply described in the section 4.1, was a voltage controlled **current** source (VCCS). It appeared that a current source is likely to oscillate when loaded with an inductor. An other possibility to drive the coil is to use a voltage controlled voltage source (VCVS) This option is examined in this section.
The drawback of this option is that the magnetic reluctance force exerted on the ball by the coil does not depend directly on the applied control voltage on the power supply. The extra transfer function of the actuator is introduced into the system, by the serial-connection of the coil with its internal resistance. (See (24)) To make it even worse, this transfer function is not constant, but depends on the distance between the ball and the coil. (See chapter 3.)
One can say that noise and stability-problems are moved from the power supply to the controller of the levitation system.

For the target of the thesis is self sensing magnetic levitation, an other restriction of the power supply is that the inductance of the coil can be measured simultaneously. Like with the current source, this is done by adding an extra high frequent voltage on top of the DC-voltage over the coil. The frequency of this extra component must be much higher than the highest frequency of the mechanical system. To add an additional signal around 1 kHz would be a good choice.

A voltage controlled voltage source can be realised as in figure 37. The extra voltage amplification by transistor T_2 is necessary because the supply voltage of the circuit is more than the supply voltage of the opamp. Diode D_1 and zenerdiode Z_1 have no function in the circuit and are only for protection of the MOSFET T_1.

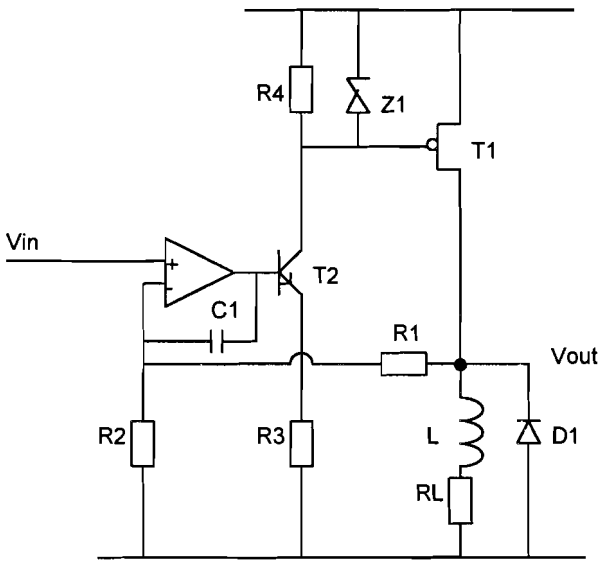

figure 37: Voltage Controlled Voltage Source

The output voltage V_{out} of the voltage controlled voltage source in figure 37 for low frequencies is given by: (When the gain of the opamp is assumed to be infinite.)

$$V_{out} = \left(1 + \frac{R_1}{R_2}\right) \cdot V_{in} \qquad (32)$$

The VCVS must have a low-pass characteristic for stability, however the bandwidth of the voltage controlled voltage source can be very high, in comparison with the voltage controlled current source. The 3dB point is given by:

$$f_{3dB} = \frac{R_1 + R_2}{2\pi R_1 R_2 C_1} \qquad (33)$$

In contrast to the current source, there are no stability or noise problems when using a voltage source.
Note that care must be taken, when designing the controller for the whole levitation system, that the actuator does not saturate at its supply voltage.

4.3 SWITCHED POWER SUPPLIES

In the current levitation system the current through the coil is supplied by a linear current supply. This has the disadvantage that a lot of energy is dissipated in the power supply. Further on, in section 4.1 it is shown that a current source leads to problems when driving a coil, and that a voltage source can be used. Because of these two reasons the possibility to use a switched voltage source has been examined. The only drawback of a switched power supply is that the dissipation in the coil is somewhat higher, because of increase of Eddy currents. However, they can be avoided by using a non-conductive coil core or laminating or sintering. The switched power supply has to meet one other restriction, namely that the inductance of the coil can be measured at the same time.

4.3.1. PULSE WIDTH MODULATED POWER SUPPLY

The first option for a switched power supply is a pulse width modulated power supply (PWM) The coil voltage is switched with constant frequency ($1/T$) between V_{ss} and V_{dd}, in such way that the average voltage over the coil is the desired voltage. The circuit is depicted in figure 38.

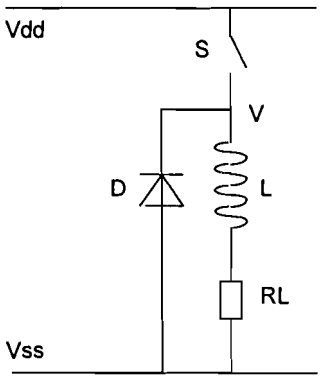

figure 38: Circuit of PWM supply

The switched power supply operates in two modes. Mode 1 is when the switch is closed and the coil is charged with magnetic energy, diode D does not conduct, because node V is higher than V_{ss}. Mode 2 is when the switch is opened and the diode conducts. When assumed that the diode is ideal, the voltage at node V is V_{ss}.
The two equivalent circuits for the two different modes are depicted in figure 39.

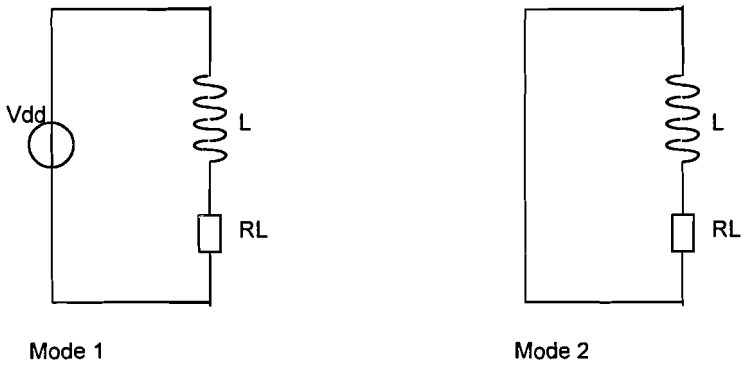

figure 39: Equivalent circuits for PWM power supply

The average current through the coil $i_{L,av}$ can be calculated as follows:

$$I_{L,av} = \frac{\delta \cdot V_{dd}}{R_L} \tag{34}$$

where δ is the duty cycle of the steering of the switch.
A high frequency saw-tooth wave form is superposed onto this average current through the coil by the switching of the power supply. The amplitude of this saw-tooth is a measurement for the inductance of the coil. The amplitude of the saw-tooth can be calculated as follows: (See also figure 40)

$$t = 0: I = I_0 = \frac{V_{dd}}{R_L} \cdot \delta$$

$$I(t) = I_0 + \left(\frac{V_{dd}}{R_L} - \frac{V_{dd}}{R_L} \cdot \delta\right)\left(1 - e^{-\frac{R_L}{L}t}\right) = \frac{V_{dd}}{R_L}\delta + \frac{V_{dd}}{R_L}(1-\delta)\left(1 - e^{-\frac{R_L}{L}t}\right)\Big|_{t \le t_1}$$

$$I(t_1) = \frac{V_{dd}}{R_L}\delta + \frac{V_{dd}}{R_L}(1-\delta)\left(1 - e^{-\frac{R_L}{L}\delta T}\right)$$

$$I(t) = \left(\frac{V_{dd}}{R_L}\delta + \frac{V_{dd}}{R_L}(1-\delta)\left(1 - e^{-\frac{R_L}{L}\delta T}\right)\right) \cdot e^{-\frac{R_L}{L}(t-t_1)}\Big|_{t>t_1}$$

$$I(t_2) = \frac{V_{dd}}{R_L} e^{-\frac{R_L}{L}(1-\delta)T} - \frac{V_{dd}}{R_L}(1-\delta)e^{-\frac{R_L}{L}T} \tag{35}$$

When assumed that $T << \frac{R_L}{L}$:

$$\left.\begin{aligned} V_R(t_1) &= V_{dd}\delta + V_{dd}(1-\delta)\left(1-1+\frac{R_L}{L}\delta T\right) \\ V_R(t_2) &= V_{dd}\delta \end{aligned}\right\} \Rightarrow$$

$$V_{R,toptop} = V_{dd}\delta + (V_{dd} - V_{dd}\delta)\frac{R_L}{L}\delta T - V_{dd}\delta = V_{dd}\frac{R_L}{L}\delta T - V_{dd}\delta^2\frac{R_L}{L}T \qquad (36)$$

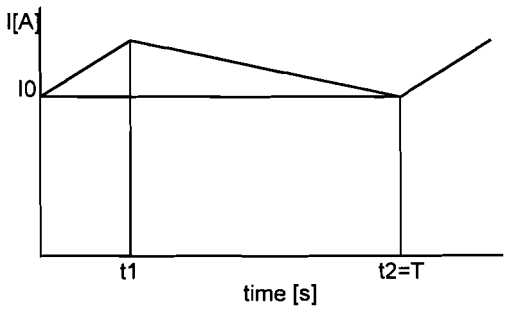

figure 40: Saw-tooth component on I

Formula (36) shows that the amplitude of the high frequency saw-tooth (measured by the voltage over a serial resistance) not only depends on the inductance of the coil, but also on the duty-cycle of the PWM-signal. So, measurement of the amplitude of the saw-tooth signal only gives not enough information to calculate the inductance of the coil. One should also measure δ or R_L accurately. (R_L depends on the temperature of the coil; δ depends on R_L) For this reason the PWM power supply is not suitable in this application.

4.3.2 PWM / FM POWER SUPPLY

In the previous section was found that the amplitude of the high frequency component on top of the average current through the coil was not a direct measurement for the inductance of the coil, when using a PWM power supply. In this section a frequency modulated / pulse width modulated power supply is examined (FM / PWM).

When using the PWM power supply described in the previous section the switching frequency 1/T is constant. When using a FM / PWM power supply this switching frequency varies with the duty cycle in a certain way. However formula (36) shows that, to be $V_{R,toptop}$ independent of $\delta, \delta \cdot T$ **and** $\delta^2 T$ must be constant. This is not possible simultaneously. So a FM / PWM power supply is not suited to drive the coil in this application, either.

4.3.3 PWM POWER SUPPLY WITH ADDITIONAL HIGH FREQUENCY COMPONENT

The previous two switched power supplies were not suitable to drive the coil in this application because the amplitude of the high frequency component of the current through the coil depends on the duty cycle of the switched voltage.

For that reason, a switched power supply with two switching frequencies is examined. The first frequency is pulse width modulated to control the current through the coil, the second has a even higher frequency and a constant duty cycle of 50%. It is examined whether the current through the coil at the highest frequency does not depend on the duty-cycle of the lowest frequency.

There are three different ways to combine two frequencies in a switched current supply. They are all Boolean functions. All three ways have a different effect on the duty cycle of the resulting signal. (See table 3.)

function	result duty cycle
AND	always < 50%
OR	always > 50%
XOR	always = 50%

table 3:Functions to combine two frequencies in switched power supply

The XOR-gate can not be used in a switched power supply, because the duty cycle is always 50%, and thus the output power of the supply can not be controlled. Only the AND-function is suitable to be used in the switched power supply for this application, because the controller must be able to reduce the output power of the supply to nearly zero.
When the AND-function is used in the PWM supply as depicted in figure 38, the voltage over the coil, will be that as in figure 41, the current through the coil will be that as in figure 42.

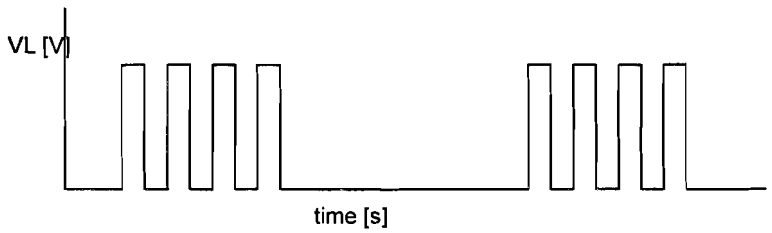

figure 41: Voltage over the coil in PWM supply with additional high frequency component

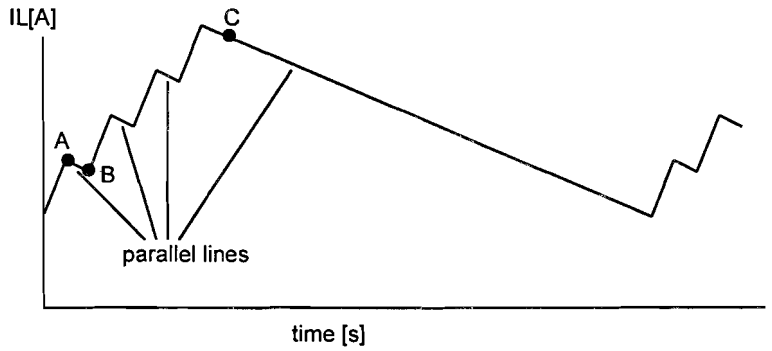

figure 42: Current through the coil in PWM supply with additional high frequency component

When assumed that $T << \frac{R_L}{L}$ the current through the coil (measured by a serial resistance) can be calculated as follows:

$$V_R(C) = V_{dd}\delta + V_{dd}(1-\delta)\frac{R_L}{L}\delta T$$

$$V_R(B) = -\frac{V_R(C)}{(1-\delta)T}\cdot\frac{1}{2f} + V_R(A) = -\frac{V_{dd}\delta}{2f(1-\delta)T} - \frac{V_{dd}\frac{R_L}{L}\delta T}{2f} + V_R(A)$$

$$V_R(A) = \frac{V_R(C) + \frac{1}{2}\delta T\frac{V_R(C)}{(1-\delta)T}}{\frac{1}{2}\delta T}\cdot\frac{1}{2f} = \frac{V_{dd}}{Tf} + \frac{V_{dd}(1-\delta)\frac{R_L}{L}}{f} + \frac{V_{dd}\delta}{(1-\delta)Tf} + \frac{V_{dd}\frac{R_L}{L}\delta}{2f}$$

(37)

The top-top value of the high frequency component in that current (voltage over the serial resistance) is:

$$V_{R,HF,toptop} = V_R(A) - V_R(B) + \frac{V_R(C)}{\delta T}\cdot\frac{1}{2f} = \frac{V_{dd}}{2}\cdot\frac{\delta + \frac{R_L}{L}\delta(1-\delta)T + (1-\delta) + \frac{1}{2}(1-\delta)\frac{R_L}{L}T}{(1-\delta)fT}$$

(38)

Formula (38) shows that, although the duty cycle of the high frequency component block wave is constant at 50%, the amplitude of the saw tooth still depends on the duty cycle of the low frequency PWM signal.
Physical explanation for this phenomenon is the serial resistance of the coil. When the switch is closed, the voltage over the coil is $V_{dd}(1-\delta)$ and not V_{dd}. When the switch is opened the voltage over the coil is $V_{dd}\delta$ and not zero. Thus the amplitude of the high frequency voltage over the coil depends on the duty cycle δ and so does the amplitude of the current.
This is true for all basic switched power supplies. So the **amplitude** of the high frequency current through the coil is not a good measurement for the inductance of the coil. For that reason in the next section, a switched power supply is proposed where the switching frequency of the supply is a measure for the inductance of the coil.

4.3.4 SERIAL RESONANT SWITCHED POWER SUPPLY

In the previous sections the amplitude of certain signals was a measurement for the inductance of the coil. It appeared that this was not easy to implement. In a resonant switched power supply not the amplitude, but the frequency of the current through the coil is measured. The circuit of a serial resonant switched power supply is depicted in figure 43.

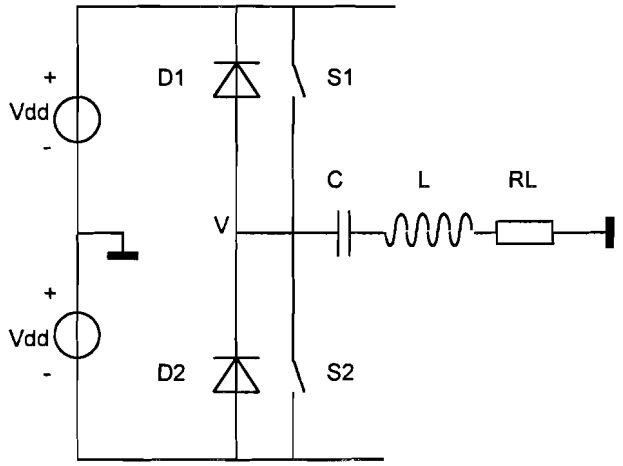

figure 43: Circuit of serial resonant switched power supply

The switches S_1 and S_2 conduct alternatively, with a certain duty cycle. So the voltage at node V is (in this sequence): $+V_{dd}$ when S_1 is closed (S_2 opened, D_1 and D_2 do not conduct), $-V_{dd}$ when D_2 conducts (S_1 and S_2 opened, D_1 does not conduct), $-V_{dd}$ when S_2 is closed (S_1 opened, D_1 and D_2 do not conduct) and $+V_{dd}$ when D_1 conducts (S_1 and S_2 opened, D_2 does not conduct).
When the sequence as described above, is repeated at the resonance frequency of the serial LC circuit, the current through the inductor can be controlled by the duty cycle of the S_1 and S_2. The current through the inductor is given by the well known equation:

$$I_L = \frac{V_{dd}\delta}{R_L} \tag{39}$$

The resonance frequency of the R_L, L and C in serial is (when $R_L << 2\sqrt{\frac{L}{C}}$):

$$f_0 = \frac{1}{2\pi\sqrt{LC}} \tag{40}$$

So the output power of the resonant power supply is controllable, given by (39), and the inductance is observable, given by (40).

However, there is one problem: The impedance of coil is $2\pi f_0 L$, so when roughly estimated values for f_0 and L are used, the impedance of the coil is:

$$Z = \sqrt{(2\pi f_0 L)^2} \approx 2 \cdot \pi \cdot 1000 \cdot 0.1 \approx 630\Omega \tag{41}$$

A current of approximately 2A is needed to levitate the ball. So, the voltage over the coil with that current will be:

$$V = Z \cdot i_L \approx 630 \cdot 2 = 1260V \tag{42}$$

This voltage is much too high for safe operation, and much to high for normal capacitors. It is not possible to force a DC-current through the coil, because of the serial capacitor. So a serial resonant switched power supply is not suited to be used in this application.

4.3.5 PARALLEL RESONANT SWITCHED POWER SUPPLY

In the previous section a resonant power supply with a capacitor in serie with the inductance was examined. In this section a parallel switched power supply will be discussed. This has the advantage that a DC-current can flow through the coil.
The circuit of a parallel resonant switched power supply is given in figure 44.

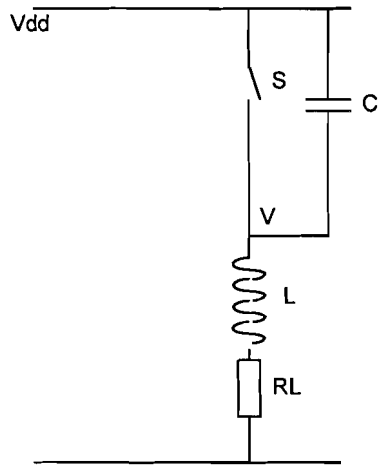

figure 44: Circuit of parallel resonant switched power supply

The circuit in figure 44 is nearly the same as in figure 38 except that the diode is replaced by a capacitor. When the switch is closed, a current starts to flow through the switch into the coil. When the switch is opened, that current continues to flow through the coil, so it is drawn from the capacitor. The capacitor charges, the inductor discharges. This process continues until the inductor is completely discharged and the capacitor is fully charged. At this point, the current is zero, and the voltage at node V has reached its minimum. Then the current starts to flow in the other direction. The capacitor is discharged and the inductor charges, however, the current is flowing in the other direction now. When the voltage over the capacitor is zero the inductor is fully charged. The current continues to flow in the other direction, until all energy in the inductor is in the capacitor again. The voltage at node V is at its maximum now. The current switches direction again, and the capacitor is discharged, until the voltage at node V is V_{dd}. Then the switch is closed again. (See figure 45)

The current through the coil can be controlled by the duty cycle of the switch. The current is given by (39). The inductance of the coil can be measured by the resonance frequency of the LC-circuit. The resonance frequency is given by (40).

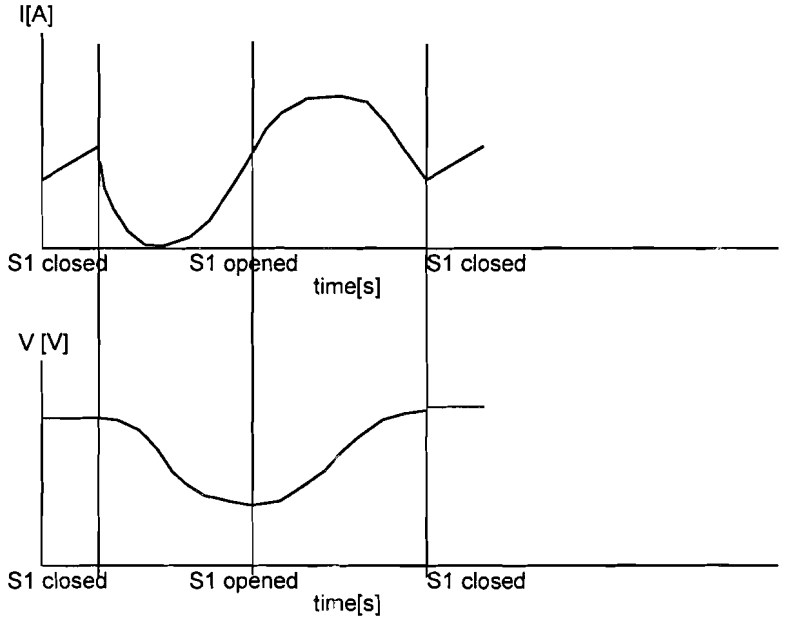

figure 45: Signals in parallel resonant switched power supply

However, there is one problem with this parallel resonant switched power supply, viz. that the energy stored in the coil must be stored in the capacitor completely. The energy in the inductor and capacitor is:

$$E_L = \frac{1}{2} L i_L^2$$
$$E_C = \frac{1}{2} C U_C^2$$

(43)

When roughly estimated values for f_0, L and i_L are used, the voltage over the maximum voltage over the capacitor will be:

$$V_C = \sqrt{\frac{L}{C}} i_L \approx \sqrt{\frac{0.1}{253 \cdot 10^{-9}}} \cdot 2 \approx 1260V$$

(44)

This voltage is much too high for safe operation.

It is not possible to enlarge the capacitor because then the resonance frequency would not be much higher than the bandwidth of the mechanical system. This would lead to high frequency movements of the ball, and therefore wrong measurement of the position.
So a parallel resonant switched power supply is not suitable as a power supply in this application.

4.4 CONCLUSIONS REGARDING THE ACTUATOR

In this chapter various actuator types were examined for the magnetic levitation system. In section 4.1 the current source was described. It appeared that a current source loaded with a coil is very likely to oscillate, and that the output voltage of the current source suffers from excessive noise. Therefore two H_∞ controllers were designed for stabilising the current source. The first H_∞ controller only observes the current through the coil, the other controller observers the current as well as the voltage over the coil. Although the latter performs better regarding to noise reduction, it cannot be used in combination with the inductance measurement schemes involving an LC oscillator.
The other type of actuator for the magnetic levitation system is the voltage controlled voltage source, described in section 4.2. It appeared that the voltage source (loaded with a coil) does not have any of the disadvantages of the current source.
Finally switched power supplies were examined as the actuator for the magnetic levitation system. It was shown that it was not possible to simultaneously use the coil as actuator and position sensor when using a switched power supply.

Regarding above, one can see that the voltage controlled voltage source is the best actuator type for the levitation system. However, as will be shown in the next chapter, it is very difficult to combine the voltage source with any sensor.

5. SENSORS

Keypoint of this thesis is (quasi) **self sensing** magnetic levitation. That means that the position of the levitated ball is not measured by an additional position sensor (such as a camera) but by measuring the inductance of the same coil that levitates the ball. This rises one big problem, namely how to measure the inductance of the coil, at the same time a control current is forced through it.
An other problem is that the coil suffers from saturation and hysterese by the control current. (See chapter 2.) This influences the measurement of the inductance, and will lead to errors in the position sensing.
Several options for the sensor are examined throughout this chapter. In the next chapter a choice is made for a particular actuator/sensor combination.

The most simple way to measure the inductance of the coil, at the same time the control current flows through it, is by alternating between the two operating modi (control and sensing) at a high frequency. The sample theorem of Nyquist requires that the frequency at which the position of the ball is measured, is at least twice the maximum frequency in the system. In [10], [11] and [12] the maximum frequency of the mechanical system is assumed to be 100Hz. This means that the sample frequency is at least 200Hz, but that 1kHz would be sensible, because of the phase shift due to sampling.
The time slot in which the coil is used as sensor can not be very long, in comparison to the time the coil is used as an actuator, because the average current through, or voltage over the coil is given by the output of the controller. Assume that for 10% of the time, the coil is used for sensing the position, and for 90% of the time the coil is used as actuator. (That means that the duty cycle δ is 0.1)
This gives a time of about $\frac{1}{f}\cdot\delta = 1\cdot10^{-3}\cdot0.1 = 1\cdot10^{-4}[s]$ in which the measurement has to take place. However, the time constant $\frac{L}{R_L}$ is about $\frac{L}{R_L} = \frac{0.1}{3.5} = 3\cdot10^{-2}[s]$. So the current flowing through the coil during the actuating modus, will continue to flow through the coil during the sensing modus. The sensor must allow this current to flow, or else the voltage over the coil will rise to very high potentials. An other effect of the continuous current through the coil is that unwanted effects, such as saturation, (still) influence the measurement.

Increasing the serial resistance of the coil, to reduce the time constant L/R_L is not a solution, because then the voltage over that resistance $V_R = I_L \cdot R_L$ would be very large: When the time constant is reduced by (only) a factor 1000, the voltage over the resistor would be enlarged by a factor 1000. That voltage would then be a few kVolt.

The above leads to the conclusion that alternating between actuating and sensing with the coil is in the practical application not possible. All proposed sensors are therefore continuous.

An other point of attention is that the serial resistance of the coil to be measured is not a constant but temperature dependent. Its value is in the range:

$$R_{L,\min} = 2.5\Omega \quad R_{L,nom} = 3.5\Omega \quad R_{L,\max} = 4.5\Omega \tag{45}$$

In the next sections various way to measure the inductance of the coil are proposed. First, three different ways to obtain the inductance of the coil involving an LC-oscillator are examined: In section 5.1. the oscillation frequency of the LC-oscillator is measured using a phase locked loop. In section 5.2 the oscillation frequency of the LC-oscillator is measured by counting pulses between two zero crossings. And finally in section 5.3 the quality factor of the LC-oscillator is examined.
In section 5.4 an additional high frequency component is added to the voltage over the coil and the high frequency current is measured, to obtain the inductance. Also the dual case (add a high frequency current and measure high frequency voltage) is examined.
In section 5.5 correlation measurement is examined as a way to obtain the inductance of the coil.
For all these different ways to measure the inductance of the coil, constraints to the circuit, the influence of the actuator on the sensor, the influence of the sensor on the actuator and the signal to noise ratio of the measurement is determined.

5.1 Measuring LC-Oscillation Frequency With PLL

One way to measure the inductance of a coil is to measure its oscillation frequency in combination with a (known) capacitor. The oscillation frequency of a LC-oscillator (when its damping is small) is given in (40). However, the actuating current must be supplied to the coil also. This gives the circuit as in figure 46.

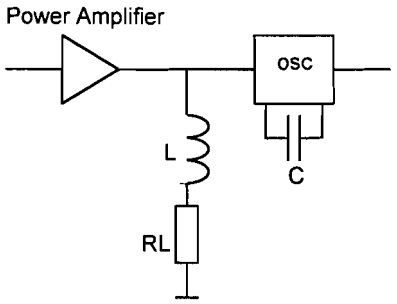

figure 46: LC-Oscillator sensor

Chapter 4 showed that the power amplifier can either be a voltage source or a current source. First the consequences of using a voltage source are examined. After that the current source is discussed.
One possibility to determine the inductance of the coil is to measure the oscillation frequency of the LC-oscillator with a *phase locked loop* (PLL). This is examined in section 5.1.3. An other way to measure the oscillation frequency is counting pulses between two zero-crossings (examined in section 5.2) The inductance of the coil can also be obtained by determining the Q-factor of the LC-oscillator (examined in section 5.3)

5.1.1 LC-OSCILLATOR WITH VOLTAGE SOURCE

The output impedance of an ideal voltage source is zero, so the LC-oscillation of the oscillator in figure 46 would be totally damped. A solution for this contradiction is to increase the output impedance of the voltage source around the oscillation frequency of the LC-oscillator. (The power amplifier is then converted to a current source, at that frequency) This can be done by an external LC-filter. (See figure 47.)

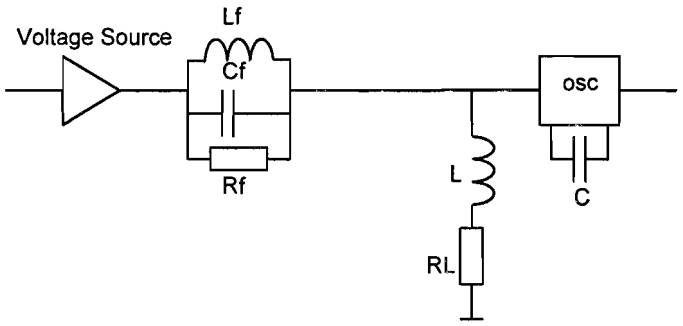

figure 47: LC-Oscillator sensor, with LC-filter

Note that the LC-oscillator in figure 46 (and figure 47 too) is a parallel LC-oscillator. A parallel LC-oscillator can be connected to a current source. The dual case, a serial LC-oscillator, can be connected to a voltage source. However when a capacitor is in serie with the coil, no (actuating) DC-current can be forced through the coil.

It is desired that the oscillation frequency of the oscillator only depends on the inductance of the coil. Therefore the influence of the various components in figure 47 is examined. They are examined separately, to avoid mathematical complexities.

Influence of R_L

In figure 48 the equivalent schematic of figure 47 is plotted, when the influences of L_f, C_f and R_f on the oscillation frequency are neglected.

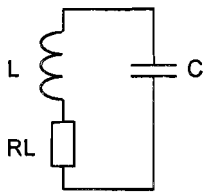

figure 48: Equivalent scheme for calculating influence of R_L

The impedance of the schematic in figure 48 is given by:

$$Z(j\omega) = \frac{\frac{1}{j\omega C}\left(j\omega L + R_L\right)}{\frac{1}{j\omega C} + \frac{1}{j\omega L} + R_L} = \frac{j\omega L + R_L}{1 - \omega^2 LC + j\omega R_L C} \qquad (46)$$

When $\frac{R_L^2}{L^2} << 4\frac{1}{LC}$, which is true in this application (1<<130000), (46) can be approximated by:

$$Z(j\omega) \approx \frac{-j\omega\frac{1}{C} - \frac{R_L}{LC}}{\left(\omega + \frac{R_L}{2L} + j\sqrt{\frac{1}{LC}}\right)\left(\omega + \frac{R_L}{2L} - j\sqrt{\frac{1}{LC}}\right)} \qquad (47)$$

Formula (47) shows that R_L has 'no' influence on the oscillation frequency, when $\frac{R_L^2}{L^2} << 4\frac{1}{LC}$. This influence decreases with increasing f_{osc}^2.

Influence of R_f

In figure 49 the equivalent schematic of figure 47 is plotted, when the influences of L_f, C_f and R_L on the oscillation frequency are neglected.

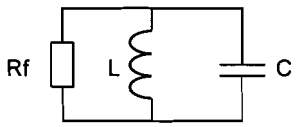

figure 49: Equivalent scheme for calculating influence of R_f

The impedance of the schematic in figure 49 is given by:

$$Z(j\omega) = \frac{1}{j\omega C + \frac{1}{j\omega L} + \frac{1}{R_f}} = \frac{j\omega R_f L}{R_f - \omega^2 R_f LC + j\omega L} \qquad (48)$$

When $R_f >> \sqrt{\frac{L}{C}}$, which can be true ($R_f$>>628), (48) can be approximated by:

$$Z(j\omega) \approx \frac{-j\omega\frac{1}{C}}{\left(\omega + \frac{1}{2R_f C} + j\sqrt{\frac{1}{LC}}\right)\left(\omega + \frac{1}{2R_f C} - j\sqrt{\frac{1}{LC}}\right)} \qquad (49)$$

Formula (47) shows that R_f has 'no' influence on the oscillation frequency, when $R_f >> \sqrt{\frac{L}{C}}$. This influence increases with increasing $\sqrt{f_{osc}}$.

In this approximation R_f is not only R_f of figure 47, but can also be the output impedance of a true current source as described in chapter 4, or the characteristic impedance of the LC-filter in figure 47.

Influence of C_f and L_f

In figure 50 the equivalent schematic of figure 47 is plotted, when the influence of R_L on the oscillation frequency is neglected.

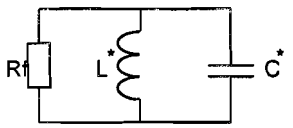

figure 50: Equivalent scheme for calculating influence of L_f and C_f

For the equivalent scheme of figure 50 the following relations apply:

$$L^* = \frac{L \cdot L_f}{L + L_f}$$
$$C^* = C + C_f \qquad (50)$$

The optimum case is when L_f equals L and C_f equals C. When this is the case L^* is decreased by a factor 2 and C^* is increased a factor 2. So the oscillation frequency is still $f_{osc} = \frac{1}{2\pi\sqrt{LC}}$.
However, in the previous paragraph it derived that to have no influence on the oscillation frequency $R_f >> \sqrt{\frac{L}{C}}$. The characteristic impedance of the parallel connection of L_f and C_f is: $Z = \sqrt{\frac{L_f}{C_f}}$. So the parallel connection of R_f and L_f and C_f has an impedance which is always smaller than $\sqrt{\frac{L}{C}}$.
This means that the filter in serie with the voltage source always influences the oscillation frequency of the LC-oscillator. In other words, when a voltage source is used as the actuator of the levitation system, and the induction sensor involves an LC-oscillator, the influence of the filter on the inductance measurement must be compensated for.

5.1.2 LC-OSCILLATOR WITH CURRENT SOURCE

In section 5.1.1 the power amplifier of figure 46 coil was a voltage source. In this section a current source is used as a power amplifier. However, it was made clear in the previous

chapter that the coil voltage suffers from a lot of noise when using a current source. An additional high-pass RC-filter is needed to limit the impedance of the load at high frequencies. The influence of this filter on the oscillation frequency of the oscillator is examined in this section.
Note that the output impedance of the current source and the serial resistance of the coil R_L also influence the oscillation frequency. The influence of the output impedance of the current source is comparable to the influence of R_f. The influence of R_f and R_L is already examined in the previous section.

When the additional high-pass filter is added to the circuit of figure 46, this leads to a equivalent circuitry as depicted in figure 51.

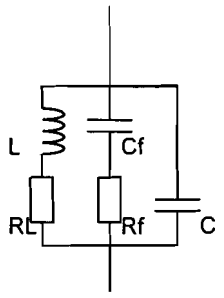

figure 51: LC-oscillator with current source

The impedance of the circuit in figure 51 is given by:

$$Z = \frac{1}{j\omega C + \frac{1}{\frac{1}{j\omega C_f} + R_f} + \frac{1}{j\omega L + R_L}} =$$

$$= \frac{\left(1 + j\omega C_f R_f\right)\left(R_L + j\omega L\right)}{-j\omega^3 LCC_f R_f - \omega^2\left(LC + CC_f R_f R_L + LC_f\right) + j\omega\left(R_L C + R_L C_f + R_f C_f\right) + 1} \qquad (51)$$

When $C_f << C$ and $R_f >> R_L$ this can be approximated by:

$$Z = \frac{\left(1 + j\omega C_f R_f\right)\left(R_L + j\omega L\right)}{\left(\omega + j\frac{1}{\sqrt{LC}}\right)\left(\omega - j\frac{1}{\sqrt{LC}}\right)\left(\omega + \frac{1}{R_f C_f}\right)} \qquad (52)$$

Formula (52) is true only when $C_f << C$ and $R_f >> R_L$, this means that C_f and R_f must be:

$$\begin{cases} C \approx 200nF \\ C_f << 200nF \Rightarrow C_f < 200pF \end{cases}$$
$$\begin{cases} R_L \approx 3.5\Omega \\ R_f >> 3.5\Omega \Rightarrow R_f > 3K\Omega \end{cases}$$

(53)

When R_f and C_f satisfy (53) no compensation is necessary in the measurement for the (known) influence of R_f and C_f.

5.1.3 MEASURING FREQUENCY WITH A PLL

The oscillation frequency of the oscillator in figure 46 can be measured by using a phase-locked loop. (See figure 52.) However, because of the additional, unavoidable noise at the input of the phase detector of the PLL (for example due to the low frequent actuating current through the coil), the measurement of the frequency of the oscillator suffers from noise.

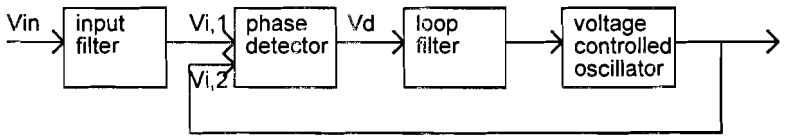

figure 52: Phase Locked Loop

In [14] the behaviour of a PLL with a noisy input signal is examined. The noise signal is assumed to have a flat spectrum in a small frequency band around the oscillation frequency of the oscillator ω_i. (Because of the input filter of the phase detector.) In that case the noise signal *n(t)* can be written as:

$$n(t) = r(t)\cos\left(\omega_i t + \varphi_i(t)\right)$$
$$r(t), \varphi_i(t) = stochastic$$

(54)

The noise signal can be decomposed in quadrature components:

$$n(t) = n_c(t)\cos\left(\omega_i t\right) - n_s(t)\sin\left(\omega_i t\right)$$

(55)

The two input signals of the phase detector of the PLL can be written as:

$$V_{i,1}(t) = V_s(t) + n(t) = \hat{V}_{i,1} \cdot \sin\left(\omega_i t + \theta_i(t)\right) + n_c(t)\cos\left(\omega_i t\right) + n_s(t)\sin\left(\omega_i t\right)$$
$$V_{i,2}(t) = V_{vco}(t) = \hat{V}_0 \cdot \cos\left(\omega_i t + \theta_o(t) + \theta_{no}(t)\right)$$

(56)

where $\theta_o(t)$ is the phase shift necessary to lock the PLL, $\theta_{no}(t)$ is the output noise of the PLL, $V_s(t)$ is the output signal of the input filter without additional noise and $V_{vco}(t)$ is the output voltage of the voltage controlled oscillator (VCO). When assumed that the phase detector is an ideal multiplier with a small gain K_d, and that the signal to noise ratio of the input signal of the phase detector is relatively high (>4dB), the output voltage V_d of the phase detector is given by:

$$V_d(t) = K_d\left[\theta_i(t) - \theta_o(t) - \theta_{no}(t) + \frac{n_c(t)}{\hat{V}_{i,1}}\cos\left(\theta_o(t) + \theta_{no}(t)\right) + \frac{n_s(t)}{\hat{V}_{i,1}}\sin\left(\theta_o(t) + \theta_{no}(t)\right)\right] \tag{57}$$

Because the loop filter is linear and the voltage controlled oscillator can be considered to have a linear transfer function from input voltage to output frequency, the signal to noise ratio of the output of the PLL $(SNR)_{out}$ can be calculated by multiplying V_d with the transfer function of the filter and VCO. This gives:

$$(SNR)_{out} = (SNR)_{in} \cdot \frac{B_i}{2B_L}, \tag{58}$$

where B_i is the bandwidth of the input filter of the PLL and B_L is the noise bandwidth of the loop filter of the PLL. For a second order loop filter with a normalised transfer function as in (59) this noise bandwidth B_L is given in (60).

$$H(j\Omega) = \left.\frac{(2\zeta - \alpha)j\Omega + 1}{(1-\Omega^2) + 2j\zeta\Omega}\right|_{\Omega=\frac{\omega}{\omega_n}} \tag{59}$$

$$\frac{B_L}{\omega_n} = \frac{1}{2\pi}\int_0^\infty |H(j\Omega)|^2 d\Omega = \frac{1}{8}\left[\frac{1}{\zeta} + 4\zeta + \alpha\left(\frac{\alpha}{\zeta} - 4\right)\right] \tag{60}$$

For different loops this relation reduces to:

$$\text{high gain: } \alpha \equiv 0: \frac{B_L}{\omega_n} = \frac{1}{8}\left[\frac{1}{\zeta} + 4\zeta\right]$$

$$\text{low gain: } \alpha \equiv \zeta: \frac{B_L}{\omega_n} = \frac{1}{8}\left[\frac{1}{\zeta} + \zeta\right]$$

$$\text{type 1: } \alpha \equiv 2\zeta: \frac{B_L}{\omega_n} = \frac{1}{8}\cdot\frac{1}{\zeta} \tag{61}$$

The bandwidth of the loop filter determines how fast the PLL is, the noise bandwidth of the loop filter determines (in combination with the input filter of the PLL) the phase jitter. The ratio between the two is therefore interesting. (See also figure 53)

$$\frac{B_L}{B_{3dB}} = \frac{\frac{1}{8}\omega_n\left[\frac{1}{\zeta} + 4\zeta + \alpha\left(\frac{\alpha}{\zeta} - 4\right)\right]}{\sqrt{2\zeta^2 - 4\alpha\zeta + \alpha^2 + 1 + \sqrt{\left(2\zeta^2 - 4\alpha\zeta + \alpha^2 + 1\right)^2 + 1}}}$$

(62)

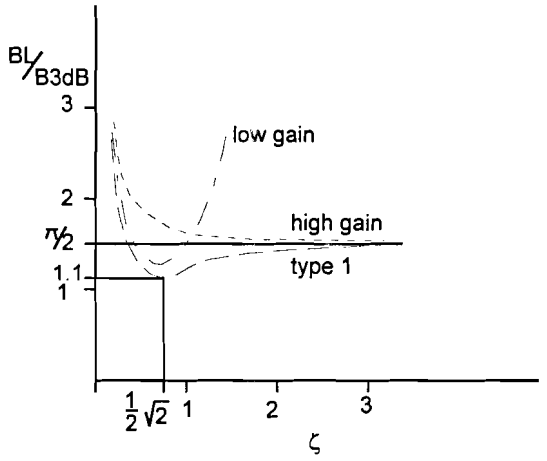

figure 53: Ratio between B_L and B_{3dB}

In figure 53 one can see that loop filter type 1 gives the best noise reduction. The maximum reduction is obtained when $\zeta = \frac{1}{2}\sqrt{2}$. The bandwidth of the loop filter is equal to the band width of the mechanical system (100 Hz): $\omega_n = 2\pi \cdot 100$. Substituting this in (61) gives:

$$B_L = \omega_n \cdot \left.\frac{1}{8\zeta}\right|_{\zeta=\frac{1}{2}\sqrt{2},\,\omega_n=2\pi\cdot 100} = \frac{100\pi}{2\sqrt{2}} \approx 110$$

(63)

The maximum frequency deviation of the LC-oscillator due to a change of the inductance of the coil is:

$$\left.\begin{aligned} L_{\min} &= 110mH \\ L_{\max} &= 115mH \\ C &= 225nF \end{aligned}\right\} \Rightarrow \begin{cases} f_{\min} = 989Hz \\ f_{\max} = 1011Hz \end{cases} \Rightarrow B_i = 22Hz$$

(64)

Substituting (63) and (64) in (58) gives for the signal to noise reduction of the PLL:

$$\frac{(SNR)_{out}}{(SNR)_{in}} = \frac{B_i}{2B_L} = \frac{22}{2\cdot 110} = 0.1$$

(65)

Substituting (65) shows that the PLL amplifies(!) the noise at the input to the output by a factor 10. Physical explanation for this phenomenon is that the PLL must get all its in formation out of a maximum frequency sweep of 22 Hz, and that this sweep can take place with a maximum frequency of 100 Hz. It is easy to understand that such a measurement comes with a lot of noise.

5.2 MEASURING LC-OSCILLATION FREQUENCY WITH HF-COUNTER

In section 5.1 the oscillation frequency of the LC-oscillator was measured using a PLL. An other way to measure a frequency is to count the number of pulses of (known) HF-source between two zero crossings of the LC-oscillator output. This gives a system which is already depicted in figure 46. The influences of various filters necessary to drive the coil are already examined in the previous section. Therefore in this section only a relation between the signal to noise ratio of the output of counter and the signal to noise ratio of the input is derived.

In figure 54 the input signal of the comparator is depicted. The comparator has hysteresis, to avoid high frequency noise at the output of the comparator at the switching point. The two detection levels of the comparator are also depicted in figure 54.

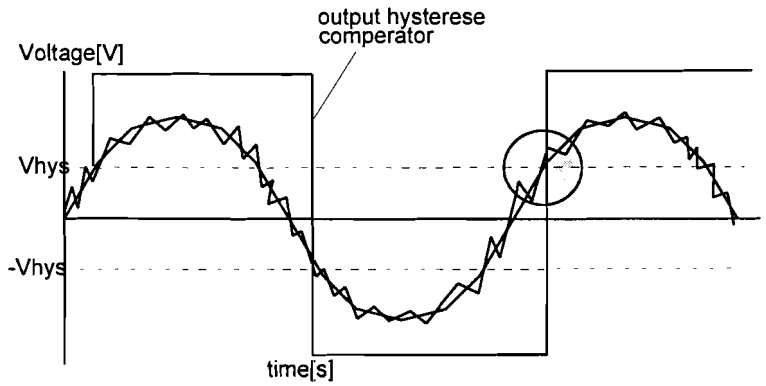

figure 54: Input signal of the hysterese-comparator

In figure 55 an enlargement of the region inside the circle of figure 54 is depicted.

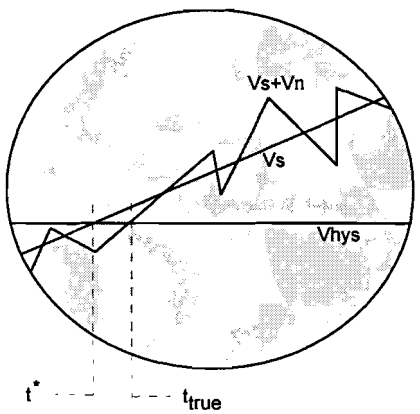

figure 55: Enlargement of noisy signal around V_{hys}

Because a very small band pass filter around the oscillation frequency of the LC-oscillator ω_s leads the comparator, to filter as much noise as possible, the noise $V_n(t)$ can be assumed to have very small band pass characteristic around ω_s (which is **not** the case in figure 55), the noise can be approximated by:

$$V_n(t) = \hat{V}_n \cdot \sin(\omega_s t + \theta_n),$$

(66)

where θ_n is stochastic and $\hat{V}_n$ is the maximum amplitude of the noise signal. (*Maximum amplitude of the noise: See later on.) The noisy signal $V_s(t)+V_n(t)$ can be written as:

$$\hat{V}_s(t) + \hat{V}_n(t) = \sqrt{1 + \hat{V}_s^2 + 2\hat{V}_s\hat{V}_n\cos(\theta_n)} \cdot \sin\left(\omega_s t + \arctan\left(\frac{\hat{V}_n \sin(\theta_n)}{\hat{V}_s + \hat{V}_n \cos(\theta_n)}\right)\right)$$

(67)

The maximum phase error of the comparator due to the additional noise can be calculated as follows:

$$\frac{d\left[\arctan\left(\frac{\hat{V}_n \sin(\theta_n)}{\hat{V}_s + \hat{V}_n \cos(\theta_n)}\right)\right]}{d\theta_n} = \frac{\hat{V}_n\left(\hat{V}_s \cos(\theta_n) + \hat{V}_n\right)}{2\hat{V}_n\hat{V}_s\cos(\theta_n) + \hat{V}_n^2 + \hat{V}_s^2} = 0$$

$$\Rightarrow \cos(\theta_n) = -\frac{\hat{V}_n}{\hat{V}_s}$$

$$\Rightarrow \theta_n = \arccos\left(-\frac{\hat{V}_n}{\hat{V}_s}\right)$$

(68)

When the result of (68) is substituted in (67), this gives for the maximum phase error of the comparator:

$$\theta_{error,\max} = \arctan\left(\frac{\hat{V}_n \sin\left(\arccos\left(-\frac{\hat{V}_n}{\hat{V}_s}\right)\right)}{\hat{V}_s + \hat{V}_n \cos\left(\arccos\left(-\frac{\hat{V}_n}{\hat{V}_s}\right)\right)}\right) = \arcsin\left(\frac{\hat{V}_n}{\hat{V}_s}\right)$$

(69)

According to the definition in (72) the signal to noise ratio of the output is:

$$(SNR)_{out} = \frac{1}{\theta_{error,\max}} = \frac{1}{\arcsin\left(\frac{1}{(SNR)_{in}}\right)}$$

(70)

Formula (70) shows that the signal to noise ratio at the output has a minimum (worst) value. This arises from the assumption that the noise has a very small band pass characteristic, and has a certain maximum value.
For small values of x $\arcsin(x) \approx x$. This reduces (70) to:

$$\frac{(SNR)_{out}}{(SNR)_{in}} = 1 \qquad (71)$$

Remark that the result of formula (71) compared to the result of formula (65) seems to be somewhat optimistic. For in both cases the frequency of an oscillator is used as a measure for the inductance of the coil. Probably, the signal to noise ratio of the sensor described in this section is much less than formula (71) shows.

(*) Note that in this section for simplicity the signal to noise ratio is **not** defined as the **power** of the signal divided by the **power** of the noise, but as the maximum **amplitude** of the signal divided by the maximum **amplitude** of the noise.

$$(SNR)_{out} \neq \frac{P_{signal}}{P_{noise}} = \frac{\frac{2\pi}{\omega_s}\sqrt{\int_0^{\frac{2\pi}{\omega_s}} (V_s)^2 dt}}{R_{Noise,Noise}(0)}$$

$$(SNR)_{out} = \frac{\hat{V}_s}{\hat{V}_n} = \frac{\|V_s\|_\infty}{\|V_n\|_\infty} \qquad (72)$$

This means that not all noise-models can be used in this approximation. For example Gaussian noise can not be used, because the 'amplitude' of Gaussian noise goes to infinity:

$$\|f_X(x)\|_\infty = \left\| \frac{1}{\sigma\sqrt{2\pi}} e^{-\frac{x^2}{2\sigma^2}} \right\|_\infty = \infty \qquad (73)$$

where $f_X(x)$ is the probability density function.

5.3 MEASURING LC-OSCILLATOR Q-FACTOR

In the previous sections the oscillation frequency of the LC-oscillator was measured. In this section the Q-factor of the oscillator in figure 47 is measured as a sensor for the inductance of the coil. The impedance of a circuit as given in figure 56 is:

$$Z(j\omega) = \frac{j\omega R_f L + R_f R_L}{-\omega^2 LCR_f R_L + j\omega L + R_L + R_f} \qquad (74)$$

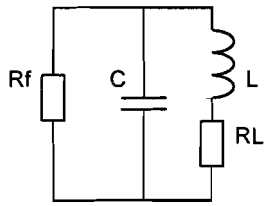

figure 56: Equivalent schematic for Q-factor measurement

This can be written as:

$$Z(j\omega) = \left.\frac{\frac{R_f(j\omega L + R_L)}{LCR_f R_L}}{-\omega^2 + j\omega\frac{\omega_p}{Q_p} + \omega_p^2}\right|_{\omega_p = \sqrt{\frac{R_L + R_f}{LCR_f R_L}},\, Q_p = \frac{\sqrt{R_L + R_f}}{\sqrt{LCR_f R_L}\cdot CR_f R_L}} \qquad (75)$$

As can be seen in (75), Q_p does not only depend on L, but also on R_L. (To be more precisely, $Q_p \propto \frac{1}{\sqrt{L}}, Q_p \propto \frac{1}{R_L}$) So, to measure L from the quality factor Q_p of the oscillator, R_L must be measured too. (R_L is temperature dependent.) For this reason Q-factor measurement is not a good method for measuring the inductance of the coil, in this application.

5.4 Measuring Additional High Frequency Component

An other option for measuring the coil inductance which will be examined in this report, is adding an extra high frequency component with a constant amplitude to the band limited control voltage over the coil or current through the coil. Because both a voltage source and a current source can be used to drive the coil, this option is examined first for voltage control, and after that for current control.

5.4.1 High Frequency Component with Voltage Control

When a high frequency component is added to the band limited control voltage over the coil, the extra high frequent current through the coil is a measurement for the inductance of the coil:

$$i_L = \frac{1}{R_L + j\omega L} \cdot U_L$$

(76)

Formula (76) shows that the current is not inversely proportional with the inductance, because of the serial resistance of the coil. There are two ways to overcome this problem. The first is to add a very high frequency, so that $\omega L >> R_L$. This will lead to certain (but small) error, depending on the measuring frequency. Problem is that a very high frequency voltage over the coil will lead to a very small current. Noise will disturb the measurement of this current.
The second solution for the problem is not to measure the amplitude of the total current, but to measure the amplitude and phase of the high frequency current. This option will be discussed in this section.

A phase diagram of the voltage over the coil V_L and its serial resistance V_R, due to a current through the coil I_L is depicted in figure 57. V_s is the voltage applied voltage over the serial connection of the coil and the internal resistance. (See also figure 58.)

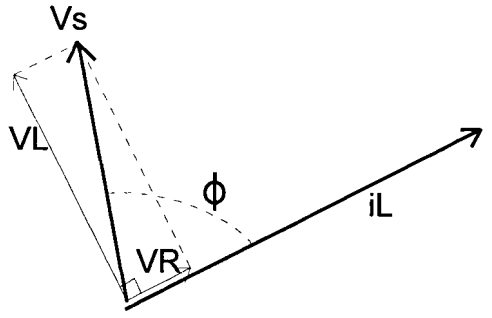

figure 57: Phase diagram of current and voltage over coil

From figure 57 the following two relations for the serial connection of the coil with its resistance can be derived:

$$\hat{V}_s = \hat{i}_L \sqrt{\omega^2 L^2 + \left(R_L + R_s\right)^2}$$

$$\phi = \arcsin\left(\frac{\omega L}{\sqrt{\omega^2 L^2 + \left(R_L + R_s\right)^2}}\right)$$

(77)

Substituting the two formulas from (77) into each other gives:

$$L = \frac{\hat{V}_s \cdot \sin(\phi)}{\hat{i}_L \cdot \omega}$$

(78)

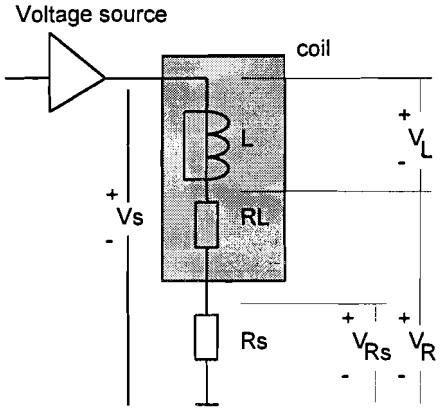

figure 58: Current sensing resistor circuitry

When the voltage over an extra serial resistance R_s with the coil (to measure the current i_L through the coil, see figure 58) is multiplied with $\cos(\omega t)$ and after that is lead through a low pass filter gives the DC-voltage: (This is also called synchronous AM-demodulation) [10], [11], [12]

$$V_{dem} = \left[\hat{V}_{R_s} \cdot \sin(\omega t + \phi) + V_{low.freq.}\right] \cdot \cos(\omega t) =$$
$$\left[\hat{V}_{R_s} \cdot \left(\sin(\omega t)\cos(\phi) + \cos(\omega t)\sin(\phi)\right)\right] \cdot \cos(\omega t) + V_{low.freq} \cdot \cos(\omega t) =$$
$$\frac{1}{2}\hat{V}_{R_s}\sin(\phi) + \frac{1}{2}\hat{V}_{R_s}\sin(2\omega t + \phi) + V_{low.freq}\cos(\omega t) \overset{low.pass.}{=}$$
$$\frac{1}{2}\hat{V}_{R_s}\sin(\phi)$$

(79)

Substituting (79) and (77) in (78) leads to:

$$L = \frac{\hat{V}_s \cdot \frac{\bar{V}_{dem}}{\frac{1}{2}\hat{V}_{R_s}}}{\frac{\hat{V}_{R_s}}{R_s} \cdot \omega} = \frac{2R_s\hat{V}_s \cdot V_{dem}}{\hat{V}_{R_s}{}^2\omega}$$

(80)

Formula (80) gives the equation which describes how the inductance (and so the position of the ball) can be measured with the DC-output voltage of the demodulator and the amplitude of the voltage over the extra serial resistance R_s. As the amplitude of the additional high frequency voltage over the coil $\hat{V}_s$, its frequency ω and R_s are constants, the relation between the inductance of the coil L and the output voltage of the demodulator V_{dem} is proportional. Note that $\hat{V}_{R_s}$ is **not** constant and must be measured separately.

Measurement of the voltage over the current sensing resistor comes with inevitable noise. This influences the accuracy of the inductance measurement of the coil. When assumed that the input voltage V_{Rs} suffers from band limited noise with frequency ω, amplitude $\hat{V}_n$ and stochastic phase θ (See section 5.2) the input of the demodulator is given by:

$$\hat{V}_{R_s} \cdot \sin(\omega t + \phi) + \hat{V}_n \cdot \sin(\omega t + \theta)$$

(81)

The output voltage of the demodulator is then given by:

$$V_{dem} = \left(\hat{V}_{R_s} \cdot \sin(\omega t + \phi) + \hat{V}_n \cdot \sin(\omega t + \theta)\right) \cdot \cos(\omega t) =$$
$$\left[\hat{V}_{R_s}\left(\sin(\omega t)\cos(\phi) + \cos(\omega t)\sin(\phi)\right) + \hat{V}_n\left(\sin(\omega t)\cos(\theta) + \cos(\omega t)\sin(\theta)\right)\right]\cos(\omega t) =$$
$$\frac{1}{2}\hat{V}_{R_s}\sin(\phi) + \frac{1}{2}\hat{V}_n\sin(\theta) + \frac{1}{2}\hat{V}_{R_s}\sin(2\omega t + \phi) + \frac{1}{2}\hat{V}_n\sin(2\omega t + \theta) \overset{low.pass}{=}$$
$$\frac{1}{2}\hat{V}_{R_s}\sin(\phi) + \frac{1}{2}\hat{V}_n\sin(\theta)$$

(82)

The measured inductance is, according to (80), given by:

$$L = \frac{2R_s\hat{V}_s V_{dem}}{\left(\hat{V}_{R_s} + \hat{V}_n\sin(\phi - \theta)\right)^2\omega} = \frac{R_s\hat{V}_s\left(\hat{V}_{R_s}\sin(\phi) + \hat{V}_n\sin(\theta)\right)}{\left(\hat{V}_{R_s} + \hat{V}_n\sin(\phi - \theta)\right)^2\omega}$$

(83)

Maximum of this function is reached when $\theta = \phi$. This maximum is:

$$L_{\max} = \frac{R_s\hat{V}_s\sin(\phi)\cdot\left(\hat{V}_{R_s} + \hat{V}_n\right)}{\hat{V}_{R_s}{}^2\omega}$$

(84)

Using (80) and (84) gives for the signal to noise ratio(*) of the inductance measurement:

$$(SNR)_{out} = \frac{L}{L_{\max} - L} = \frac{\dfrac{R_s\hat{V}_s\hat{V}_{R_s}\sin(\phi)}{\hat{V}_{R_s}{}^2\omega}}{\dfrac{R_s\hat{V}_s\sin(\phi)\cdot\left(\hat{V}_{R_s} + \hat{V}_n\right)}{\hat{V}_{R_s}{}^2\omega} - \dfrac{R_s\hat{V}_s\hat{V}_{R_s}\sin(\phi)}{\hat{V}_{R_s}{}^2\omega}} = \frac{\hat{V}_{R_s}}{\hat{V}_n} = (SNR)_{in}$$
$$\frac{(SNR)_{out}}{(SNR)_{in}} = 1$$

(85)

Formula (85) shows that the signal to noise ratio of the inductance measurement is equal to the signal to noise ratio of the input signal of the sensor. (which is R_s)

(*) Again, in this section the signal to noise ratio is defined as the maximum amplitude of the signal devided by the maximum amplitude of the noise. See section 5.2 for details.

5.4.2 HIGH FREQUENCY COMPONENT WITH CURRENT CONTROL

In the previous section a high frequent component is added to the **voltage** over the coil. When a current source is used a high frequent component can be added to the **current** through the coil. This has some advantages, as will be made clear in this section.
The high frequency voltage over the coil is not a direct measurement for the inductance of the coil, because of the serial resistance of the coil:

$$U_L = \left(R_L + j\omega L\right) \cdot i_L \qquad (86)$$

Like with voltage control, there are two ways to overcome this problem:
The first is to add a very high frequency, so that $\omega L >> R_L$. This will lead to certain (but small) error, depending on the measuring frequency. Problem is that a very high frequency currents can not be supplied to the coil, due to the high impedance of the inductor at that frequency.
The second solution for the problem is not to measure the amplitude of the total voltage, but to measure the amplitude of the voltage which is 90° out of phase with the applied current. This option will be discussed in this section.

A phase diagram of the voltage over the coil V_L and its serial resistance V_R, due to a current through the coil i_L is depicted in figure 59. Note that this is the same diagram as in figure 57, except for the fact that now i_L is known, and V_s (not V_L) can be measured.

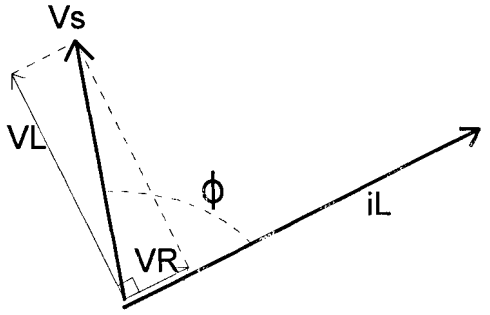

figure 59: Phase diagram of current and voltage over coil

The vector diagram in figure 59 shows that the voltage over the inductive part of the coil impedance is always 90° out of phase with the applied high frequency current. This has some advantages:

When the voltage over the serial-connection of the coil inductance and resistance (V_s) is multiplied with $\cos(\omega t)$ and after that is lead through a low pass filter this gives the DC-voltage:

$$V_{dem} = \left[\hat{V}_s \cdot \sin(\omega t + \phi) + V_{low.freq.}\right] \cdot \cos(\omega t) =$$
$$\left[\hat{V}_s \cdot \left(\sin(\omega t)\cos(\phi) + \cos(\omega t)\sin(\phi)\right)\right] \cdot \cos(\omega t) + V_{low.freq} \cdot \cos(\omega t) =$$
$$\frac{1}{2}\hat{V}_s \sin(\phi) + \frac{1}{2}\hat{V}_s \sin(2\omega t + \phi) + V_{low.freq}\cos(\omega t) \overset{low.pass.}{=}$$
$$\frac{1}{2}\hat{V}_s \sin(\phi)$$

(87)

Substituting (87) in (78) leads to:

$$L = \frac{\hat{V}_s \cdot \sin(\phi)}{\hat{i}_L \cdot \omega} = \frac{2V_{dem}}{\hat{i}_L \omega}$$

(88)

Formula (88) gives the equation which describes how the inductance (and so the position of the ball) can be measured with the DC-output voltage of the demodulator. Remark that the amplitude of the applied high frequent current through the coil $\hat{i}_L$ and its frequency ω are constants. This means that, in contrary to the voltage controlled coil, **only** the output voltage of the demodulator V_{dem} must be measured.

Like with the voltage controlled coil, the measurement of the coil voltage comes with inevitable noise. When assumed that the input voltage V_S suffers form band limited noise with frequency ω, amplitude $\hat{V}_n$ and stochastic phase θ (See section 5.2) the input of the demodulator is given by:

$$\hat{V}_s \cdot \sin(\omega t + \phi) + \hat{V}_n \cdot \sin(\omega t + \theta)$$

(89)

The output voltage of the demodulator is then given by:

$$V_{dem} = \left(\hat{V}_s \cdot \sin(\omega t + \phi) + \hat{V}_n \cdot \sin(\omega t + \theta)\right) \cdot \cos(\omega t) =$$
$$\left[\hat{V}_s\left(\sin(\omega t)\cos(\phi) + \cos(\omega t)\sin(\phi)\right) + \hat{V}_n\left(\sin(\omega t)\cos(\theta) + \cos(\omega t)\sin(\theta)\right)\right]\cos(\omega t) =$$
$$\frac{1}{2}\hat{V}_s \sin(\phi) + \frac{1}{2}\hat{V}_n \sin(\theta) + \frac{1}{2}\hat{V}_s \sin(2\omega t + \phi) + \frac{1}{2}\hat{V}_n \sin(2\omega t + \theta) \overset{low.pass}{=}$$
$$\frac{1}{2}\hat{V}_s \sin(\phi) + \frac{1}{2}\hat{V}_n \sin(\theta)$$

(90)

The measured inductance is according to (88) given by:

$$L = \frac{2V_{dem}}{\hat{i}_L \omega} = \frac{\hat{V}_s \sin(\phi) + \hat{V}_n \sin(\theta)}{\hat{i}_L \omega}$$

(91)

Maximum of this function is reached when $\theta = \phi$. This maximum is:

$$L_{\max} = \frac{(\hat{V}_s + \hat{V}_n) \cdot \sin(\phi)}{\hat{i}_L \omega}$$

(92)

Using (88) and (92) gives for the signal to noise ratio(*) of the inductance measurement:

$$(SNR)_{out} = \frac{L}{L_{\max} - L} = \frac{\frac{\hat{V}_s \sin(\phi)}{\hat{i}_L \omega}}{\frac{(\hat{V}_s + \hat{V}_n)\sin(\phi)}{\hat{i}_L \omega} - \frac{\hat{V}_s \sin(\phi)}{\hat{i}_L \omega}} = \frac{\hat{V}_s}{\hat{V}_n} = (SNR)_{in}$$

$$\frac{(SNR)_{out}}{(SNR)_{in}} = 1$$

(93)

Formula (93) shows that the signal to noise ratio of the inductance measurement is equal to the signal to noise ratio of the input signal of the sensor, which is the voltage over the coil.

Also, the high frequent current through the coil suffers from noise. It is assumed that the amplitude of the current through the coil is given by:

$$\hat{i}_L + \hat{i}_n,$$

(94)

where $\hat{i}_n$ is stochastic.

Substituting (94) and (77) in (87) gives:

$$V_{dem} = \frac{1}{2}\sqrt{R_L^2 + \omega^2 L^2}\left(\hat{i}_L + \hat{i}_n\right)\frac{\omega L}{\sqrt{R_L^2 + \omega^2 L^2}} = \frac{1}{2}\left(\hat{i}_L + \hat{i}_n\right)\omega L$$

(95)

Using (88) leads to:

$$L_{measured} = \frac{L_{real}\left(\hat{i}_L + \hat{i}_n\right)}{\hat{i}_L}$$

(96)

This gives for the signal to noise ratio(*):

$$(SNR)_{out} = \frac{L_{measured}}{L_{measured} - L_{real}} = (SNR)_{in}$$

$$\frac{(SNR)_{out}}{(SNR)_{in}} = 1$$

(97)

Remark that for this sensor the voltage sensing current source, as described in section 4.1.3, can be used. That means that no additional filter is necessary to stabilise the current source. This has the advantage that no compensation is necessary for the influence of such a filter on the inductance measurement.

(*) Again, in this section the signal to noise ratio is defined as the maximum amplitude of the signal devided by the maximum amplitude of the noise. See section 5.2 for details.

5.5 CORRELATION MEASUREMENT

In the previous sections the inductance of the coil is measured by adding a particular sensing signal to the control current or voltage over the coil. Problem of all these options was the noise at the output of the power amplifier. In this section this noise is used as sensing signal to measure the inductance of the coil. This can be done by correlation measurement.

The impedance of the serial connection of the inductance L and the resistance R_L of the coil is given by:

$$|Z(j\omega)| = |R_L + j\omega L| = \sqrt{R_L^2 + \omega^2 L^2}$$

(98)

This means that the spectrum of the noise in the current through the coil is given by:

$$\Phi_{noise,current}(j\omega) = \left|\frac{1}{Z(j\omega)}\right|^2 \cdot \Phi_{noise,voltage}(j\omega)$$

(99)

And that the spectrum of the noise in the voltage over the coil is given by:

$$\Phi_{noise,voltage}(j\omega) = |Z(j\omega)|^2 \cdot \Phi_{noise,current}(j\omega)$$

(100)

So when the spectrum of the noise in the coil voltage and the spectrum of the noise in the current through the coil can be measured, the impedance of the coil can be calculated by:

$$|Z(j\omega)| = \sqrt{\frac{\Phi_{noise,voltage}(j\omega)}{\Phi_{noise,current}(j\omega)}} \qquad (101)$$

However, the inductance of the coil can not be calculated when only the impedance of the serial connection of the inductance and the resistance is known. So an other measurement is necessary to determine R_L. This can only be done by using one of the methods described in the previous sections. This means that correlation measurement can not be used to determine the impedance of the coil in this application.

5.6 Conclusions Regarding the Sensor

In this chapter various sensors for the self sensing magnetic levitation system were examined. The sensor must be adapted to the actuator type (voltage source or current source), however the actuator influences the sensor. This influence must be compensated for.
First the sensor examined was to measure the oscillation frequency of an LC-oscillator with a phase locked loop. It appeared that this combination has a very bad signal to noise ratio (compared to other sensors) Therefore it will not be used in the levitation system.
The second sensor which was examined, was the HF-pulse counting between two zero crossings. Although the signal to noise ratio of this sensor seemed much better than the inductance sensor using the PLL, it was remarked that the calculations of the signal to noise ratio was probably much too optimistic. Therefore this way to measure the inductance of the coil will not be used in the levitation system.
Next, the Q-factor of an LC-oscillator was examined as a way to obtain the inductance of a coil. It was shown that the Q-factor not only depends on the inductance of the coil, but also on its serial resistance R_L. As the serial resistance R_L of the coil is temperature dependent, this type of sensor cannot be used in this application.
The fourth type of inductance sensor which was examined was adding a high frequency signal to the current through the coil or voltage over the coil. It appeared that, when a using current controlled coil, this type of sensor is accurate and simple.
Finally the last sensor discussed was correlation measurement. It was shown that when using correlation measurement only, the inductance of the coil cannot be obtained. For this reason this inductance sensor is not used in the magnetic levitation system.

One can say that, from the sensor's point view, a current controlled coil with an additional high frequency component is the best option for the actuator/sensor combination in this application.

6. CHOOSING ACTUATOR / SENSOR COMBINATION

In the previous two chapters various actuator and sensor types were discussed. Problems with practical realisation and noise problems were examined. In this chapter a particular actuator/sensor combination is chosen.

6.1 CHOOSING ACTUATOR/SENSOR COMBINATION

In table 4 the combinations of actuators and sensors discussed in the previous two chapters are summarised.

Actuator type	Sensor type	Sensor Noise Reduction	Additional Circuitry	Circuitry Constraints
current source	PLL	0.1	- high pass filter parallel to coil	$R_p >> \sqrt{\frac{L}{C}}$ $C_f < 200pF$ $R_f > 3K\Omega$
voltage source	PLL	0.1	- serial LC-filter with source - compensation for L_f and C_f	$R_f >> \sqrt{\frac{L}{C}}$
current source	HF-counter	1(?)	- high pass filter parallel to coil	$R_p >> \sqrt{\frac{L}{C}}$ $C_f < 200pF$ $R_f > 3K\Omega$
voltage source	HF-counter	1(?)	- serial LC-filter with source - compensation for L_f and C_f	$R_f >> \sqrt{\frac{L}{C}}$
current source	Q-factor		- high pass filter parallel to coil - measurement of R_L	$R_p >> \sqrt{\frac{L}{C}}$ $C_f < 200pF$ $R_f > 3K\Omega$
voltage source	Q-factor		- measurement of R_L - serial LC-filter with source - compensation for L_f and C_f	$R_f >> \sqrt{\frac{L}{C}}$
current source	HF-amplitude	1	- complex current source	
voltage source	HF-amplitude	1	- two measurements necessary	
current source	correlation		- measurement of R_L	
voltage source	correlation		- measurement of R_L	

table 4: Summarisation of actuators and sensors

Out of the ten possible actuator/sensor combinations in table 4, the **current controlled coil with additional high frequent component for inductance sensing** is chosen. (Shaded dark) Although the H_∞ controller for the current source requires complex electronics, the electronics for inductance measurement are relatively simple, and no compensation is required for additional filters.
Last but not least, the current controlled levitation system is of the second order, a voltage controlled system is third order. Also the pole location of the current controlled system does not depend on the operation point of the system, in contrary to the voltage controlled system. (Compare (17) and (24))

These three reasons make that the **current controlled coil with additional HF-component for inductance sensing** is the best option in this application.

6.2 SENSOR TUNING

As every sensor, the sensor chosen for the self sensing magnetic levitation system has a few system parameters which can be varied to optimise the sensor for the system it is used in. This can be visualised as in figure 60.

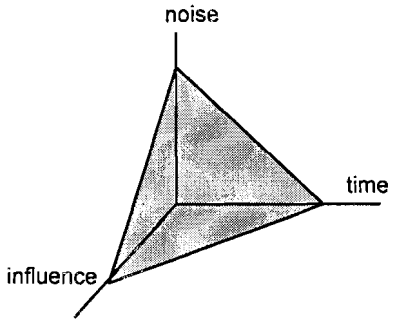

figure 60: Time / influence / noise exchange

The graph in figure 60 shows that when measurement of the inductance of the coil has to take place very fast, this measurement suffers from a lot of noise, or has a great influence on the levitation system. This can be explained on the basis of an example as follows:
The three performance parameters which can be varied in the current controlled coil with additional HF-component are the frequency of the additional high frequency component, the amplitude of the additional high frequency component, and the bandwidth of the low pass filter in the synchronous AM-demodulator. When the inductance measurement must be very fast, the bandwidth of the low pass filter following the AM-demodulator must be broad. However, then the noise bandwidth of the AM-demodulator is broad too. Signal to noise ratio can be improved if the amplitude of the additional high frequency component is enlarged, however then the influence of the sensor on the levitation system is larger.
A similar contemplation can be set up for the minimum influence and minimum noise.
(Note that in figure 60 the performance of the system is assumed to be a plane. As it is impossible to measure without noise, influence or time, this plane must be a three dimensional hyperbole.)

In the levitation system under study, the bandwidth of the mechanical system is assumed to be 100 Hz. This means that the low pass filter in the AM-demodulator must have a bandwidth of at least 100 Hz.
Further more the Nyquist criterion requires that the sample frequency is at least two times the highest frequency to be measured. So this criterion demands that the frequency of the additional high frequency is at least 200 Hz. However, because the band pass input filters of the AM-demodulator cannot be infinitely steep, the frequency of the additional component must even be as much as 1 kHz, to avoid noise caused by the actuating current.
Finally, the amplitude of the additional high frequency component must be chosen. When the actuating current is zero, still a DC-voltage must be supplied to the coil to be able to source the inductance sensing signal. The DC-current by this DC-voltage must be compensated for by the current through the opposite coil, and thus must be a small as possible. On the other hand, when the inductance sensing signal is very small, the signal to noise ratio of the inductance sensor is very low.

Regarding the restrictions as stated above the three system parameters for the inductance sensor are chose as follows:

$$
\begin{aligned}
f_{HF} &= 1 \text{ kHz} \\
B_{low\ pass\ filter\ AM\text{-}demodulator} &= 100 \text{ Hz} \\
V_{inductance\ measurement,\ DC} &= 1.5 \text{ V} \\
V_{inductance\ measurement,\ AC} &= 1.5 \text{ V} \\
i_{inductance\ measurement,\ DC} &= 285 \text{ mA} \\
i_{inductance\ measurement,\ AC} &= 2.38 \text{ mA}
\end{aligned}
\qquad \textit{(102)}
$$

7. CONTROLLER DESIGN

In the previous chapter the current controlled coil with additional HF-component was chosen as the actuator/sensor combination for the self sensing magnetic levitation system. This gives the system as depicted in figure 61.

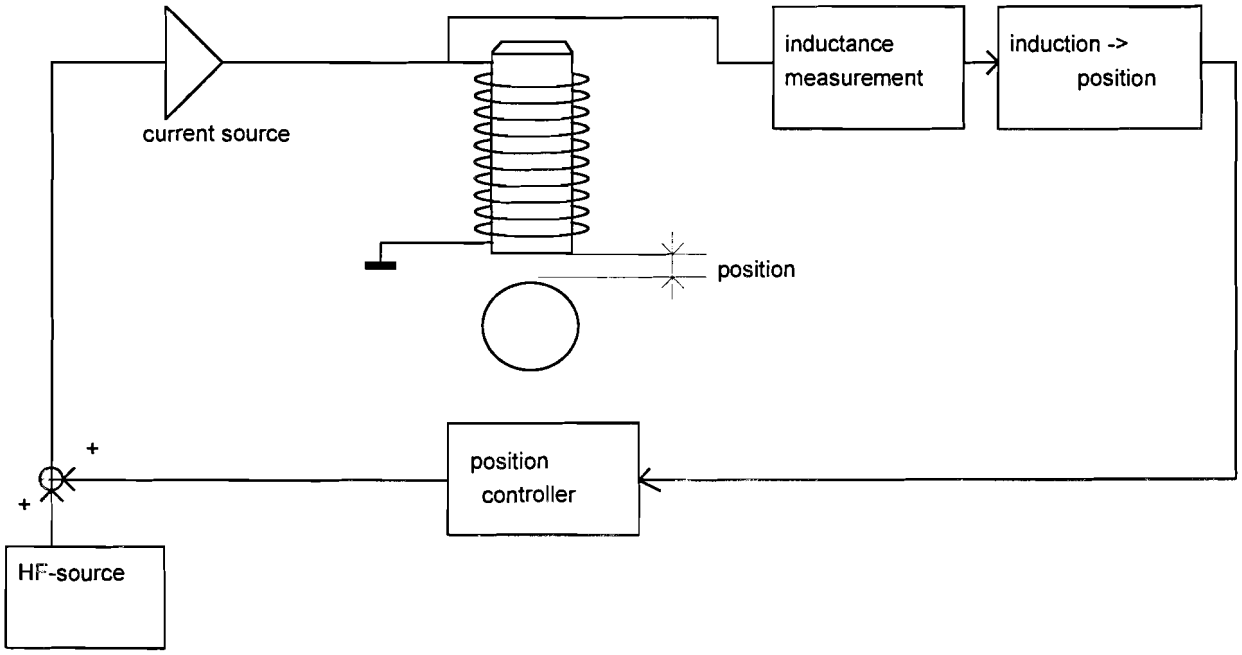

figure 61: Block scheme of magnetic levitation system

In chapter 4, section 4.1.4, the transfer function and phase shift form input voltage to output current of the current and voltage sensing H_∞ controller is plotted. As already indicated, the bandwidth of the H_∞ controller is much more than the bandwidth of the mechanical system. Also the phase shift for low frequencies is very small. This means that the current source has a unity gain transfer function (in the concerned frequency band) and introduces no delay time into the levitation system.
Further more, as the additional high frequency component in the current through the coil to measure its inductance is at least two time higher than the highest frequency in the mechanical system (that means is at least 200Hz), the output signal of the inductance sensor does not suffer from aliasing. Because operation of the sensor is continuous, the sensor does not introduce a time delay into the system.
So, the actuator as well as the sensor are designed such that they do not have any influence on the transfer function of the magnetic levitation system, as derived in chapter 3.

When the model parameters, given in chapter 2, are substituted into the linearised transfer function given in chapter 3 by (17) a controller for this linearised process can be designed using several design tools, e.g. Matlab. The model parameters are summarised in (103)

$$H(s) = \frac{x(s)}{i(s)} = -\sqrt{\frac{2ABge^{-Bx_0}}{m}} \frac{1}{\left(s+\sqrt{gB}\right)\left(s-\sqrt{gB}\right)}$$

$$A = 4.941 \cdot 10^{-3}[H]$$
$$B = 138[m^{-1}]$$
$$x_0 = 0.005[m]$$
$$g = 9.81[ms^{-2}]$$
$$m = 0.05[kg]$$

(103)

As already indicated in chapter 3, the position of the poles does not depend on the linearisation point x_0. Only the gain of the system varies with x_0. The pole map of the linearised open loop system is depicted in figure 62.

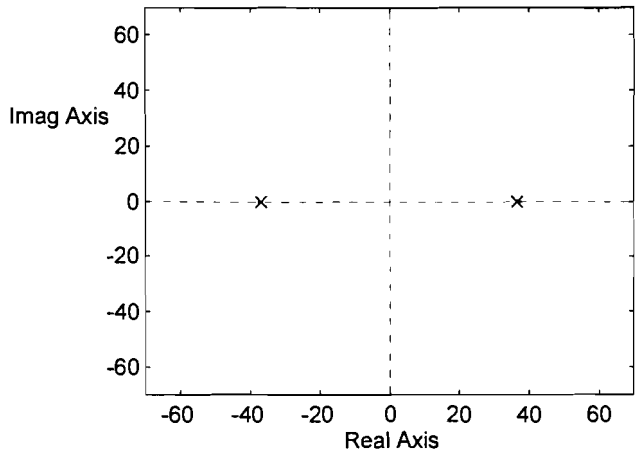

figure 62: Pole and zero map of the open loop system

7.1 SECOND ORDER LINEAR CONTROLLER

A stabilising controller for the linearised process described in the previous section should have the lowest order possible. A second order controller can stabilise the process with zero steady state error, as will be discussed below.

The application of the controller demands that the steady state error of the close loop system is zero. So, an extra pole will be positioned in the origin of the complex plane. This system in figure 61 can be stabilised using a linear controller, with the transfer function:

$$C(s) = K \frac{(s+z_1)(s+z_2)}{(s+p_1)(s+p_2)}\Bigg|_{K=-900, z_{1,2}=21\pm 10j, p_1=0, p_2=100}$$

(104)

This controller has a complex zero-pair at $z_{1,2} = 21 \pm 10j$ and one additional pole far left in the complex plane, to make its transfer function proper. The root loci of this system are plotted in figure 63.

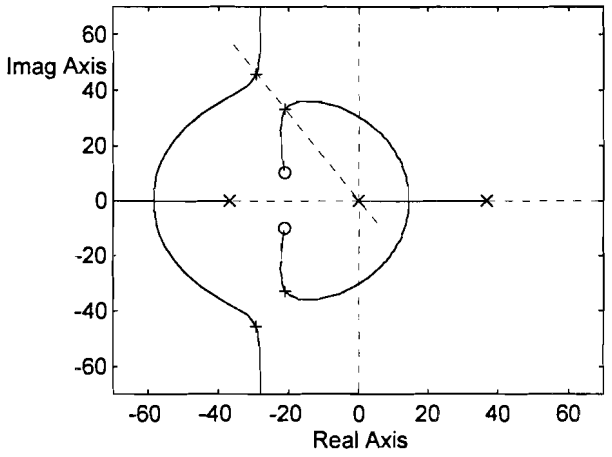

figure 63: Rootloci of controlled system, K=-900, $z_{1,2}$=-21±10j

When the zeros of the controller are located more to the right, the inner pole-pair would be less damped, so the zeros must be located as far to the left as possible. However, when the two zeros are located more to the left than that they are in figure 63, the outer pole-pair would go to the zeros in stead of the inner, and the latter pair would be much less damped. So the position of the zeros in figure 63 is the optimum.
The gain K of the controller is chosen at K_{opt} such that a line through the two poles with a positive imaginary part leads through the origin. (See dashed line in figure 63.) In that case the system is damped optimal: When the gain K set lower than K_{opt}, the inner pole-pair would be less damped than in the case K is equal to K_{opt}, and when the gain is set higher than K_{opt}, the outer pole-pair would be less damped.
Remarkable is that the gain of the controller is negative. This is because the process has also a negative gain. Physical interpretation of this phenomenon is that (when in equilibrium) the current through the coil i_L increases, the distance between the ball and the coil x decreases.

Note that it is possible that the gain K is such high that the actuator is not able to supply the demanded current at all times, or that the magnetic material of the coil saturates. This will be examined in detail in section 7.5.

7.2 THIRD ORDER LINEAR CONTROLLER

Simulations (see section 7.5) show that the second order controller designed in the previous section is not able to stabilise the **non linear** process. Therefore a third order controller which effects much more damping is designed in this section. Simulations show that this controller can stabilise the non linear process. Formula (105) shows the transfer function of a third order controller which can be used in the control scheme in figure 61.

$$C(s) = K\left.\frac{(s+z_1)(s+z_2)(s+z_3)}{(s+p_1)(s+p_2)(s+p_3)}\right|_{K=-2775,z_1=40,z_2=z_3=60,p_1=0,p_2=p_3=140} \qquad (105)$$

This controller has one zero at s=-40 to cancel one open loop system pole, two zeros at s=-60 and two additional poles far left in the complex plane, so that its transfer function is proper. The root loci of this system are plotted in figure 64.

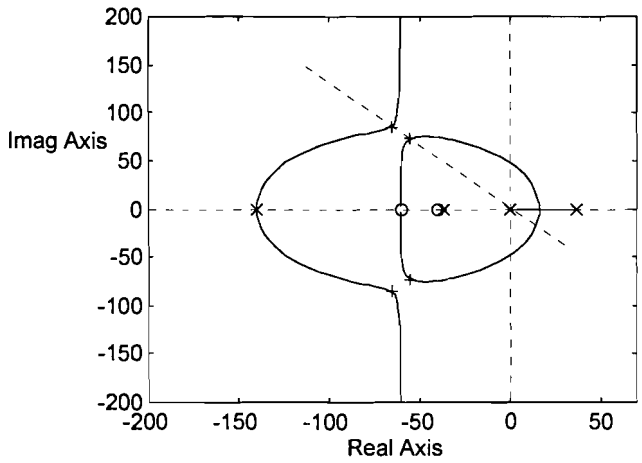

figure 64: Root loci of controlled system, K=-2775, z_1=40,z_2=z_3=60

A comparison between figure 63 and figure 64 shows that the poles of the closed loop system are located more to the left in the complex plane. This implies that the system is more damped.
Disadvantage of a third order controller in comparison with the second order controller is that the former has an extra differentiator, and thus suffers more from noise.
As with the previous controller, the position of the zeros and the gain of the controller are optimised using a iterative process.

Note that again, saturation of the current source and the magnetic material of the coil core is examined in section 7.5.

7.3 THIRD ORDER NON LINEAR CONTROLLER

In the previous two sections the root loci were plotted for the controlled linearised system in the **nominal** operation point x_0 (=0.005[m]) However, when the system is not in the nominal operation point, but in $x=x^*$ the root loci of the controlled linearised system differ, as can be seen in figure 65.

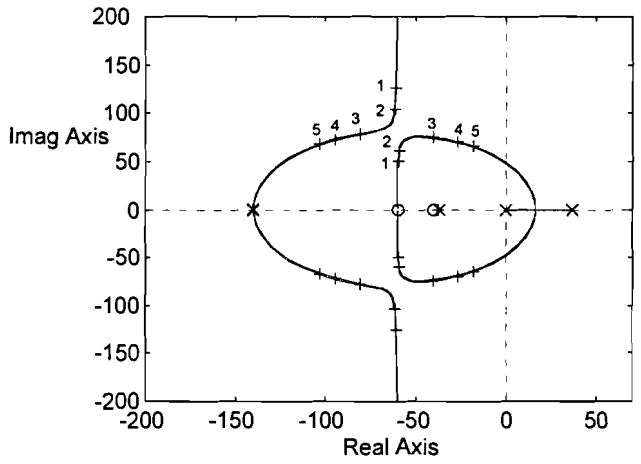

figure 65: Root loci of the controlled linearised system, around the nominal operation point

In figure 65 for $x^*=0.002$ *(point 1)*, $x^*=0.004$ *(point 2)*, $x^*=0.006$ *(point 3)*, $x^*=0.008$ *(point 4)* and $x^*=0.010$ *(point 5)* the root loci and the position of the poles are calculated, using the linear third order controller of the previous section. One can see that the trajectory on which the poles are located does not depend on the operation point x^*, but that the gain of the process (and thus the optimal gain K_{opt} of the controller) changes significantly. It is therefore sensible to design a controller which takes the operation point into account.

Formula (17) shows that the transfer function(*) of the process can be described by:

$$H(s,x) = A(x)\frac{1}{(s+p)(s-p)},$$

(106)

where:

$$A(x) = -\sqrt{\frac{2ABge^{-Bx_0}}{m}}$$
$$p = \sqrt{gB}$$

(107)

It is then easy to correct for the dependence of the gain on x by taking:

$$C(s,x) = K(x)\frac{(s+z_1)(s+z_2)(s+z_3)}{(s+p_1)(s+p_2)(s+p_3)}\Bigg|_{z_1=40,z_2=z_3=60,p_1=0,p_2=p_3=140}$$

(108)

and:

$$K(x)\cdot A(x) = G_{opt}$$

(109)

The relative difference in the gain of the linearised process in the operating x and the nominal operating point x_0 is:

$$\frac{-\sqrt{\frac{2ABge^{-Bx}}{m}}}{-\sqrt{\frac{2ABge^{-Bx_0}}{m}}} = e^{\frac{1}{2}B(x-x_0)}$$

(110)

This difference in the gain of the process must be compensated in the non linear gain of the controller. This gives the transfer function(*) of the non linear controller by:

$$C(s,x) = e^{\frac{1}{2}B(x-x_0)} \cdot \left[K_{opt} \frac{(s+40)(s+60)(s+60)}{s(s+140)^2} \right] = e^{\frac{1}{2}B(x-x_0)} \cdot \left[-2775 \frac{(s+40)(s+60)(s+60)}{s(s+140)^2} \right]$$

(111)

According to (14) a DC-current must be added to the output of the controller to set the process in the equilibrium point the controller is designed for. So, the current through the coil to levitate the ball is given by:

$$i_L = \sqrt{\frac{2mg}{ABe^{-Bx}}} + i_{controller}$$

(112)

The technique described in this section, can also be applied to other linear controllers (Such as H_∞-controllers, see next section.) to adapt them to the non linear process. This technique is also known as exact linearisation. [16]
In figure 66 the procedure of exact linearisation is plotted.

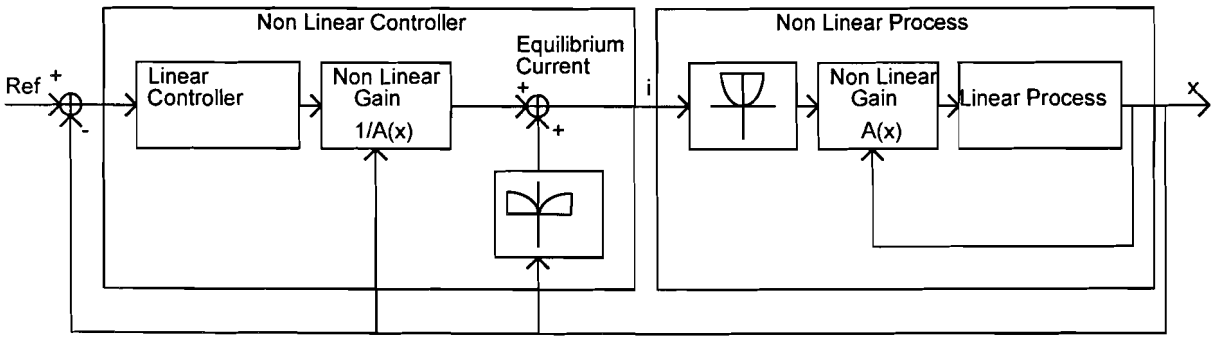

figure 66: Exact linearisation

(*) Formally this is not a transfer function. A transfer function does only depend on the frequency ($j\omega = s$) and not the operation point x. Transfer functions **must** be linear. Nevertheless, in this report a transfer function multiplied with a non linear function which only depends on x is also called a transfer function.

7.4 H_∞-CONTROLLER

As with the current source (see section 4.1) an H_∞-controller can be designed for the process to find an optimal balance between noise reduction, overshoot, step response, actuator saturation etc. A non linear H_∞-controller will be designed in this section using the exact linearisation scheme as described in the previous section. Therefore, a linear H_∞ controller will be designed first and after that, this controller will be adapted to the non linear process.

In figure 67 the augmented plant is plotted for the system linearised in the operating point x_0. (103) The generalised plant is depicted in figure 68.

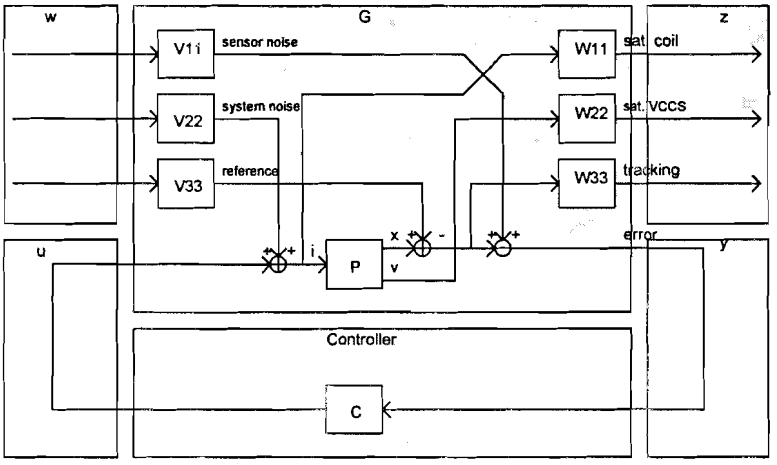

figure 67: Augmented plant

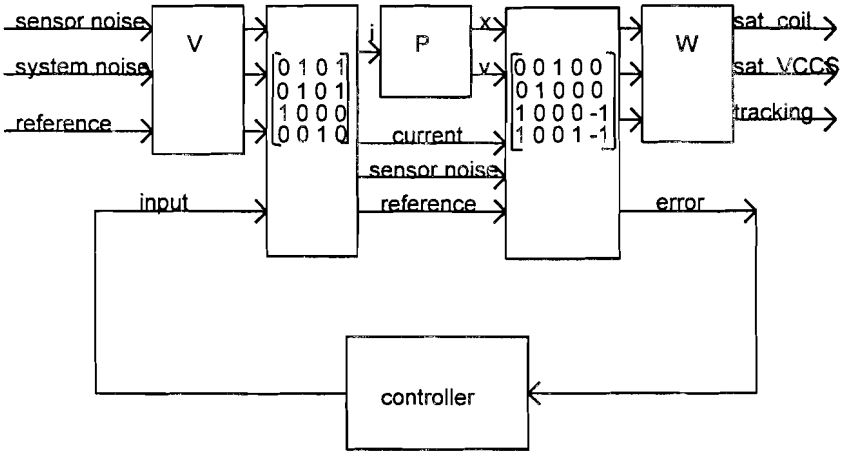

figure 68: Generalised plant for MHC-Toolbox

In figure 67 the plant is the coil, controlled by the voltage controlled current source, as in section 4.1, and the ball. The input of the plant is the input voltage of the VCCS, the two outputs are the position of the ball, and the voltage over the coil. As already indicated in section 7, the voltage controlled current source and the inductance sensor have no influence on the transfer function of the magnetic levitation system as derived in chapter 3. (In the concerned frequency band.) This leads to the transfer functions of the plant P as in (113)

The plant has three exogenous inputs. The first is sensor noise, with its shaping filter V_{11}. The position sensor with its additional electronics is assumed to have a signal to noise ratio of at least 60dB. This leads to V_{11}=-60 dB=0.001
The second exogenous input of the plant is system noise, with its shaping filter V_{22}. System noise is added mainly for modelling coil saturation but also for modelling the signal to noise ratio of the electronics in the controller, and the influence of the high frequency inductance sensing signal. When the currents through the coil are not too large, the influence of saturation effects is relatively small. V_{22} is chosen as: V_{22}=-60 dB=0.001
The last exogenous input of the plant is the reference signal for the position, with its shaping filter V_{33}. The reference signal is assumed to consist of low frequencies only.
Finally it is assumed that: $\|w_1\|_2, \|w_2\|_2, \|w_3\|_2 < 1$

The plant has three exogenous outputs. First of all the current through the coil, with its shaping filter W_{11}. This exogenous input is to model saturation effects of the magnetic material of the coil core. W_{11} is chosen at 0.33.
Note that weighting filter W_{11} as state above does **not** guarantee that the input signal of the current source is small enough to avoid saturation of the current source. It only gives an rough estimation of the output signals of the current source for designing the H_∞ controller for the levitation system.
The second exogenous output of the plant is the output voltage of the current source with its shaping filter W_{22}, to model saturation of the output voltage of the voltage controlled current source. The maximum output voltage of the current source is bounded by its supplied voltage, which is assumed to be 30V. This leads to W_{22}=0.0333
Note that, again, W_{22} gives no guarantee that the desired output voltage of the current source never exceeds 30V
The last exogenous input of the plant is the tracking error of the ball, with its shaping filter W_{33}. The tracking error must be small for low frequencies can be large for high frequencies.
Finally it is assumed that: $\|z_1\|_2, \|z_2\|_2, \|z_3\|_2 < 1$

The transfer functions of the plant are: (Remark that the position of the ball is expressed in millimetres rather than in metres)

$$P_{11} = \frac{1000}{-0.1092s^2 + 147.8048}$$
$$P_{12} = \frac{691s + 21980}{s + 6280} \qquad (113)$$

The transfer functions of the weighting filters are: (Remark that the position of the ball is expressed in millimetres rather than in metres.)

$$V_{11} = 0.001$$
$$V_{22} = 0.001$$
$$V_{33} = \frac{10 \cdot 62.8^3}{(s+62.8)^3}$$
$$W_{11} = \frac{1}{3}$$
$$W_{22} = \frac{1}{30}$$
$$W_{33} = \frac{30 \cdot 6.28^4 \cdot (s+6.28)^2}{(s+0.628)^2 (s+62.8)^2}$$

(114)

As formula (113) shows, the plant is linearised in the operating point x_0.
The transfer functions of the plant and the weighting filters are plotted in figure 69.

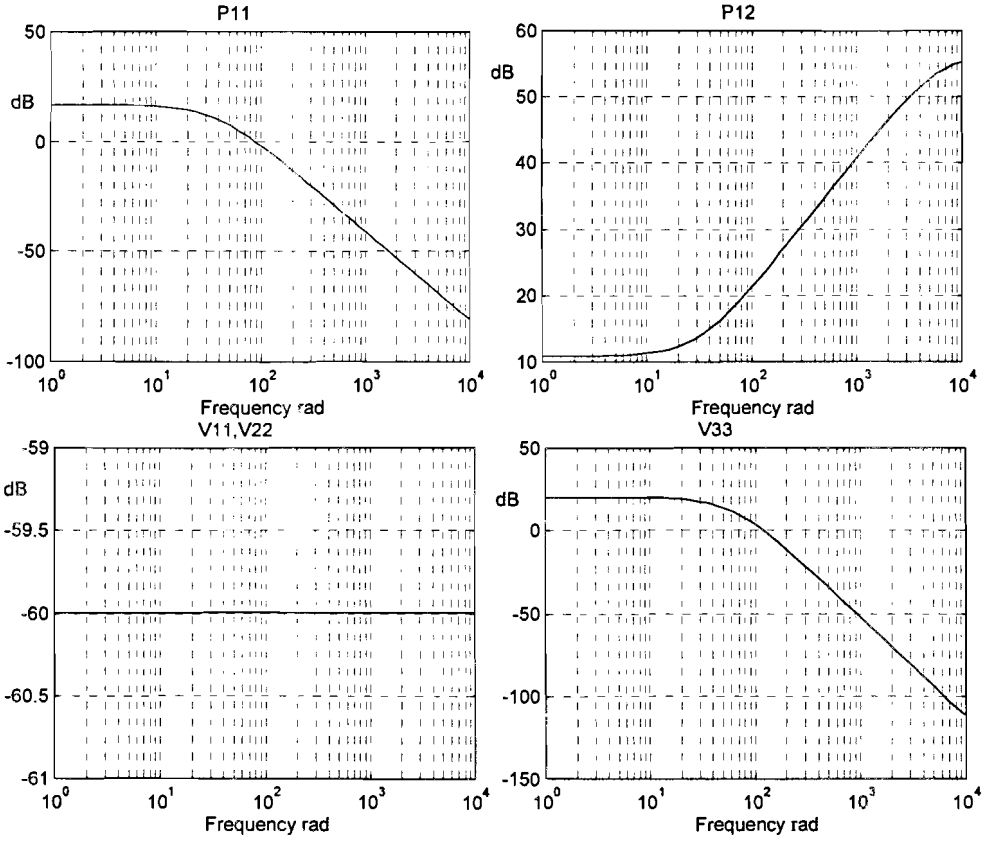

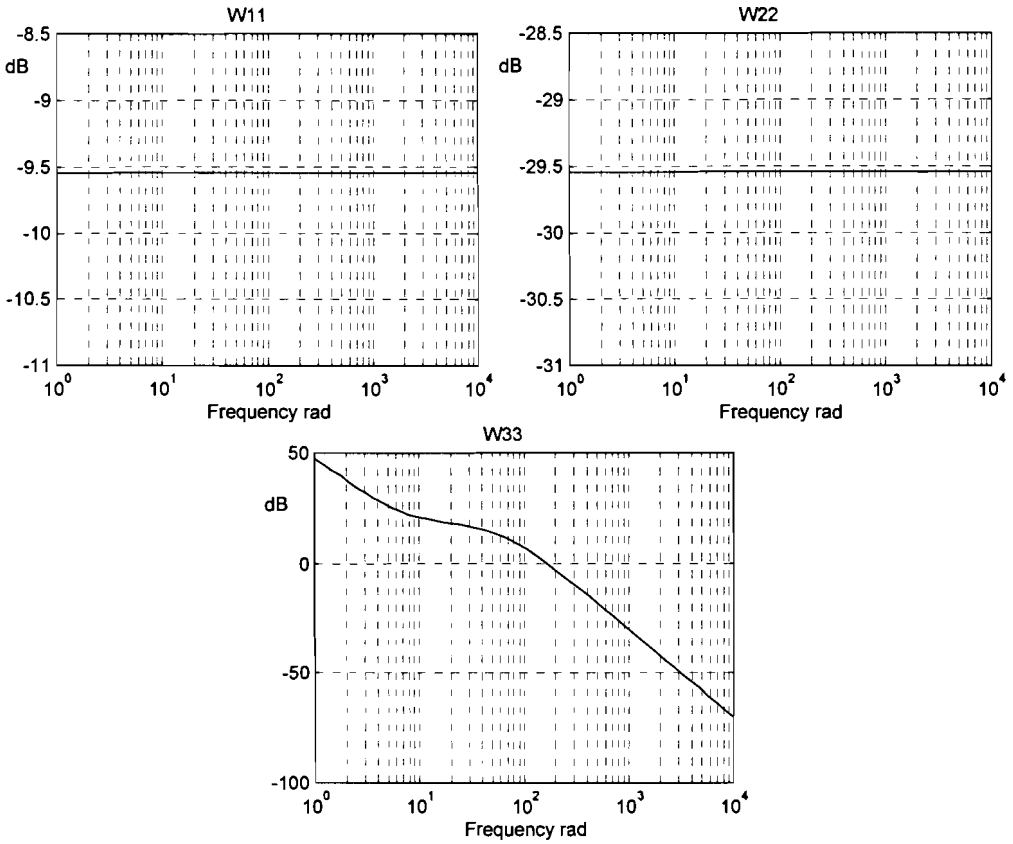

figure 69: Weighting filters for MHC-Toolbox

When a controller is designed using the weighting filters as in (114) MHC gives the results as in figure 70. The solid line is the transfer function from a certain input of the augmented plant to a certain out. The dashed line is the boundary of stability. The optimum for γ was found to be 1.138, which is close to 1, as it should be.

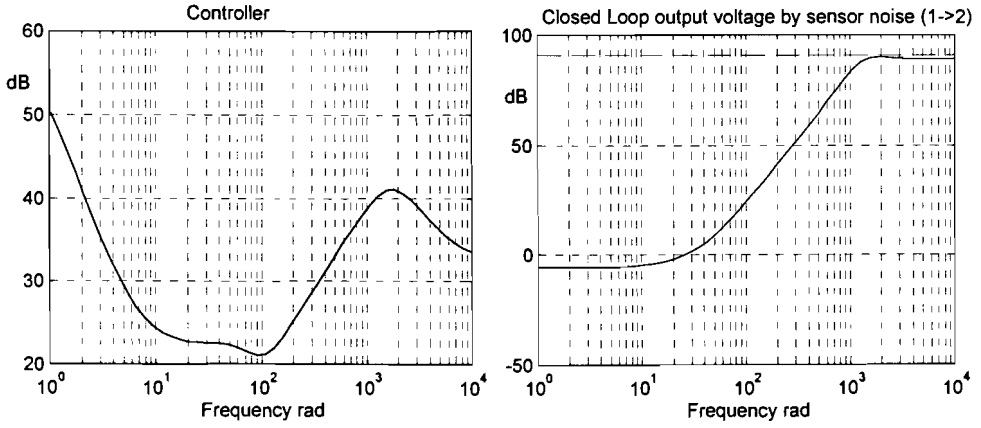

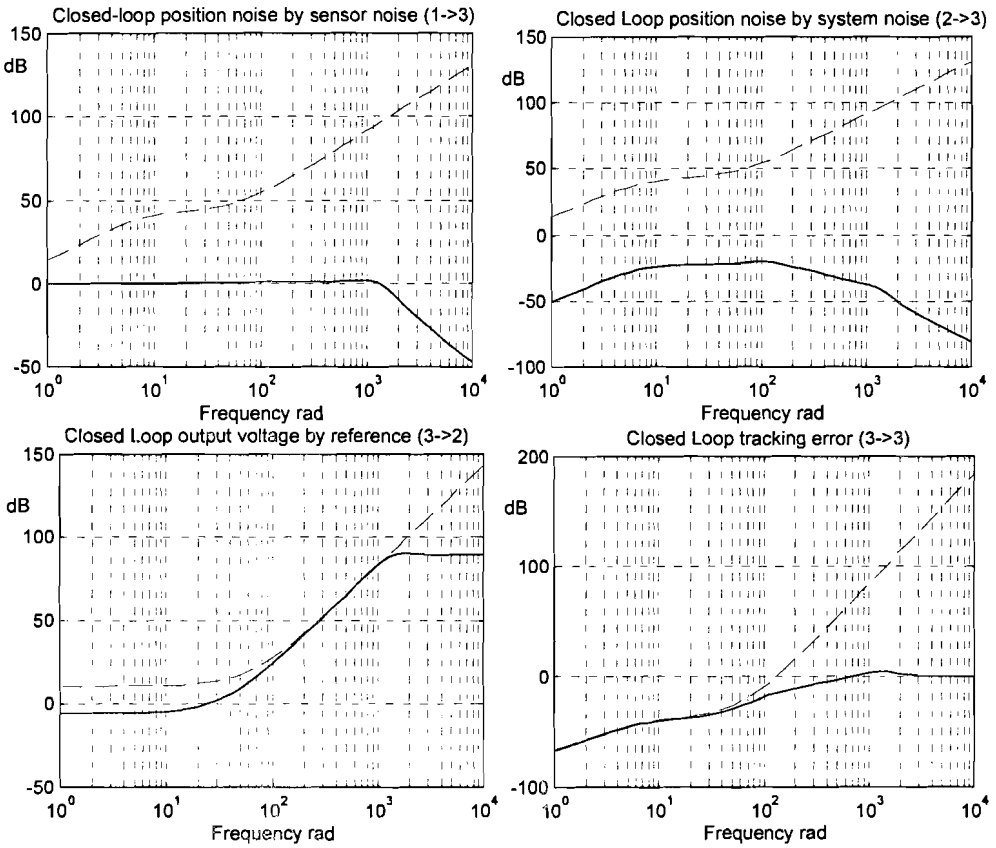

figure 70: Controller designed by MHC-Toolbox

The upper left plot in figure 70 shows the transfer function of the controller. The controller is of the tenth order.
The upper right part of figure 70 shows the bottle neck of the system for high frequencies. The plot of bottom left part shows the bottle neck for frequencies around 100Hz. Apparently, the maximum output voltage of the voltage controlled current source is for high frequencies the limiting factor for the system. This can be understood by the fact that the output voltage is the third(!) derivate of the position.
The tracking error for low frequencies is -60dB (0.1%)
For all frequencies system-noise is damped very well.

In figure 71 the rootloci of the system controlled by the H_∞-controller are plotted. The plot on the right is an enlargement of the shaded area in the left plot.

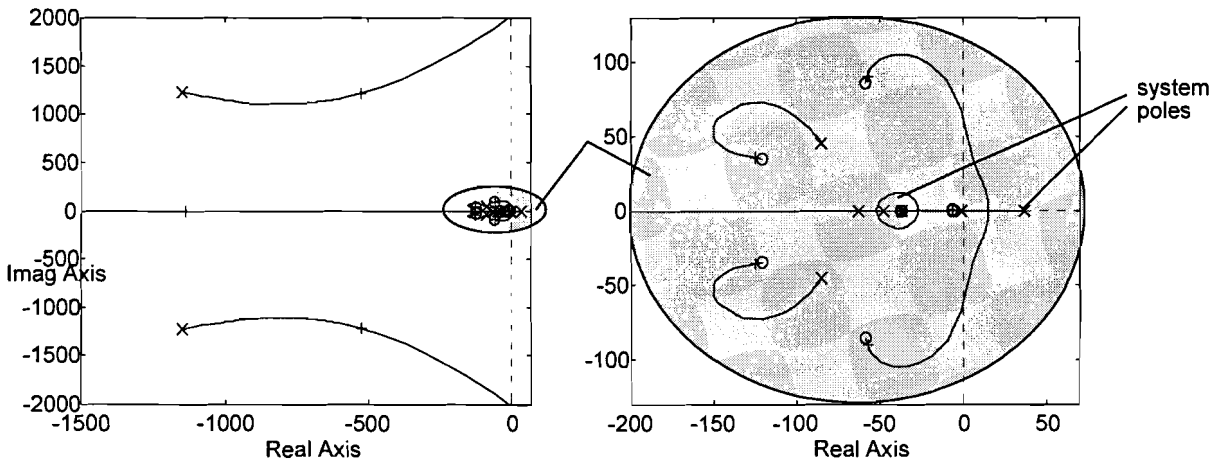

figure 71: Rootloci of the H_∞ controlled system

Until now the designed H_∞-controller was a linear controller. However, like with the third order linear controller designed in section 7.2, a non linear H_∞-controller can be designed using exact linearisation. The same non linear functions as in section 7.3 can be used. This gives the following transfer function(*) for the non linear H_∞-controller:

$$C(s,x) = e^{B(x-x_0)} \cdot H_{lin.H_\infty - controller}(s) \qquad (115)$$

Again the process must be set in the equilibrium point the controller is designed for. Therefore a DC current must be added to the output of the controller. So, the current through the coil to levitate the ball is given by:

$$i_L = \sqrt{\frac{2mg}{ABe^{-Bx}}} + i_{controller} \qquad (116)$$

(*) Formally this is not a transfer function. A transfer function does only depend on the frequency ($j\omega = s$) and not the operation point x. Transfer functions **must** be linear. Nevertheless, in this report a transfer function multiplied with a non linear function which only depends on x is also called a transfer function.

7.5 SIMULATIONS

In this section the non linear process controlled by the various controllers designed in the previous sections is simulated, using Matlab 4.2c.1 with Simulink.

Although a certain DC-current i_0 given by (14) necessary to keep the process in its operating point, preliminary simulations show that, to stabilise the process, the control current $\tilde{i}$ can exceed i_0 in the negative direction. This means that in those situations in spite the gravitational force the controller wants to 'push' the ball away from the upper coil. However, because the electromagnet can only 'pull' at the ball, the control current must flow through the bottom coil, in stead of the upper coil. [11] This gives the control scheme as in figure 72.

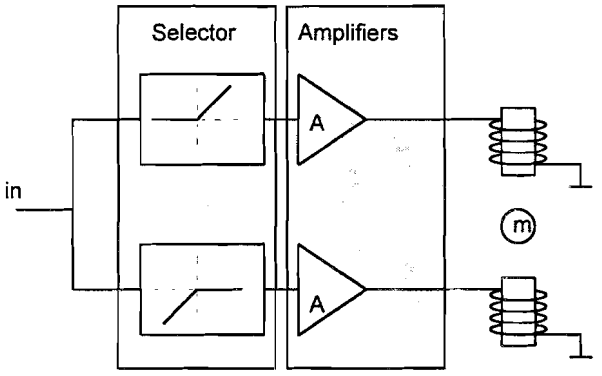

figure 72: Two-coil-control

When simulating the two-coil-control scheme as in figure 72 one can use the following operation for the square in (7)

$$f_m = -\frac{1}{2} AB \cdot e^{-B \cdot x} \cdot i_L^2 \cdot \mathrm{sgn}(i_L), \qquad (117)$$

where f_m is the total magnetic reluctance force on the ball by the **two** coils and i_L is the current through (one of) the coils.

Using (117) gives the Simulink model as in figure 73, figure 74 and figure 75 for the controlled non linear system.

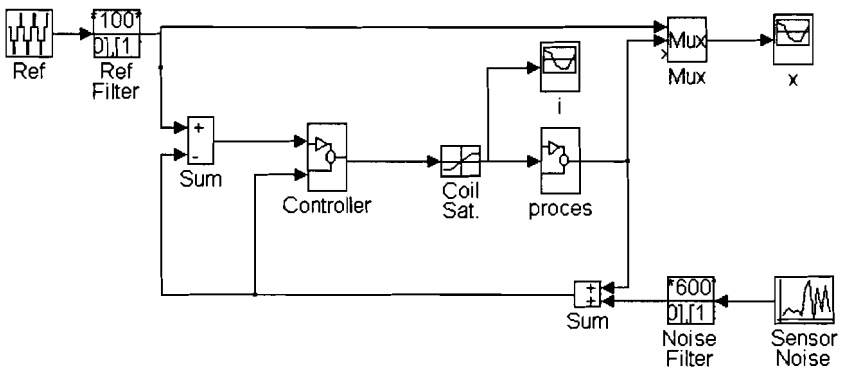

figure 73: Simulink block scheme of controlled levitation system

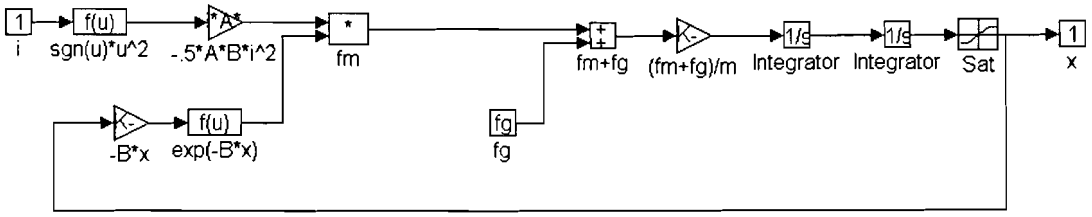

figure 74: Simulink block scheme of non linear process

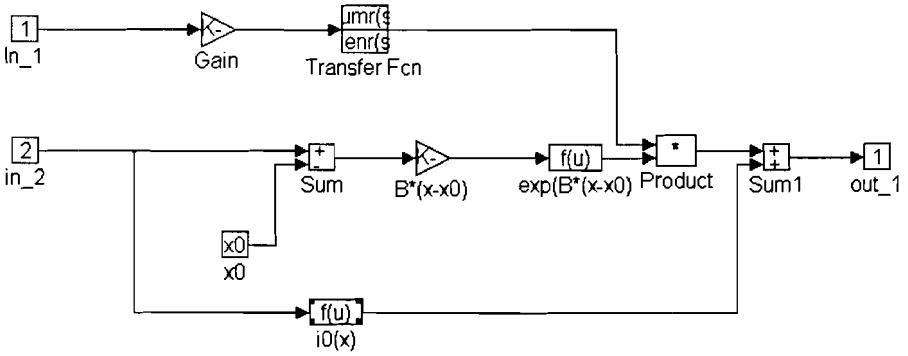

figure 75: Simulink block scheme of non linear controller

In figure 73 the reference signal consists out of six steps to different operating points. The higher harmonics in these steps are filtered by the third order filter *Ref Filter.* This filtered reference signal is plotted.
In the bottom right part of figure 73 the sensor noise is added to the position measurement. The sensor noise is assumed to have a maximum amplitude of 0.001, frequencies above 100Hz are filtered by the third order filter *Noise Filter.*

The measured position of the ball is subtracted from the reference signal, and then supplied to the controller. The block scheme of the (non linear) controller is depicted in figure 75.
The output signal of the controller is clipped at +4A (upper coil) or -4A (bottom coil) by the saturation block, to simulate the saturation of the coil. (Magnetic hysterese is **not** modelled.)
The output of the saturation block supplied as the input signal of the process. The block scheme of the non linear process is depicted in figure 74.

In figure 75 an additional gain block is added in series with the linear transfer function of the controller. This is because the input signal of the H_∞ controller designed in section 7.4 was expressed in millimetres rather than in meters. Also, as already indicated in chapter 2, the gain of the process is negative. Therefore this amplifier block must have a gain of **-1000**.

In figure 76 the simulation with the third order non linear is depicted. The plot on the left is the position of the ball, the plot on the right is the current through the coil. Obviously the controller cannot stabilise the ball very well: High frequencies are poorly damped. (The second order controller, and the linear third order controller are unable to stabilise the ball at all.) In the reference signal all frequencies above 15Hz are filtered by the reference filter.

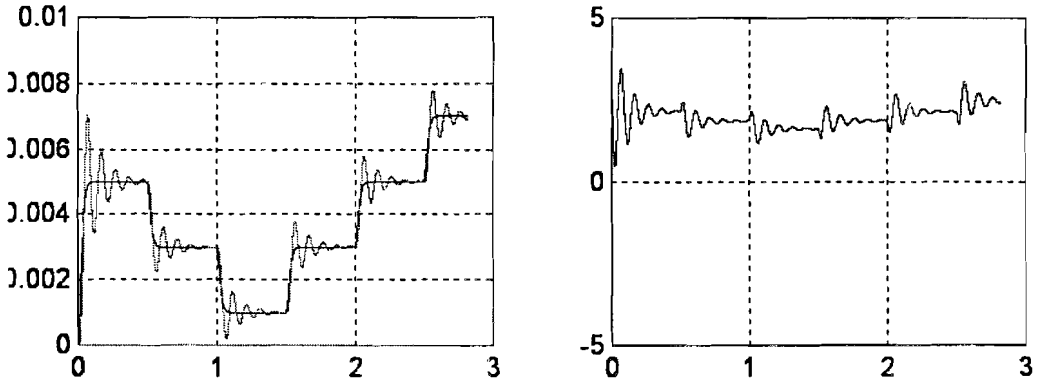

figure 76: Simulation of the third order non linear controller

In figure 77 simulation of the non linear H_∞-controller is depicted. One can see that the tracking of the reference signal is very well. In the reference signal all frequencies above 15Hz are filtered by the reference filter. The current through the coil never exceeds the saturation value of approximately 4A.

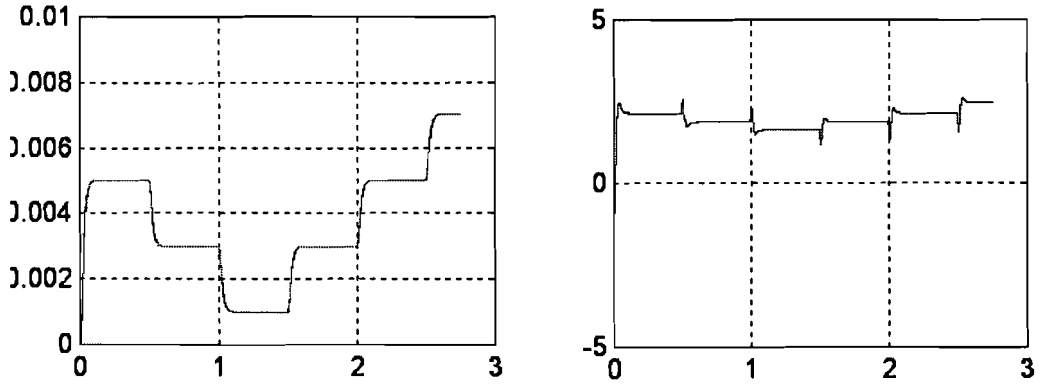

figure 77: Simulation of the H_∞ non linear controller

In figure 78 the H_∞-controlled process is simulated, when a reference signal is applied above the design criteria of the H_∞-controller. (Note that for visibility the time axis is expanded a factor three.) Now in the reference signal all frequencies above 50Hz are filtered by the reference filter. This leads to more overshoot in position of the ball, and the current through the coil saturates.

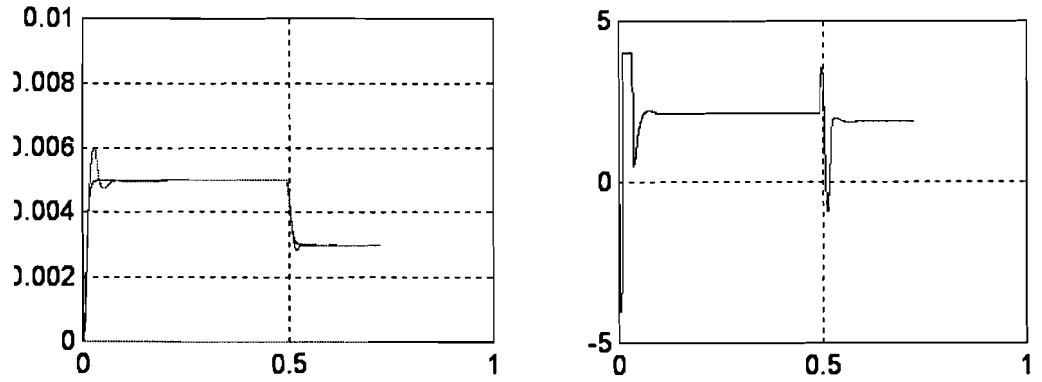

figure 78: Simulation of the H_∞ non linear controller, frequencies above specs.

In figure 79 the H_∞-controlled process is simulated, when noise is added to the position measurement signal. (Note that for visibility the time axis is expanded a factor three.) As stated before, the maximum amplitude of the noise is 0.001m, and it is low pass filtered by a third order filter at 100Hz. One can see that the coil does saturate. Sensor noise has a very large influence on the performance of the controller.

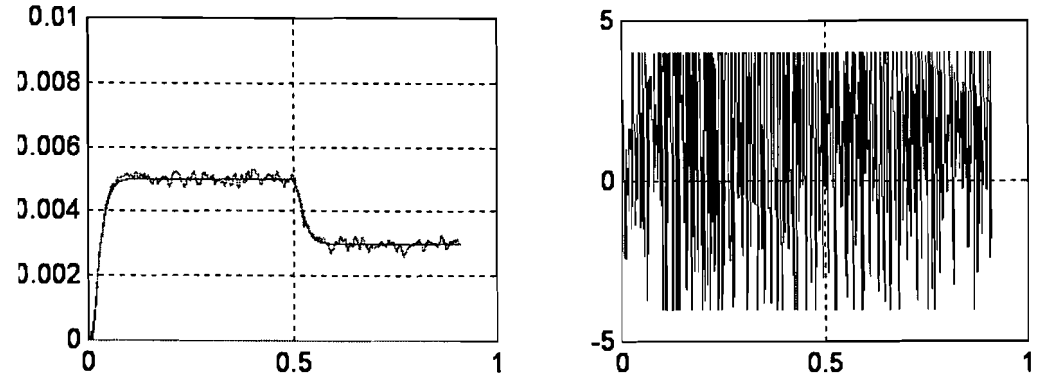

figure 79: Simulations of the H_∞ controller, noisy position measurement

7.6 CONCLUSIONS

In this chapter a non linear H∞ controller is designed for controlling the magnetic levitation system. The controller was designed for the linearised system, and then adapted to the non linear system using a technique called exact linearisation. The performance of the designed controller has been examined by simulating its behaviour in the non linear process. The performance of the designed controller has been compared to linear and non linear PID controllers.
It appeared that the designed non linear H∞ controller was able to stabilise the position of the ball very accurate. However, noise deteriorates the performance of the controller.

8. PRACTICAL IMPLEMENTATION

In the previous chapters a magnetic levitation system has been designed. Due to lack of time, the complete system is not tested in practice. Only the H_∞ voltage controlled current source with voltage and current sensing, and the inductance sensor are tested.
The preliminary results will be discussed in this chapter

8.1 TESTING ACTUATOR

The H_∞ controller for the voltage controlled current source as designed in section 4.1.3 is tested in practice, with the actual coil connected at the output of the current source. It appeared that the current source was not able to stabilise the current through the coil. However, with a few minor adjustments the current source works perfectly fine. The schematic of the adjusted VCCS is depicted in figure 80.

The first adjustments to the scheme in figure 24 is that two operational amplifiers are replaced by other types. Texas Instruments (the manufacturer of the NE5534) specifies that its opamp is stable for gains larger than 3. So the most left and most right opamp are replaced by LF356 type opamps.
The other adaptation of the circuit is that two very small capacitors are added to the circuit, otherwise that amplification for very high frequencies was very high. This lead to instabilities.

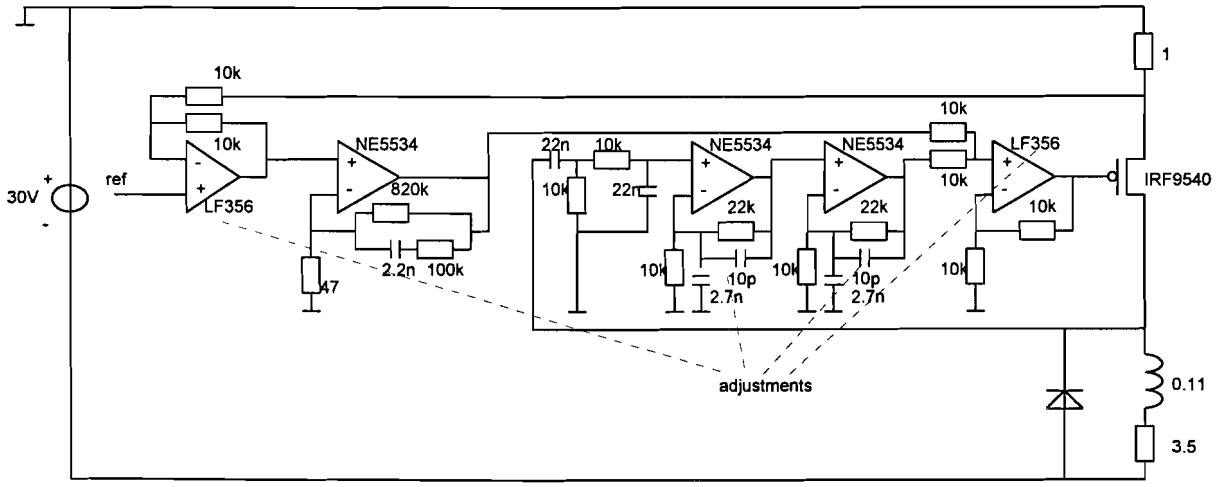

figure 80: Circuitry of VCCS source, with minor adjustments

8.2 TESTING INDUCTANCE SENSOR

The inductance measurement scheme as described in section 5.4.2 is tested in practice. The circuitry as in figure 81 was used.

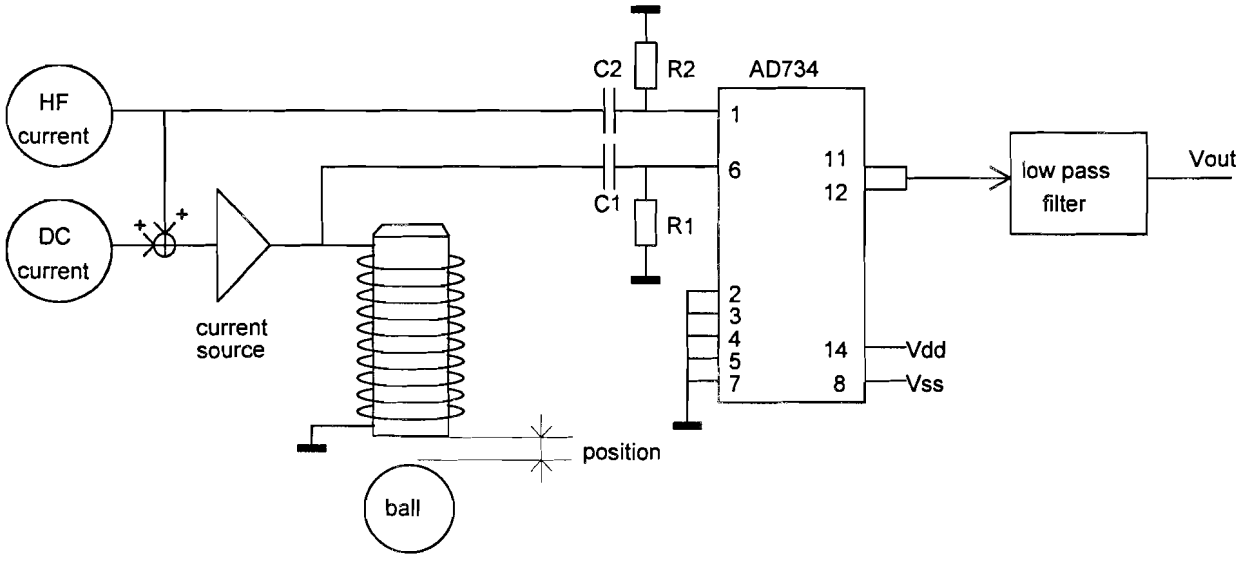

figure 81: Circuitry of inductance sensor

The inductance sensor works as expected. However, due to lack of time the phase shift of the filters R_1/C_1 and R_2/C_2 could not be optimised, so the dependence of the output voltage of the inductance sensor V_{out} and the DC-current flowing through the coil is not measured.

Note that a true multiplier (AD734) is used as synchronous AM-demodulator. In [10], [11] and [12] a so called lock-in amplifier is used as AM-demodulator. The switching and the misadaption of the input signals and gains of the lock-in amplifier caused much noise at the output of the inductance sensor. Therefore a true multiplier is used.

9. REFLECTING ACHIEVED GOALS TO MIRROR DEFLECTION SYSTEM

As already indicated in chapter 1, the levitated ball as described in this report, is a pilot project for a magnetic levitated mirror. In this chapter the achieved goals for the ball will be reflected on to the magnetic levitated mirror.

The magnetic levitated mirror for the laser deflection system has five degrees of freedom (DOF): three degrees for the position of the centre point of the mirror (x, y, z); and two for the angle of the mirror (θ, φ). See figure 82.

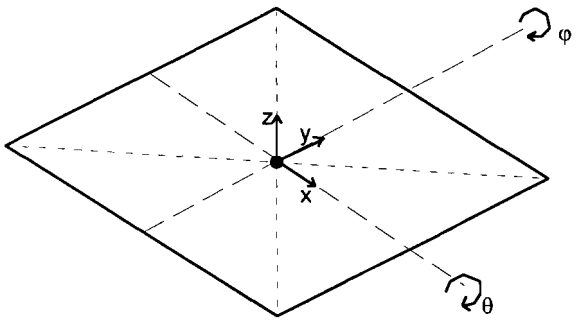

figure 82: Degrees of freedom of magnetic levitated mirror

In the application the mirror is used for (a laser interferometer), both the position and the orientation of the mirror must be known very accurately: the accuracy of position of the mirror determines the accuracy of the laser interferometer (distance), and the accuracy of the orientation of the mirror determines the accuracy of the 3D-measurement of the position of the object.
In contrary to the accuracy, the bandwidth and tracking ability specifications are very different for the position and the orientation of the mirror. First of all, the position of the mirror must be the same at all times. This leads to high noise reduction in a broad frequency bandwidth, but no tracking requirements of a reference signal. The bandwidth and tracking ability requirements of the orientation on the other hand are very stringent.
This leads to the following observations or recommendations for the mirror levitation system:

1. In the current levitation system for the ball, I-shaped coils are used. In this case only a few flux lines lead through the ball, but most of them go around the ball. This leads to large L_s and small L_m, which means that the induction of the coil is very large, and that the induction is only slightly dependent of the position of the ball. Because of this the magnetic reluctance force f_m, is very small compared to the current through the coil i_L, and the sensitivity of the coil as sensor is poor.
   It is much better to use U-shaped coils to levitated the ball (and the mirror). This will solve the above problems.

2. To levitate the mirror, a large current is needed. This leads to saturation of the magnetic material and excessive heat production in the coil windings. The current necessary for

levitation can be (much!) smaller when the mirror is close to the levitation magnets. ($\approx 1\mu m$)
For the orientation of the mirror a large air gap is inevitable. However because the inertia of the mirror is much smaller than the mass of the mirror (118), a smaller current is needed for the same tracking error and bandwidth.

$$J_{half\ sphere} = \frac{1}{5}mr^2 = \frac{1}{5}m \cdot 0.005^2 = 5 \cdot 10^{-6} m \text{ [kg m}^2\text{]}, \qquad (118)$$

where m is the mass of the mirror and r the radius of the half sphere mirror.

3. The mirror levitation system must be much smaller than the current ball levitation system. This will lead to scaling of the dimensions of the system in all three directions. The mass of the ball (mirror) will decrease with the third power of the scaling factor, the area of the coils with the square of the scaling factor. This will lead to less saturation of the coils, and better heat radiation. Also, this will lead to a faster system.

4. In the current levitation system the material of the coil is ferrox cube. This material suffers form saturation at low flux densities (≈ 0.1T) When weak iron (>99.98% Fe) or silicon iron (SiFe) is used as the core material for the coil, the coil will suffer much less from saturation ($\approx 1..2$T) (See also section 2.1)
Furthermore, in the current levitation system the ball to be levitated is a steel ball. Steel (<99% Fe) has poor magnetic properties. It is better to use a weak iron, silicon iron or ferrox cube ball. In that case the magnetic reluctance force exerted on the ball f_m at a certain current i_L is much larger. Also the influence of the position of the ball x on the inductance of the coil L would be much higher.
Note that to avoid Eddy current losses, the coils must be laminated or sintered when using weak iron or silicon iron. The ball nor the mirror must not be laminated because else they would be anisotrope

5. More research is needed to examine the saturation characteristics of the magnetic material of the coil. It is unknown (at the section MBS of the TUE) whether saturation is temperature dependent, frequency dependent, time dependent, etc. When this is all **not** the case saturation can easily be compensated for by using a look-up table.

6. Also hysterese of the magnetic material of the coil must be examined in detail. Maybe hysterese can be eliminated by adding a high frequency current to the actuator current. Note that this is already the case because of the inductance measurement.

7. Biggest problem of the magnetic levitated mirror for the laser interferometer is to measure the position (and orientation) of the mirror sufficiently accurate. Up till now this is done by measuring the inductance of the coil. (self sensing) Apart from saturation and hysterese, there is one other major problem: the inductance of the coil changes only very slightly when the mirror (or ball) moves.
Using the parameters of the current levitation system, the necessary accuracy of the inductance measurement is calculated as follows:

$$\left.\begin{aligned} &\Delta x = 10\cdot 10^{-3} m \leftrightarrow \Delta L = 4\cdot 10^{-3} H \Rightarrow \\ &\Delta x = 1\cdot 10^{-6} m \leftrightarrow \Delta L = 4\cdot 10^{-7} H \\ &L_s = 100\cdot 10^{-3} \end{aligned}\right\} accuracy.L = 0.1000004H$$

(119)

Formula (119) shows that the inductance of the coil L must be measured with 7(!!!) significant digits. This must be considered as impossible, all the more because of the effects of saturation and hysterese.

An other way to measure the position of the ball is to use a capasitive sensor as in figure 83.

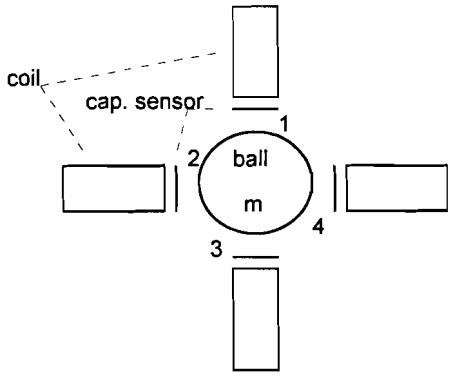

figure 83: Magnetic levitated ball with capasitive sensor

Because no additional wiring to or from the ball (or mirror) is desired, one cannot measure the distance between the ball and the coil by sensing the capacity of the capacitor formed by one capasitive sensor as one plate and the ball as the other plate. Therefore two capasitive sensors are needed. The two capacitors are serie connected through the (conducting!) ball. Those two capacitors cannot lie on opposite sides of the ball (e.g. not sensor 1 and 3 or 2 and 4 in figure 83) because then the position of the ball has no influence on the capacity of the serie connection of the two capacitors. (See (120), where K is a constant determined by the geometry of sensor and ball, x is the distance between the first sensor and the ball and a-x is the distance between the second sensor and the ball.)

$$C = \frac{\frac{K}{x}\cdot\frac{K}{a-x}}{\frac{K}{x}+\frac{K}{a-x}} = \frac{K}{x+a-x} = \frac{K}{a}$$

(120)

However, when the capacity of the four capacitors formed by the serie connection of sensor 1 and 2, 2 and 3, 3 and 4, and 4 and 1 are measured, the position of the ball can be calculated in 2D, using a formula which will not be derived here.

An other possibility to use capasitive position measurement (which can only be used for **very** small gap widths is depicted in figure 84. The capacity between the bar in the middle of the sensor and its shield (shaded in grey) is influenced by the position of the mirror. When designed correctly the inductance of the wires compensates the capacity

between shield and conductor in the wire (as with coaxial cables). So the capacity is zero when the mirror is very far away. (ideally)

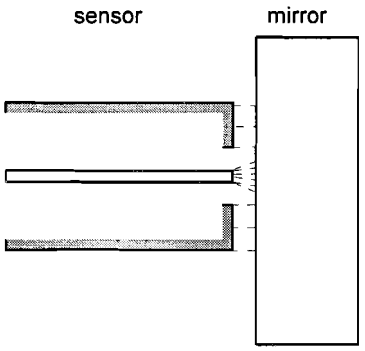

figure 84: Alternative capasitive sensor for magnetic levitated mirror

Position measurement based on capasitive sensors can be much more accurate then the inductance measurement principle.

LITERATURE

[1] Vischer, D. and H. Bleuler.
A New approach to Sensorless and Voltage Controlled AMBs Based on Network Theory Concepts.
Magnetic Bearing. Proc. 2nd. Int. Symp. (1990), p. 301-306
July 12-14, 1990, Tokyo, Japan.

[2] Mizuno, T. and H. Bleuler and C. Gähler and D. Vischer
Towards Practical Applications of Self-Sensing Magnetic Bearings.
Magnetic Bearings. Proc 3rd. Int. Symp. (1992), p. 169-175.
Technomic Publishing Co., Inc., Lancaster.

[3] Vischer, D. and H. Bleuler.
Self-Sensing Active Magnetic Levitation.
IEEE Transactions on Magnetics, Vol. 29 (1993), No. 2, p. 1276-1281.

[4] Mizuno, T.
Phase-Locked Loops for the Stabilization of Active Magnetic Suspensions.
JSME International Journal, Series A, Vol. 37 (1994), No. 3, p. 499-503.

[5] Bleuler, H. and D. Vischer and G. Schweitzer and A. Traxler and D. Zlatnik.
New Concepts for Cost-effective Magnetic Bearing Control.
Automatica, Vol. 30 (1994), No. 5, p. 871-876.

[6] Kurita, Y.
Displacement-Sensorless Control Using Electromagnets (Vibration Control by Current and Magnetic Flux Feedback).
JSME International Journal, Series C, Vol. 38 (1995), No. 2, p. 233-239.

[7] Jayawant, B.V. and R.J. Whorlow and B.E. Dawson.
New transducerless magnetic suspension system.
IEE proc.- Sci. Meas. Technol., Vol. 142 (1995), No. 3, p. 255-261.

[8] Mizuno, T. and H. Bleuler
Self-Sensing Magnetic Bearing Control System Design Using the Geometric Approach.
Control Eng. Practice, Vol. 3 (1995), No. 7, p. 925-932.

[9] Sivadasan, K.K.
Analysis of Self-Sensing Active Magnetic Bearings Working on Inductance Measurement Principle.
IEEE Transactions on Magnetics, Vol. 32 (1996), No. 2, p. 329-334.

[10] J.H.H. Kop, A Magnetic levitation system, Master Science Thesis, Eindhoven University of Technology, Department of Electrical Engineering, Measurement and Control Group.

[11] M.L. Thijssen, A 2-dimensional magnetic levitation-system, Master Science Thesis, Eindhoven University of Technology, Department of Electrical Engineering, Measurement and Control Group.

[12] P.B. Houtkamp, Preparatory study of a two axis mirror deflection system with magnetic bearings, Master Science Thesis, Eindhoven University of Technology, Department of Electrical Engineering, Measurement and Control Group.

[13] A. Vandenput. Elektromechanica en vermogenselektronica, College diktaat, Eindhoven University of Technology, Department of Electrical Engineering, EMV.

[14] G.G. Persoon. Cursus Moderne Analoge Electronica. Phase-Locked Loops. College dictaat , Eindhoven University of Technology, Department of Electrical Engineering, SES.

[15] Heinz Falkus. Multivariable H_∞ Control Design Toolbox User Manual, Eindhoven University of Technology, Department of Electrical Engineering, MBS.

[16] T. Sugie, K. Simizu, and J. Imura. H_∞ control with exact linearization and its application to magnetic levitation systems. IFAC, Vol. 4, pages 363-366, 1993.

APPENDIX A. MEASUREMENT OF SATURATION OF MAGNETIC MATERIALS

ferrox-cube:

I (A)	B (mT)
0.00	0.0
0.08	2.0
0.16	3.8
0.22	5.25
0.26	6.25
0.30	7.20
0.34	8.05
0.43	10.2
0.47	11.2
0.53	12.5
0.60	14.5
0.67	16.0
0.74	17.9
0.81	19.5
0.85	20.5
0.88	21.2
0.94	22.8
1.00	24.0
1.06	25.5
1.15	27.8
1.21	29.0
1.28	30.5
1.36	32.5
1.43	34.2
1.51	36.5
1.56	37.8
1.62	39.5
1.68	40.0
1.80	42.7
1.90	45.5
1.99	47.5
2.07	49.5
2.16	52.0
2.23	53.5
2.32	54.9
2.41	57.5
2.49	59.5
2.55	60.5
2.64	62.0
2.72	62.5
2.80	64.2
2.89	65.5
3.01	66.5
3.13	68.5
3.25	69.5
3.39	71.0
3.51	72.0

I (A)	B (mT)
3.63	72.0
3.71	72.5
3.84	74.0
3.99	75.0
4.26	77.8
4.37	78.2
4.48	79.5
4.58	80.5
4.71	81.5
4.80	82.0
4.91	82.6
5.02	83.8
4.85	82.1
4.78	81.9
4.65	80.8
4.55	80.0
4.45	79.0
4.35	78.0
4.16	76.5
4.04	75.5
3.92	74.2
3.68	72.0
3.47	70.2
3.36	69.0
3.17	66.5
3.05	66.0
2.91	64.0
2.82	62.5
2.65	60.5
2.46	57.8
2.24	53.0
2.12	50.0
1.96	46.5
1.84	43.5
1.75	40.5
1.61	38.0
1.47	34.5
1.30	30.5
1.14	27.5
0.92	21.8
0.82	19.2
0.65	15.5
0.46	11.0
0.33	7.40
0.14	3.05
0.00	0.0

Steel-37:

I (A)	B (mT)
0.00	1.0
0.02	1.5
0.04	1.8
0.06	2.2
0.08	2.6
0.11	3.2
0.13	3.6
0.14	3.9
0.16	4.2
0.18	4.6
0.20	5.0
0.22	5.5
0.25	6.1
0.27	6.6
0.29	7.0
0.32	7.6
0.35	8.1
0.38	8.8
0.40	9.2
0.42	9.6
0.44	10.0
0.47	10.5
0.51	11.5
0.53	11.9
0.57	12.6
0.59	13.2
0.63	14.0
0.66	14.7
0.69	15.5
0.75	16.8
0.81	18.1
0.86	19.2
0.88	19.7
0.92	20.5
0.96	21.3
1.02	22.5
1.05	23.1
1.08	23.9
1.12	24.9
1.17	25.9
1.22	26.9
1.25	27.5
1.32	29.0
1.36	30.0
1.41	30.9
1.43	31.5
1.49	32.1
1.52	32.5
1.58	34.1
1.63	35.8
1.69	37.0
1.74	38.0
1.79	39.0
1.86	40.2
1.91	41.8
1.97	42.5
2.05	44.8
2.15	46.8
2.21	48.1
2.27	49.5
2.35	51.0
2.44	53.5
2.53	55.0
2.60	56.2

I (A)	B (mT)
2.66	58.0
2.71	59.3
2.78	60.5
2.89	62.5
2.98	65.0
3.04	66.0
3.12	68.0
3.16	68.5
3.25	70.5
3.38	73.0
3.44	74.2
3.50	76.0
3.54	76.5
3.62	78.2
3.69	80.0
3.76	81.5
3.88	83.9
3.94	85.0
4.00	86.1
4.06	87.5
4.13	88.5
4.20	90.1
4.29	92.0
4.37	93.8
4.52	96.5
4.62	99.0
4.69	100
4.76	103
4.84	105
4.94	106
5.03	108
4.93	106
4.87	104
4.73	101
4.64	99.0
4.54	98.0
4.34	94.0
4.25	92.0
4.12	89.0
4.07	88.0
3.99	86.5
3.90	85.0
3.68	80.0
3.39	74.0
3.17	70.0
2.94	64.5
2.64	58.5
2.48	55.0
2.31	51.0
2.17	48.0
2.02	44.5
1.86	41.0
1.73	38.5
1.54	34.0
1.33	29.5
1.17	28.0
0.94	21.5
0.84	19.4
0.64	15.0
0.48	11.2
0.38	9 2
0.30	7.5
0.16	4.2
0.00	1.0

weak iron:

I (A)	B (mT)
0.00	0.0
0.08	1.85
0.23	4.95
0.41	8.70
0.53	11.2
0.67	14.2
0.78	16.6
0.88	18.8
1.00	21.2
1.11	23.8
1.27	27.0
1.46	30.8
1.67	35.0
1.84	38.2
1.99	42.0
2.09	44.0
2.21	46.5
2.29	48.0
2.39	50.5
2.49	53.0
2.62	55.0
2.72	57.8
2.85	60.2
2.93	62.2
3.03	64.2
3.12	66.2
3.21	68.2
3.31	70.0
3.39	71.8
3.52	74.2
3.63	76.5
3.76	80.0
3.89	82.5
4.01	85.0
4.16	88.0
4.27	90.0
4.38	92.2

I (A)	B (mT)
4.48	94.2
4.59	96.5
4.73	100
4.83	101
4.96	105
5.06	107
5.20	110
5.44	112
3.70	78.0
3.56	75.0
3.46	72.5
3.35	70.5
3.23	68.0
3.09	65.5
2.92	61.5
2.74	57.8
2.61	54.5
2.51	53.0
2.40	50.0
2.28	47.8
2.14	44.2
1.98	41.0
1.85	39.0
1.69	35.0
1.56	32.2
1.43	30.0
1.33	28.0
1.17	24.0
1.06	21.8
0.91	18.5
0.72	14.5
0.66	12.0
0.43	8.7
0.27	5.5
0.17	3.8
0.00	0.0

APPENDIX B. MEASUREMENT OF POSITION / INDUCTANCE RELATION

ferrox coil, steel ball

x [mm]	L [mH]	L_m [mH]
0.7	107.41	4.52
1.2	107.10	4.21
1.3	107.10	3.97
1.7	106.74	3.85
1.8	106.80	3.66
2.2	106.44	3.55
2.3	106.55	3.39
2.7	106.19	3.30
2.8	106.28	3.17
3.2	106.06	3.04
3.3	105.93	2.96
3.7	105.95	2.84
3.8	105.73	2.74
4.2	105.63	2.66
4.3	105.55	2.56
4.7	105.45	2.50
4.8	105.39	2.39
5.2	105.28	2.32
5.3	105.21	2.24
5.7	105.13	2.16
5.8	105.05	2.09
6.2	104.98	2.03
6.3	104.92	1.96
6.7	104.85	1.92
6.8	104.81	1.85
7.2	104.74	1.78
7.3	104.67	1.73
7.7	104.62	1.65
7.8	104.54	1.62
8.2	104.51	1.57
8.3	104.46	1.52
8.7	104.41	1.47
8.8	104.36	1.43
9.2	104.32	1.40
9.3	104.29	1.35
9.7	104.24	1.28
9.8	104.17	1.21
10.2	104.10	1.19
10.8	104.08	1.07
11.2	103.96	1.04
11.8	103.93	0.83
13.2	103.72	0.82
13.8	103.71	0.66
15.2	103.55	0.64
15.8	103.53	0.35
20.2	103.24	0.34
20.8	103.23	0.09
30.2	102.98	0.07
30.8	102.96	0.07